Master's thesis

NTNU
Norwegian University of Science and Technology
Faculty of Engineering
Department of Geoscience and Petroleum

Tanja Marie Gjerde

Pegmatite petrogenesis and PT-calculations regarding the magmatic-hydrothermal-transition in Tørdal, SE Norway

Compared to The Land's End Granite, SW England

Master's thesis in Bedrock and Resource Geology
Supervisor: Rune Berg-Edland Larsen
Co-supervisor: Kristian Drivenes

June 2021

NTNU
Norwegian University of
Science and Technology

Tanja Marie Gjerde

Pegmatite petrogenesis and PT-calculations regarding the magmatic-hydrothermal-transition in Tørdal, SE Norway

Compared to The Land's End Granite, SW England

Master's thesis in Bedrock and Resource Geology
Supervisor: Rune Berg-Edland Larsen
Co-supervisor: Kristian Drivenes
June 2021

Norwegian University of Science and Technology
Faculty of Engineering
Department of Geoscience and Petroleum

NTNU
Norwegian University of
Science and Technology

Abstract

A 3 km wide belt comprising over 300 pegmatite bodies is emplaced in the Tørdal-Treungen granite, SE Norway (Rosing-Schow, Müller, & Friis, 2018b; Steffenssen et al., 2020). This thesis is a contribution regarding recent ideas of their petrogenesis and the magmatic-hydrothermal-transition. Rune Wilberg (1983) performed a detailed mapping around Kleppsvatnet, identifying five generations, where the most mineralizing events with Sn-Mo signatures occurred in the final phases. In a commonly accepted model are the pegmatitic melt derived from highest differentiated, water-saturated portions of the cupola zone in large granitic intrusions. Here are short travel distances of the pegmatitic-melt noted by field observations and both observations are contributing to the pegmatites being formed directly by anatectic (Rosing-Schow, 2020; Steffenssen et al., 2020). The presence of rare earth elements (REE) is usually associated with Nb-Y-Fe (NYF) pegmatites. However, the Tørdal-pegmatites was a long time defined as Li-Ce-Ta (LCT), despite its enrichments of REE. A detailed EPMA-mapping of an Nb-Rutile reveal NYF-affinity, despite LCT characteristics, and a mixed-class pegmatite system is supported.

A more detailed investigation of the hydrothermal veins is also performed, aiming to answer the magmatic-hydrothermal transition. To obtain this goal was SEM-CL photos and Ti-variations of both hydrothermal and magmatic quartz analysed. Observations of phyllic alteration products suggest a system of acidic fluids percolating through a cooler host-rock. Hydrolysis of feldspar moved the fluid properties towards oxidizing conditions and increasing pH, causing precipitation of the ore-forming minerals. The mineral assemblage and alteration products match the calculated pressure and temperature condition. Temperatures ranging from 450-550 °C and a pressure of 3,4-5,2 Kb was calculated based on microthermometry from fluid inclusion measurements and TitaniQ, for the hydrothermal event.

Sammendrag

Ett 3 km langt belte bestående av 300 pegmatittkropper er lokalisert i Tørdal-Treungen granitten, SØ Norge. Denne oppgaven er ett bidrag til nylige ideer om deres petrogenese og den magmatisk-hydrotermale overgangen (Rosing-Schow et al., 2018b; Steffenssen et al., 2020). Dannelsesteorier av pegmatitter kompleks, men en akseptert modell foreslår at smelten stammer fra de meget differensierte, vannmettede delene av store granitt-intrusjoner. Rune Wilberg utførte en detaljert kartlegging rundt Kleppsvatnet, og identifiserte fem generasjoner, der den mest mineraliserende hendelsen med Sn-Mo mineraliseringer er knyttet til sluttfasene. En kort migreringsvei for den pegmatittiske smelten er også bemerket av feltobservasjoner. Begge disse faktorene bidrar til teorien om at pegmatittene er dannet direkte av anatektisk. Tilstedeværelsen av sjeldne jordartselementer (REE) er vanligvis assosiert med Nb-Y-Fe (NYF) pegmatitter. Tørdal-pegmatittene var imidlertid lenge definert som Li-Ce-Ta (LCT), til tross for sin berikelse av REE. En detaljert EPMA-kartlegging av en Nb-Rutil avslører en NYF affinitet, til tross for LCT kjennetegn. Dette støtter at pegmatittene klassifiseres som en mikset klasse.

En detaljert undersøkelse av de hydrotermale væskene ble også utført for å kunne forstå den magmatisk hydrotermale overgangen. For å oppnå dette ble SEM-CL bilder og variasjoner av Ti innholdet i både hydrotermal og magmatisk kvarts analysert. Basert på observasjoner av phyllic omvandlingsprodukter i optisk mikroskop, er ett system hvor sure væsker strømmer gjennom en kjøligere vertsbergart foreslått. Hydrolyse av feltspat endrer væskeegenskapene mot ett mer oksiderende system med økende pH, som forårsaket utfelling av de malmdannende mineralene. Mineralselskapet og omvandlingsproduktene passer godt med de beregnede trykk og temperaturforholdene. Temperaturene strekker seg fra 450 til 550 °C med et trykk mellom 3,4-5,2 Kbar. Det ble beregnet basert på mikrotermometriske målinger av væske inneslutninger i kvarts og TitaniQ, fra den hydrotermale kvartsen.

Acknowledgement

My master thesis has been accomplished at the Norwegian University of Science and Technology (NTNU) Trondheim, at the Department of Science and Technology. First, I want to express my gratitude to everyone that has contributed to this thesis. Especially my supervisor Rune Berg-Edland Larsen, for good guidance and solution-oriented attitude when things didn't turn out the way I imagined. A great thank you to my co-supervisor Kristian Drivenes for method expertise and understanding, notably when the time flies in the bunker at PTS. I am so grateful for Sabina Strmic Palinkas allowing me to use their equipment at The Arctic Univeristy of Norway when a perfect storm hit the equipment at NTNU. My field work in Tørdal would not have been the same without local knowledge and boat-loan by Lars Kristian Bronken, and good assistance from my childhood friend Hanne Sørvik (and the polardog Føyke).

I am happy with all the facilities at Petroleum Technical Centre and this journey would not have been the same without all my co-students, showing great engagement for my geological discussions, excel-help, and intervals at 7 am.

A great appreciation is appointed to my sister, Lene Kristin Gjerde and her partner Olaf Sissener, for great support always and proofreading.

Trondheim, 17.06.2021

Tanja Marie Gjerde

Content

Abstract....iii
Sammendrag....v
Acknowledgement....vii
Content....ix
List of Figures....xi
List of Tables....xiii

1. INTRODUCTION 1

2. THEORY 2

2.1 MAGMATIC HYDROTHERMAL CONTINUUM....2
2.1.1 Formation of water....2
2.1.2 Solubility of economic metals and other species 5
2.1.3 Deposition of Sn....7
2.4.5 Atomic lattice of quartz as indicator of magmatic events....9
2.2 FLUID INCLUSION....10
2.3 GRANITIC PEGMATITES....12

3. GEOLOGICAL SETTING....15

3.1 THE CORNUBIAN BATHOLITH....15
3.2 THE LAND'S END GRANITE....16
3.3 THE SVECONORWEGIAN OROGEN....18
3.4 PEGMATITES LOCATED AT KLEPPSVATN....20

4. METHODOLOGY....23

4.1 FIELD WORK....23
4.2 SAMPLE PREPARATION....25
4.2.1 Thin sections....25
4.2.2 Fluid Inclusion sections....26
4.3 MICROTHERMOMETRY....26
4.3.1 Salinity, pressure, and temperature estimations....27
4.4 SCANNING ELECTRON MINCROSCOPE (SEM)....28
4.5 CATHODOLUMINESCENCE (CL)....28
4.6 ELECTRON MICROPROBE ANALYSIS (EMPA)....29
4.6.1 Titanium in quartz (TitaniQ) thermobarometer....29

5. RESULTS....31

5.1 FIELD DESCRIPTIONS....31
5.2 PETROGRAPHIC DESCRIPTIONS....32
5.2.1 Quartz vein....32
5.2.2. Aplite....33
5.3 SEM....35
5.4 CL....36
5.5 EPMA....40
5.5.1 Feldspar analysis....40
5.5.2 Quartz analysis....41
5.5.3 Rare earth elements....45
5.6 MICROTHERMOMETRY....47
5.7 PRESSURE AND TEMPERATURE ESTIMATES....52
5.7.1 Fluid inclusions....52
5.7.2 EPMA....54

6. DISCUSSION 55

6.1 THE MINERAL ASSEMBLAGE 55
6.2 PRESSURE AND TEMPERATURE ESTIMATE 57
6.3 THE MAGMATIC HYDROTHERMAL TRANSITION IN TØRDAL 58
6.2.1 Igneous differentiation 58
6.4 ORIGIN OF THE TØRDAL PEGMATITE FIELD 61
6.5 COMPARISON TO PEGMATITES OF LAND'S END 63
6.5.1 Petrogenesis 63
6.5.2 Magmatic hydrothermal transition 64

7. CONCLUSION 70

8. REFERENCES 71

List Of Figures

Figure 1: *A section through a granodioritic intrusion, showing hydrofracturing and the formation of breccia pipe. From (Burnham, 1979).* _____ *4*

Figure 2: *Illustrating how the salinity decrease as proportions of H_2O are separated from the melt. The concentration of cations in the melt is a function of the cation acceptor Chlorine (i.e. salinity). Cl has strong affinity to H_2O so the concentration of Cl is dependent on the amount of exsolved H_2O from the melt.* _____ *6*

Figure 3: *Distribution of K/Rb vs Rb in K-feldspar from South Norway compared with other localities from around the world. From(Larsen, 2004).* _____ *7*

Figure 4: *Phase diagram of pure H2O (solid, liquid, vapor). At 0,008 ºC and 0,06 bar is the coexisting triple point. The critical point is at 374 ºC and 221 bars, where liquid and vapour no longer can be physical distinctive (Robb, 2005).*_____ *10*

Figure 5: *Illustration of how primary, secondary and pseudo-secondary inclusions acts in a crystal (modified from gems-inclusions).* _____ *11*

Figure 6: *Petrogenetic classification of granitic pegmatites by the family system after Černý & Ercit (2005).* _ *13*

Figure 7: *Overview over the Land's End plution, the granite types with textural variations. The location of the pluton within the Batholith is showed in the inset, after (Müller et al., 2006).*_____ *17*

Figure 8*: A simplified map covering Southern Norway illustrating The Sweconorwegian pegmatite provinces (Solid blue lines encircling the areas). 1) Mandal, 2) Setesdal, 3) Bamle, 4) Nissedal, 5) Hardanger, 6) Buskerud, 7) Østfold-Halland. Our interest lies with the letter T for the Tørdal-granite. From (Müller, Romer, & Pedersen, 2017; Rosing-Schow, 2020).* _____ *19*

Figure 9: *Map of pegmatites and quartz veins around Siljestølen at Kleppsvatn. The green color is amphibolite, blue is pegmatite, purple aplite, red is quartz veins. Mo, Sn and B and the generations are also marked. The samples collected from field work was in the final quartz generation quartz vein, highlighted with a red circle. Modified from (Wilberg, 1983)*_____ *24*

Figure 10: *Hand sections sampled in field that the thin sections are made of.*_____ *25*

Figure 11: *Example of well-preserved fluid inclusions from section TG20-001A (left) and TG20-003 (right).* __ *26*

Figure 12: *Field observations. A) Example of a sonation pattern in a pegmatite. B) Amazonitepegmatite cutting the pale quartz-feldspar gneiss. Black lines are amphibolite bonding. C) Close up photo of the amazonitepegmatite. Coarse grained amazonite and smoky quartz.*_____ *31*

Figure 13: *Example of variations in grain boundaries in hydrothermal quartz from thin section TG20-003 and TG20-004. See appendix A for whole scan of the thin section.* _____ *32*

Figure 14: *Quartz and feldspar from thin section TG20-001A. Chessboard texture in the quartz. See appendix A for whole scan of the thin section.* _____ *33*

Figure 15: *Example from thin section TG20-004 in cross polarized light. Neighboring quartz veins of a feldspar with both saussuritization and sericitization. See appendix A for whole scan of the thin section.*_____ *34*

Figure 16: *SEM photo with spectrum and normalized weight percent from spectrum 55. Cassiterite has the brightest signatures due to higher densities. See appendix B for several examples.* _____ *35*

Figure 17: *SEM photo of spectrum 64 (rutile), 65 (magnetite) and 66 (cassiterite) with normalized weight percent. Taken from the borderline between cross cutting hydrothermal vein and magmatic aplite. See appendix B for several examples.* _____ *36*

Figure 18: *CL photo of the quartz vein cutting through the aplite in section TG20-004. The chessboard formation is caused by the stitching program and scans. Main result is the small contrasts in grey-color, also found in Appendix C.* _____ *37*

Figure 19: *CL image from thin section TG20-004. A sonation pattern with a lighter contrast close to the rim and darker inwards to the core. See appendix C for whole section.* _____ *38*

Figure 20: *Photos of thin section TG20-004 from both CL (A), CPL (B) and PPL(C).* _____ *39*

Figure 21: *Composition from felspar in thin section TG20-04. Measurements was sampled from both plagioclase and K-feldspar.* _____ *40*

Figure 22: *K/Rb plot against Rb/Sr from K-feldspar from sample TG20-004.* _____ *41*

Figure 23: *Plot of Ti against Al. Hydrothermal quartz with orange and magmatic with blue.* _____ *42*

Figure 24: *Plot of Al/Ti relationship. The upper panels show correlation coefficients, and the lower panels draw line between the datasets. A flat line indicates a typical non-related.* _____ *43*

Figure 25: *Overview of the points sampled from EPMA and CL photo. A plot of TG20-005, analyze point 21-3044*

Figure 26: *The grain of interest, a Nb-Rutile with a characteristic texture.* _____ *45*

Figure 27: *High concetrations of Nb and Y in Nb-Rutile mapped from EPMA.* _____ *46*

Figure 28: *EPMA photo showing correlation between U and Th.* _____ *46*

Figure 29: *Fluid inclusions in thin section TG20-002 (38850) a) At -15℃ after sufficient undercooling at -197℃ and gradually heating. Three phases are observed, solid ice crystal, gas and a liquid. During the observations, final melting temperature (T_{mf}) noted. b) Inclusions at room temperature, vapor, and liquid phase. c) Heated to 200℃, the gas bubble sublimates in the liquid. d) Only liquid phase remains, and the temperature of homogenization (Th) is noted.* _____ *47*

Figure 30: *Histogram of homogenization temperature and melting temperature for alle measurements performed on thin section TG20-001 to TG20-005.* _____ *48*

Figure 31: *Histogram of first melting temperature and wt% Nacl from thin section TG20-001 to TG20-005.* __ *49*

Figure 32: *Plot diagram of hydrothermal and magmatic quartz regarding to melting temperature and homogenization temperature of the fluid inclusions.* _____ *49*

Figure 33: *Plot of T_h against wt% NaCl. Hydrothermal quartz and magmatic quartz show opposite trendlines.* *50*

Figure 34: *Plot of all thin sections in a wt% NaC and density diagram illustrating small degree of variation.* _ *51*

Figure 35: *Pressure and salinity plotted against each other. The blue dots are hydrothermal Quartz analyzed from section TG20-001 to TG20-004. FI measurements from the pegmatite were difficult to collect, and only eight samples were politely and included.* _____ *53*

Figure 36: *Isochores from fluid inclusion plotted with average composition ± standard deviation, against TitaniQ isochore from Wark and Watson, 2010.* _____ *54*

Figure 37: *A) From The Land's End granite, light core with decreasing intensities towards the rim. B) Opposite trends from Tørdal, with a dark core and light randzone.* _____ *65*

1. Introduction

For several years has researchers worked to gain information regarding the petrogenesis of the coarse-grained pegmatites. No models are universally accepted and a satisfactorily way to describe all the diverse features is still missing. Researchers favourite the model of residual melts being derived from a crystallizing granitic pluton. But it is ubiquitous that almost all ore deposits around the world has a direct connection to hydrothermal ore-forming processes (Robb, 2005). Comprehensive amounts of research have especially been located around The Central Cornwall district in SW-UK. It has for centuries supplied the world with imperative metals for the industrial revolution, and due to its famous occurrences of Sn-W-Cu deposit is it remaining to be so.

Investigations on the meta-cystic, coarse-grained granites of the Land's End was recently studied by Müller et al., (2006) and Drivenes et al., (2016) with the aim of deciphering the magmatic evolution of the granite and to understanding the timing of the magmatic hydrothermal transition that is so important for the formation of ore-deposits. A two-stage emplacement process is proposed by analyzing fluid inclusions, cathodoluminescence textures of quarts and trace elements (Drivenes et al., 2016).

The Cornwall Sn-Cu-W deposits are in this study compared to the less known Sn-Mo occurrences in pegmatites in Telemark, Norway where Rune Wilberg did a detailed study in 1983, and recent studies of the Scandium enrichment performed by Steffensen et al. (2020) and Rossing-Schow (2020) has greatly improved our knowledge about this area (Steffenssen et al., 2020; Wilberg, 1983). Occurrences of cassiterite, molybdenum and beryl in quartz veins are of great interest. The aim of this study is to contribute to a better understanding of the petrogenesis of the Tørdal pegmatites and compare it to the genesis of Cornwall; particularly with respect to pressure, temperature, and the composition of the magma-derived ore-forming hydrothermal fluids. To obtain these goals we conducted microthermometry on fluid inclusions, we studied the trace elements in quartz and feldspar and added SEM-CL to obtain a detailed structural control.

2. Theory

This chapter begins with the origin exsolution of magmatic hydrothermal fluids, solubility and transportation of metals, vein formation in the cupola allowing the fluids to escape, and the formation of the hydrothermal veins, together termed the magmatic hydrothermal continuum. A chapter will address fluid inclusions since this is the thesis's primary method and the key evidence substantiating mineral deposits formed from hydrothermal solutions.

2.1 Magmatic hydrothermal continuum

2.1.1 Formation of water

The water incorporating magma is derived from several sources and is one of the main components regarding the transportation of elements and deposition. The earth processes are progressively dominated by plate tectonics, and considerable amounts of the water are extensively recycled, known as metamorphic water. Water that has not taken part in this recycling loop is known as juvenile water and is derived directly from the mantle. Hydrated subduction zones contribute to mixing of seawater with mantle-derived, more primitive fluids. However, most of the water content in granitic magmas originate from dehydration of minerals, giving volatiles of different character (Robb, 2005).

The proportions of water dissolved in a melt are predominantly controlled by P, T and the composition of the silicate melt. For calc-alkaline silicate melts, the amount on the hydrous mineralogy of the protolith that is partially melted. For example, amphiboles ($NaCa_2(Mg, Fe, Al)_5(Al, Si)_8O_{22}(OH)_2$) contains three times less water than muscovite - $Al_2K_2O_6Si$. Accordingly, the amount of H_20 in muscovite is 8-10%, compared to 3-5% in biotite and 2-3% in hornblende (Robb, 2005). A sedimentary, muscovite rich protoliths producing S-type melt will contain more water than I-type magma derived from an amphibolite rich igneous rock.

The total solubility of water in a silicate melt is proportional to the concentration of SiO_2 and pressure. Water is dissolved as OH- in Si-O-Si-O- polymers where hydrogen bonds at bridging oxygen sites. Meaning that dissolved silica in water exists at the form of H_4SiO_4 who explains the common occurrence of quartz in veins (Robb, 2005). This dissolved silica is percolating through fractures by hot aqueous solutions before they precipitate and form quartz veins.

Water result as a powerful solvent and significant quantities of rock-forming minerals are dissolved. An important actuality is that the water concentration in the melt is doubled from 1 to 3 kBar. When an undersaturated melt is exposed for a pressure decrease is the volatiles released and separates into a fluid phase. As the magma rises towards shallower depths, P and T decreases, and volatile fluids become saturated in the melt with two different approaches. The fist approach is undersaturated melt exposed to decreasing pressure and volatiles released from the melt and separated into a fluid phase. This process is termed "first boiling" and usually occur in the upper crustal or volcanic environments. "Second boiling" is a process driven by cooling isobaric magma, i.e. heat is lost to the host rock, and water concentration in the residual melt is increased due to crystallization of anhydrous minerals. Second boiling generally occurs in a more deep-seated magmatic environment when more immense proportions of the magma are solidified.

Boiling imposes some mechanical effects upon the magma chamber. Exsolved H_2O appearing in the magma chamber is accompanied by the release of mechanical energy, which may results in an overpressure of the chamber interior (Burnham, 1979). The volatile fluids have a lower density than the magma and will migrate towards the roof of the magma chamber. This generates an overpressure in the roof of the magma chamber and cause hydro brecciation, a path for the fluids to migrate towards shallower depths along fractures trough the lithologies (**Figure 1**). The hot aqueous solutions percolating through fractures in the Earth's crust is an important transportation of economic metals and leave us with veins of different character.

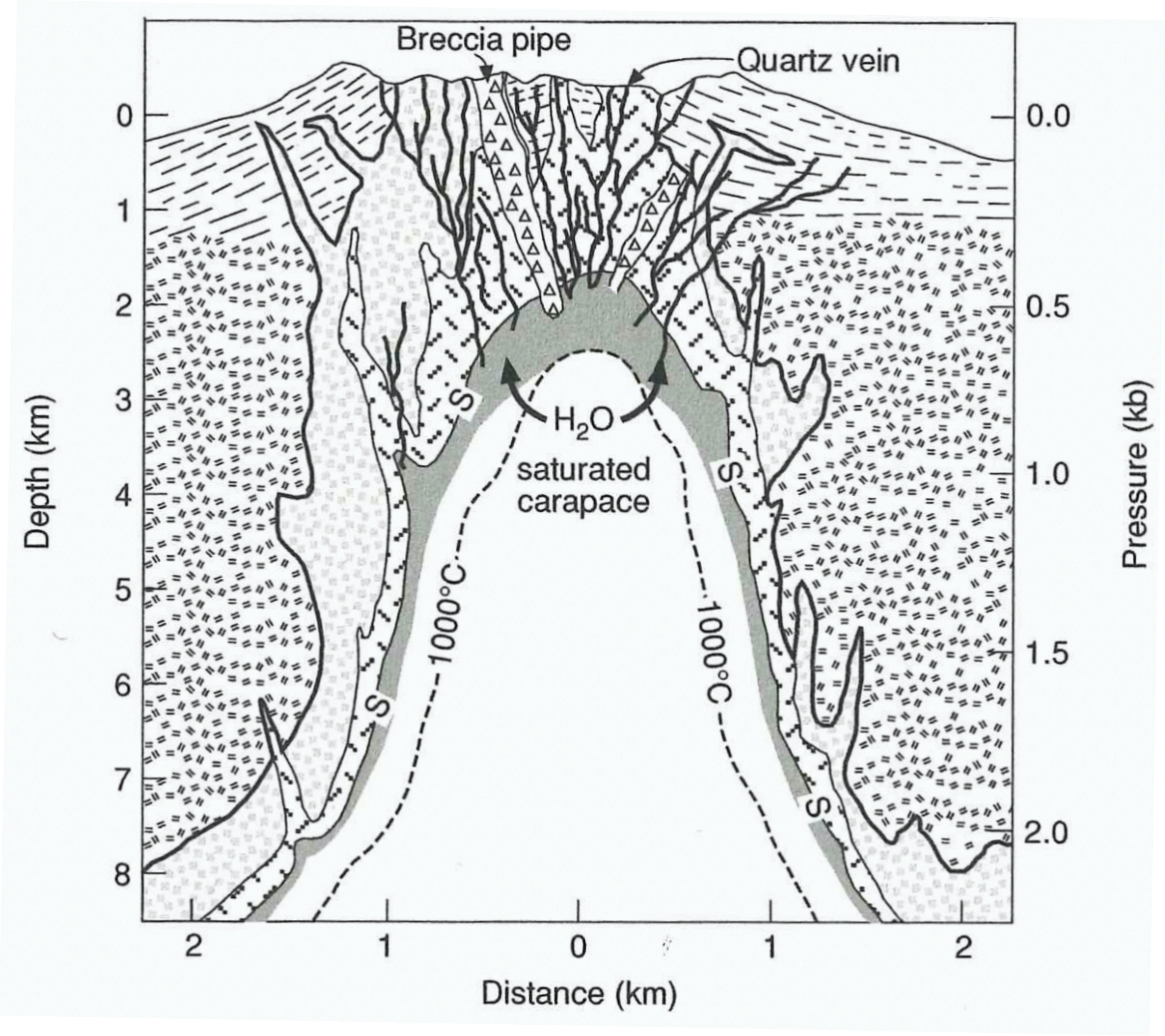

Figure 1: *A section through a granodioritic intrusion, showing hydrofracturing and the formation of breccia pipe. From (Burnham, 1979).*

Development of mineral assemblages that differ from the original composition occurs as the solutions passage through the crust. These mineral assemblages typically reveal information regarding the original rock composition and properties of the fluids. The hydrothermal pathway is therefore represented as zones of alteration being a great guideline when exploring ore-deposits. A description of the most normal alteration types will follow.

The highest temperature condition is found in potassic alteration. It is defined by the formation of K-feldspar and/or biotite, connected with chlorite, sericite, and quartz. Magnetite, hematite, and anhydrite can be companied as accessory minerals. The next alteration type is most common in hydrothermal ore deposits and forms over a wide range of temperatures, known as phyllic alteration.

The process is dominated by feldspar hydrolysis forming sericite, possibly accompanied by quartz, chlorite, and pyrite. The probably most widespread alteration type is propylitic alteration, with assemblages alike those forming of the metamorphism of greenschist. The composition is mainly epidote and chlorite with occurrences of albite, calcite and zoisite. Both the fluid/rock ratios and temperatures are low to intermediate, typically between 200-350 °C. The final type included is argillic alteration, where the magnitude of the breakdown of host mineral is causing subdivisions; intermediate or advanced. The formation of clay minerals, such as smectite and kaolinite is the characterizing factors and the dominating mechanism are H^+ metasomatism with temperatures below 250 °C.

2.1.2 Solubility of economic metals and other species

A silicate magma may dissolve and transport metals that are needed to form a hydrothermal ore deposit. Hydrothermal fluids can transport metals, mainly as a complex ion with negative ions/ionic complexes and/or neutral molecules. The metals and ligand are classified as soft or hard, and Pearson's principle defines that hard metals predominantly are attracted to hard ligands and soft metals to soft ligands (Pearson, 1963). Hard ions have a small atomic radius, are highly charged and slightly polarizable. Soft ions have a larger atomic radius, lower charge and are polarizable. Metals situated in the transition may complex with both soft and hard, for example, Cu, Pb and Zn. They tend to complex with the intermediate anion Cl-, which makes Cl- the most essential complexing ligand in hydrothermal solutions (**Figure 2**). After the aqueous volatiles has exsolved from the silicate melts, they migrate upwards in the magma chamber and scavenge the melt for incompatible elements, including many economic elements (Robb, 2005).

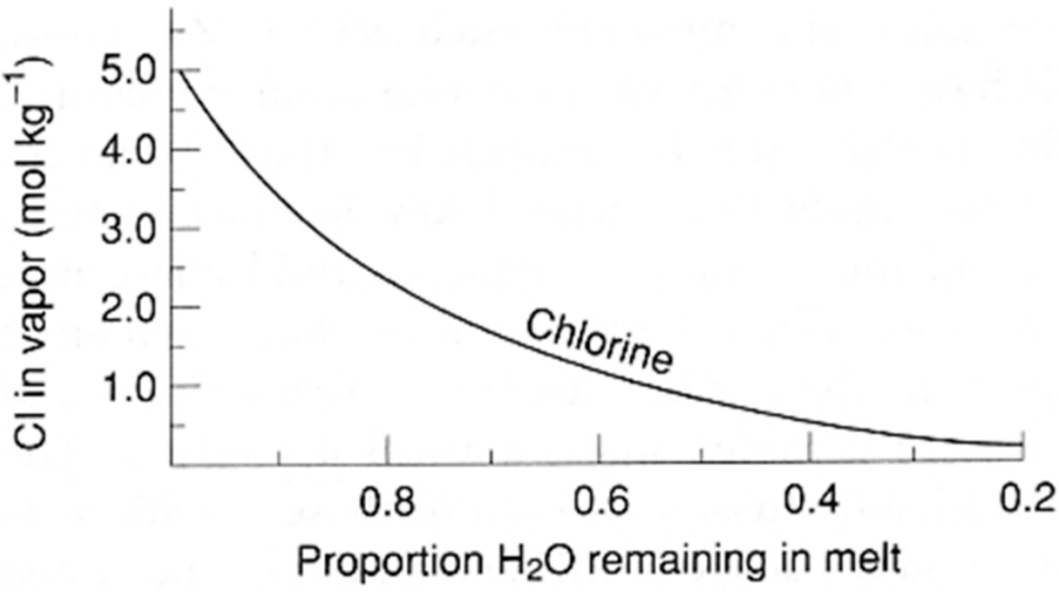

Figure 2: *Illustrating how the salinity decrease as proportions of H_2O are separated from the melt. The concentration of cations in the melt is a function of the cation acceptor Chlorine (i.e. salinity). Cl has strong affinity to H_2O so the concentration of Cl is dependent on the amount of exsolved H_2O from the melt.*

Other factors playing an essential role for metals entering the aqueous solutions are oxidation stage, Ph, temperature, and fluid composition. The oxidation state of an ion is determining its properties. For example, Sn2+ is soft while Sn4+ is hard. Precipitation of metals from hydrothermal fluids, therefore, requires the stability of a host mineral. It can result from boiling, host-rock properties, chemical changes due to fluid mixing (pH, Eh), temperature or pressure variations (Pirajno, 2008). Information of these factors are used as indications of how evolved the system is. A typical methodology is the K/Rb and Rb/Sr distribution in K-feldspar as Sr is compatible and Rb is the least compatible elements, making them sensitive to igneous differentiation. They give an initial ratio because ^{87}Rb will decay to ^{87}Sr in all rocks. By these methods are some of the pegmatites of Southern Norway relatively primitive compared to other localities around the world, even though great variations within the field is observed (**Figure 3**)(Larsen, 2004).

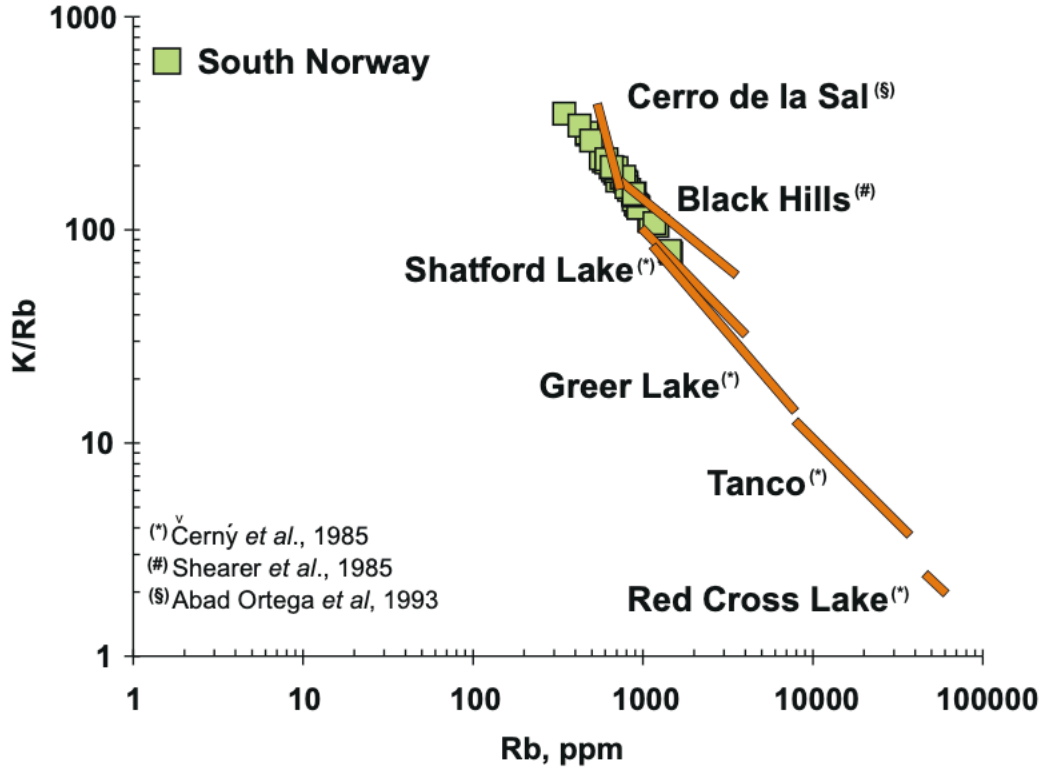

Figure 3: *Distribution of K/Rb vs Rb in K-feldspar from South Norway compared with other localities from around the world. From(Larsen, 2004).*

2.1.3 Deposition of Sn

To make an economically viable ore body must a metal in solution be extracted from that fluid and precipitated as a mineral in an accessible and sufficiently restricted part of the crust (Robb, 2005). Dramatic modifications in the fluid properties are an important mechanism associated with precipitating metals from the ore-forming solutions that transported them. In the upper levels of the crust is fluid pressure drop an essential factor causing phase separation from one to two or more fluids (Robb, 2005). The transition from a one-phase supercritical fluid to two fluids may dramatically destabilize the metal complexes, e.g. by separating CO_2 from solution and changing pH as well as the Eh (Drummond & Ohmoto, 1985).

Overall, the system's oxidation-reduction equilibria should be considered to determine the stability of ore-minerals. In a silicate magma is the solubility of water governed the equilibria:

$$2H_2 + O_2 \rightleftarrows 2H_2O \quad (1)$$

That would be a strong pH-Eh buffer at high temperatures (Drummond & Ohmoto, 1985). The bridging O_2 polymerizes the silicate structure, and a low viscous basaltic magma has fewer portions than a granitic magma. The lower content of bridging O_2 and OH groups make basaltic melts unable to dissolve the same amount of water as a granitic melt. However, at high enough pressure is the water solubility totally reliant on pressure and to a smaller degree affected by magma composition (Robb, 2005).

Tin (Sn) is a metal that theoretically can be dissolved by complexing with several different ligands since it exhibits both hard acid quadrivalent (as Sn4+) and borderline divalent (as Sn2+). At oxidizing conditions is the dominant complex Sn4+ hydroxychloride complex $Sn(OH)_2Cl_2$, but the solubility is low. At more reducing conditions, both Sn4+ and Sn2+ may complex with Cl, forming very soluble complexes. At alkaline, low temperature conditions are the Sn-hydroxide complexes ($Sn(OH)_4$ and $Sn(OH)_2$) stable. However, their solubilities are low compared to those exhibited by the dominant Sn-Cl complex, formed at lower pH and higher temperatures (Robb, 2005). The dominant tin solubility is probably of the equilibria type deriving from aqueous solution to Cassiterite:

$$SnCl_x^{2-x} + 2H_2O = SnO_2 \quad (2)$$

Again, the amount of solubility is connected to system and temperature. Temperatures of 400 °C are required to achieve solubilities of 10 ppm or more in acid conditions, so the normal precipitation temperatures lie between 350-500 °C, while solubilities of 100-1000 times higher are supported in feldspar-absent at redox conditions with a given T. A feldspathic host rock may work as an incomplete chemical buffer for the fluids in an ore depositional environment with temperatures less than 400 °C degrees.

The buffer causes transportation of economic amounts of tin over far distances and it occurs when hydrothermal fluids flow through a confined channel relatively more rapid than the controlling kinetics of the interaction with fresh wall rock.

According to Patterson et al. (1981) does Sn^{+2} readily complex with F^-, OH^- and Cl^- particularly in high temperature, alkaline fluids (Patterson, Ohmoto, & Solomon, 1981). Precipitation of cassiterite (SnO_2) occur when the transporting complexes destabilize, either by Eh or pH increase, decrease in temperature or a combination of these physio-chemical factors (Pirajno, 2008).

2.4.5 Atomic lattice of quartz as indicator of magmatic events

The reliability of genetic information from quartz has been low hence the difficulty to constrain conventional analytical methods. Studies of whole-rock samples concerning minor and major element chemistries are the standard approach. The strong bond configuration of Si-O causes a minimum of elements allowed into the atomic lattice structure. Larsen (2004) concerned a study with Al, B, Be, Fe, Ge, K, Li, Na, P and Ti that comprised >99% of the trace elements, and three situations were presented. 1.) With atomic lattice in the “low quartz”, were trace elements configurated of tetravalent ions (Ge and Ti) that single substituted for Si. 2.) To facilitate charge equilibrium is two Si-ions substituted in neighbouring Si-O tetrahedrons by a trivalent (Al) ion and a pentavalent ion (P) 3.) Trivalent ions (Al, Fe, B) substitutes for Si, but the charge results in inequality of 1+, so to facilitate charge balance is a monovalent ion (Li, Na, K) accommodated. The TiO_2 content in quartz can be counter to thermobarometry of magmatic rocks. If a TiO_2 rich phase shall survive and crystallize in a silica melt, is TiO solubility and relations of activity-compositions necessary. This causes great variations within quartz, that is already observed in the field. Quartz of undisturbed presence in pegmatite bodies appears sub- to euhedral, glassy clear or smoky. As the distance to K-feldspar crystal increase will smoky quartz gradually abate into clear quartz.

2.2 Fluid inclusion

Fluid inclusions comprise microscopic cavities mostly <20 µm in diameter and composed of various volatiles, dissolved species and mineral (Roedder, 2005). The inclusions may be trapped as imperfections when crystal growth occurred in the presence of a fluid phase. During cooling and pressure decrease, differentiate the homogeneous fluids to a multi-phase system due to re-equilibration to new existing pressure and temperature. This process can be reversed by heating the inclusion and record the T when only one phase is forming hence the minimum T at which the inclusion initially was trapped (Sorby, 1858). They form especially in quartz but also in other rock- and ore-forming minerals. FI are the only evidence that document if a mineral deposit formed from a hydrothermal solution (Robb, 2005).

As the fluid is trapped, it may contain both liquid and vapour at the supercritical stage. This supercritical stage is an exceptional condition where water cannot be accurately described as gas or liquid (**Figure 4**). Both the chemical and physical properties are not distinguishable and act as a single homogenous phase. Brines of various salinity, pure water, gas or gas-bearing liquids, silicate, carbonate or sulphide also may be observed (Robb, 2005).

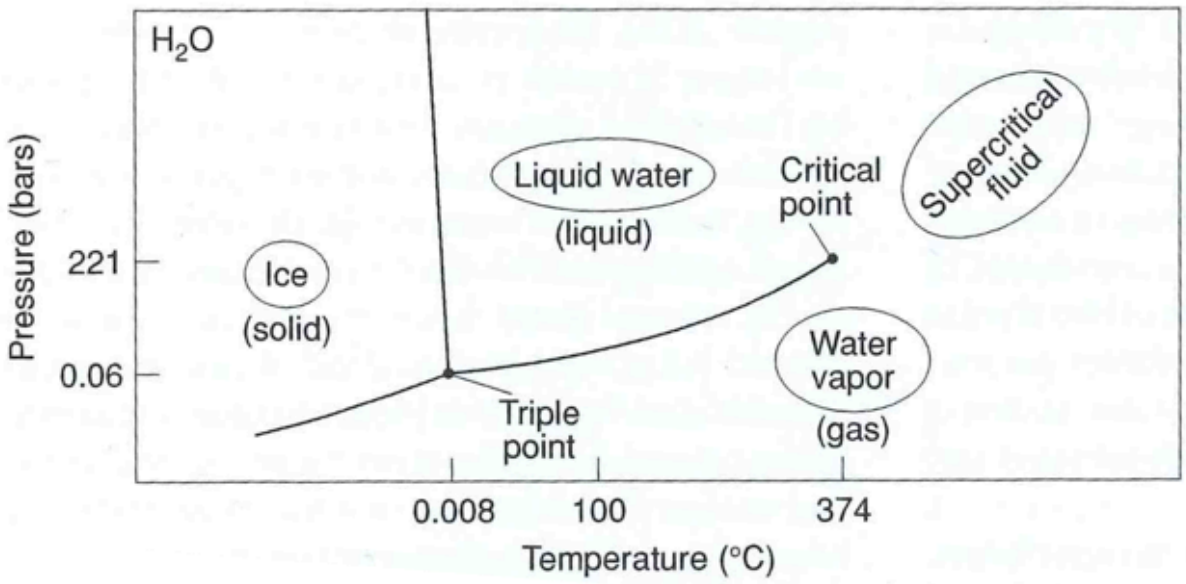

Figure 4: *Phase diagram of pure H2O (solid, liquid, vapor). At 0,008 ºC and 0,06 bar is the coexisting triple point. The critical point is at 374 ºC and 221 bars, where liquid and vapour no longer can be physical distinctive (Robb, 2005).*

Fluid inclusions may be defined into three principal types: (1) Primary fluid inclusions: as the surrounding host crystal grew, the inclusion was trapped by the crystal. (2) Secondary fluid inclusions: may have entered the system after the crystal growth is finished during fracture formation and subsequent healing. (3) Pseudosecondary fluid inclusions: could be trapped when fracturing occurred during the crystal's growth (**Figure 5**)(Roedder, 2005). In some cases, it may be challenging to correctly classify the FI (J. Goldstein et al., 2003).

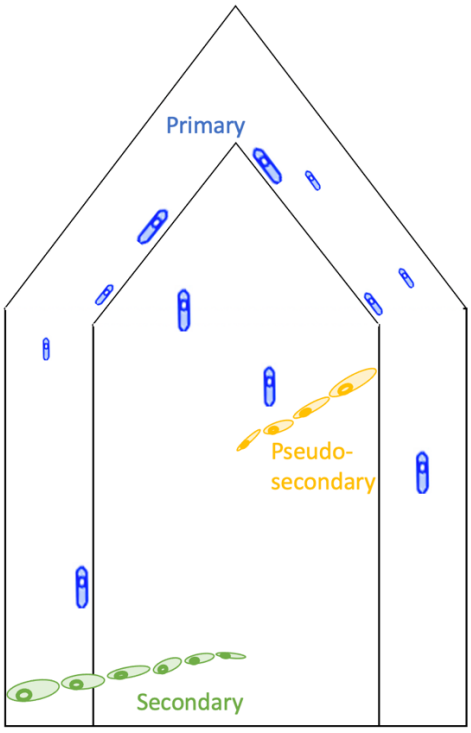

Figure 5: *Illustration of how primary, secondary and pseudo-secondary inclusions acts in a crystal (modified from gems-inclusions).*

Inclusions that are clustered together might represent the same pressure and temperature conditions during entrapment and represent equal compositions. Fluid inclusion assemblage (FIA) were therefore introduced in 1994 with the purpose is to describes a group of inclusions that were trapped at the same time, rather than inclusion for inclusion (R. H. Goldstein & Reynolds, 1994). A FIA represent the history of those inclusions, and different FIA's may represent other fluid events.

The phase relationship between inclusions may vary and the understanding of the entrapment history is therefore required. It is separated between homogeneous and heterogeneous entrapment. Homogeneous entrapment implies inclusions from a one-phase fluid with identical physiochemical properties. During heterogeneous entrapment is the temperature equal, but the chemical composition varies, and the phase relationship implies that more than one phase is trapped that during inclusion formation (Samson, Anderson, & Marshall, 2003).

2.3 Granitic pegmatites

Granitic pegmatites are often derived from granitic melts, but the characteristic coarse-grained rocks separate them from each other. The silicate melts that facilitate the growth of pegmatites dissolve large quantities of volatile constituents (H_2O, CO_2, Li, F, Cl, B etc.). Dominating minerals are quartz, feldspar, and micas. However, pegmatites can also contain a certain number of high field strength and large ion lithophile elements, e.g., Sn, W, Th, Li, Be, B, Ta, Nb, Sc and Cs.

The classification of pegmatites is predominantly based on the Cerny's (1991) model (Černý, 1991). The first mineral assemblage is the NYF suite (Nb-Y-Fe), affiliated with sub-alkaline to metaluminous granites derived from I- or A-type granite (**Figure 6**). The preponderance is Nb-dominant oxides and enrichment in REE, and the accessory minerals zircon and Ti-oxides and silicates. LCT suite (Li-Cs-Ta) is the second mineral assemblage. Generally, often peraluminous and dominantly originated from S-type granites. Associated enrichments next to the three signature elements is Sn, Ta, Ga, Nb, Sn, B, Br, Rb, P and F often present (**Figure 6**). The high silica content contributes to makes REE insoluble in LCT pegmatites (London, 2018).

Family	Dominant subclass of pegmatites[§]	Geochemical signature	Bulk composition of pegmatites *	Associated granites	Bulk composition of granites *	Source lithologies **
LCT	REL-Li MI-Li	Li, Rb, Cs, Be, Sn, Ga, Ta>Nb, (B, P, F)	peraluminous to subaluminous	(synorogenic to) late-orogenic (to anorogenic); largely heterogeneous	peraluminous, S, I or mixed S + I types	undepleted upper- to middle-crust supracrustal rocks and basement gneisses
NYF	REL-REE MI-REE	Nb>Ta, Ti, Y, Sc, REE, Zr, U, Th, F	subaluminous to metaluminous (to subalkaline)	(syn-, late, post-) to mainly anorogenic; quasi-homogeneous	(peraluminous to) subalum-inous and metaluminous; A and I types	depleted middle- to lower-crust granulites, juvenile granites, mantle-metasomatized crust
Mixed	Cross-bred LCT and NYF	mixed	(metaluminous to) moderately peraluminous	(postorogenic to) anorogenic; heterogeneous	subaluminous to slightly peraluminous	mixed protoliths or assimilation of supracrustal rocks by NYF granites

Figure 6: *Petrogenetic classification of granitic pegmatites by the family system after Černý & Ercit (2005).*

The petrogenesis and origin of pegmatites are complex and currently much debated. They may result from partial melting and the formation of minor dykes in high-grade metamorphic terranes. Some cases are also genetically linked to the most highly differentiated, water-saturated portions of cupolas zones of large granitic intrusions. It was suggested that the point of H_2O fluid saturation marks the transition from granite to pegmatite (Jahns & Burnham, 1969). This substantiates increased diffusion rates and lower melting points due to the high H_2O content, allowing high crystallization rates causing extreme grain sizes obtained over a short cooling interval.

The low crystallization temperature could also explain how the melt could travel far in a cold host rock. This model was attractive due to the demonstrations of lab experiments implying that aqueous fluid can dissolve very significant proportions of solute at high pressure and temperatures. Pegmatites are suggested to be generated from an undersaturated granitic melt by several models. The London model (1990, 1992 and 1996) explained the typical mineral zonation observed in many pegmatites. The following zonation pattern may be recognized at several places worldwide, and each zone is formed by fractional crystallization. The contact zone is dominated by quartz, plagioclase, K-feldspar, and mica with average granitic grain size.

A wall zone with plagioclase, K-feldspar, some mica, and quartz are recognized closer to the centre. Several intermediate zones appear within the border zone and are dominated by K-feldspar and quartz before the core assemblage is dominated by quartz. Pegmatites are rarely organized in a concentric pattern, but this general trend is accepted as the general geometry by most researchers.

London agrees that higher H_2O content lowers the crystallization temperature. Nevertheless, he proposed that the melts could be undersaturated with H_2O rather than oversaturated. By undercooling the granitic melt below its average liquidus temperature, the other volatile components such as B, Li, Fe and P facilitate metastable conditions and non-equilibrium crystal growth. These elements individually and collectively lower the granite solidus from 700 to < 500 °C while increasing the range of temperatures the magmatic crystallization may occur. Low crystal seed density and high diffusion rates ensure the formation of coarse crystals. Combined with this is the solubility of H_2O in the melt increased. Pegmatites could conceivably form in these situations, where the H_2O solubility is so high that saturation is not obtained at all. Several models can explain the genesis of a specific pegmatite event, and no "super unified theory" may not even exist. Components from different models may be connected in one case or even specific zones within one setting (Thomas, Davidson, & Beurlen, 2012).

3. Geological setting

This chapter is addressing the geological setting of the investigated field areas. The first area is in Cornwall, located in the south-western part of UK. A short introduction of the origin of the Cornubian batholith, emplaced during the Varascan Orogeny will be discussed. Subsequently the petrography and geochemistry combined with a deeper understanding of the Land´s End granite will be discussed.

The second area is in Telemark, located in South-Norway and formed during the formation and collapse of the Sveconorwegian Orogeny and the Tørdal-pegmatites around Kleppsvatn are defined in this framework.

3.1 The Cornubian batholith

The Cornubian batholith has an NE-SW extent over 200 km and comprises of five major plutonis complexes: Dartmoor, St. Austell, Bodmin, Carnmenellis, Land's End and the Scilly Isles granites (Goode et al., 1988). The plutons were emplaced during the late stages of the Variscan Orogeny, over a period of ca. 20 million years (Chen et al., 1993; Chesley et al., 1993). This was a result of the convergence of Gondwana and Laurassia during closing and deformation of the Rheic ocean. Subsequently rifting and increased volcanism accompanied the collapse of the orogeny, resulting in sedimentary basin formation (LeBoutiller, 2002). The orogeny extends continentally from Poland over Portugal to Cornwall.

The batholith intrudes deformed, low-grade metamorphic sediments and magmatic rocks with Devonian- to Carboniferous ages. The morphology of the batholith is elongated while the exposed granites forms cupolas and extends to depths between 8 and 20 km (Bott, Day, & Masson-Smith, 1958). The batholith is strongly peraluminous with high K/Na ratios, which characterizes an oversaturation in Al compared to the alkalises (Müller et al., 2006). A high content of radioactive elements such as Th, K and U facilitates a steep geothermal gradient and high temperatures.

S-type monzo- and syeno granites with trace-alkali elements, Nb, F, and Sn and high initial $^{87}Sr/^{88}Sr$ composes over 90% of the batholith. In addition, extreme enrichments in elements such as P, Rb, B, Sn, W and Cs are observed (Chappell & Hine, 2006).

The origin of the batholith is somewhat controversial, but partial melting of crustal material with a small degree of mantle contribution are agreed upon to imply the origin of the granites, from a single reservoir. The granites have intruded in multiple events and were emplaced in a laccolitic manner (Pownall, Waters, Searle, Shail, & Robb, 2012).

3.2 The Land's End granite

The Land's End pluton is normally not associated with significant ore-deposits, but the magmatic-hydrothermal transition and the formation of Sn-Cu mineralization. This granite is the youngest pluton with U/Pb age of ca. 275 Ma (Chen et al., 1993; Chesley et al., 1993) with varying textures and mineralogy (**Figure 7**). Land's End is the second largest plutonic complex in the Batholith, covering an area of 190 km^2 (Chappell & Hine, 2006). The field area presented in this thesis will focus on this area.

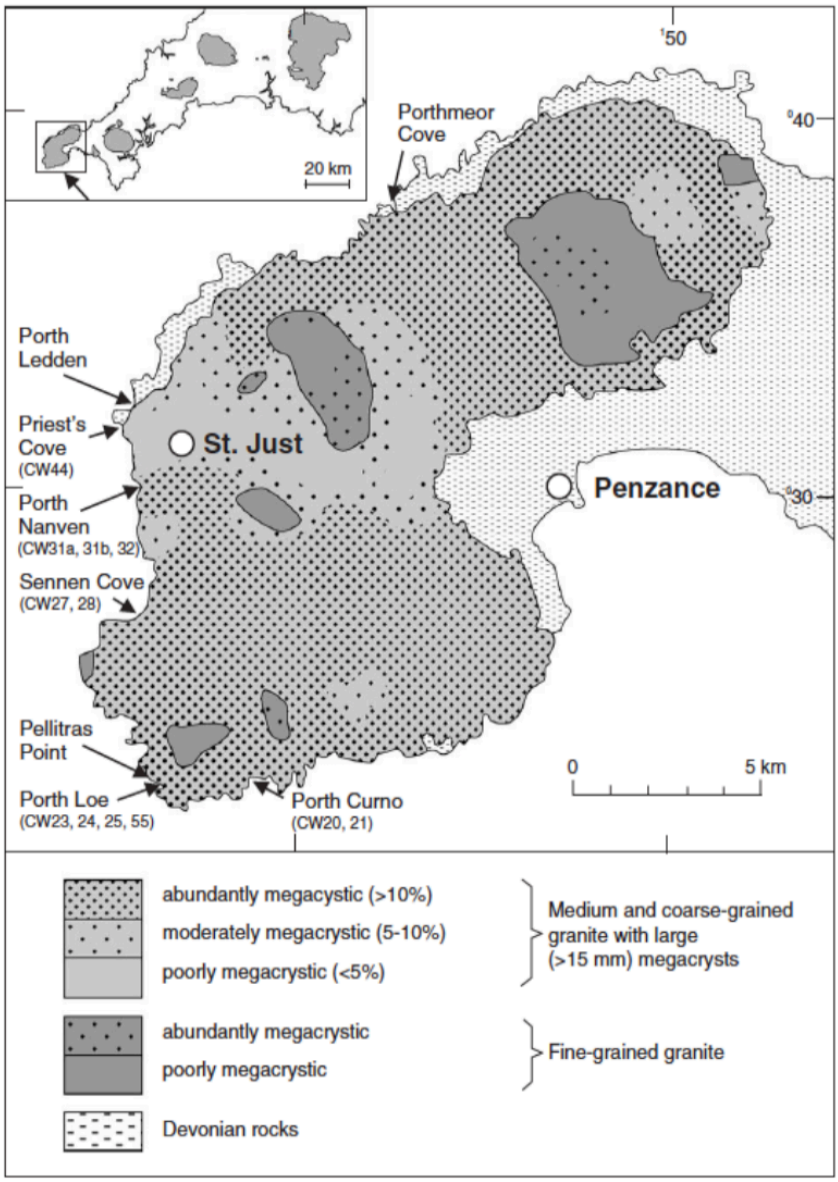

Figure 7: *Overview over the Land's End plution, the granite types with textural variations. The location of the pluton within the Batholith is showed in the inset, after (Müller et al., 2006).*

Until 2012, the origin of the Land´s End batholith was interpreted as a diapiric structure. Pownall et al. (2012) proposed that this theory was unlikely. Their mapping of the aureole implied that the Land's End batholith was a shallow laccolitic body. They suggested the successive emplacement of narrow dyke-fed sills during roof uplift and laccolith inflation. This explains the domed roof with a flat base.

In 2006 Müller et al. suggested four main stages of the intrusion at Land´s End complex. From oldest to youngest: (1) Fine grained porphyritic biotite granite (FGG) which appear as enclaves up to 50 cm in diameter. (2) Medium to coarse-grained porphyritic biotite granite (CGG), formed at the outer crust and the inward's in of the pluton. (3) Equigranular Li-mica-tourmaline granite. (4) Porphyritic Li-siderophyllite granite with K-feldspar phenocrysts. The dominating plagioclase is oligoclase with normal zoning, while siderophyllite is the dominant mica occurring as mm large phenocrysts. Muscovite acts as inclusions in quartz and contain lower Mg compared to the muscovite disseminated in the matrix (Drivenes et al., 2015). A great understanding of the magmatic hydrothermal transition in the Land's End granite were obtained from studying tourmaline signatures in massive quartz tourmaline (MQT). They are interpreted to represent the final magmatic event, before the melt separated into hydrothermal phase (Drivenes et al., 2016).

Overall are the Land's End granites being coarse grained, calc-alkaline rocks. They have high K, Ti and Mg content, compared to the other plutons of the batholith. Additionally, they are strongly peraluminous and has low phosphorus contents (Müller et al., 2006).

3.3 The Sveconorwegian Orogen

The pegmatites involved in this study is geologically located in the Sveconorwegian orogen that covers the southern parts of Norway (**Figure 8**). It is one of the largest provinces in the world with up to 5000 bodies in seven pegmatite fields (Bingen, Nordgulen, & Viola, 2008; Rosing-Schow et al., 2018b; Slagstad, Roberts, & Kulakov, 2017). This orogen was formed by collision between the tectonic shields of Amazonia and Baltica, approximately between 1.1 to 0.9 Ga. The collision, combined with the growth and re-merging of fractured crustal blocks made the supercontinent Rodinia (Bingen et al., 2008; Slagstad et al., 2017). The metamorphic grade varies from amphibolite facies in the east and increasing to granulite facies in the west (Bingen et al., 2008). Tectonic boundaries appear to be ignored during the emplacement throughout the region.

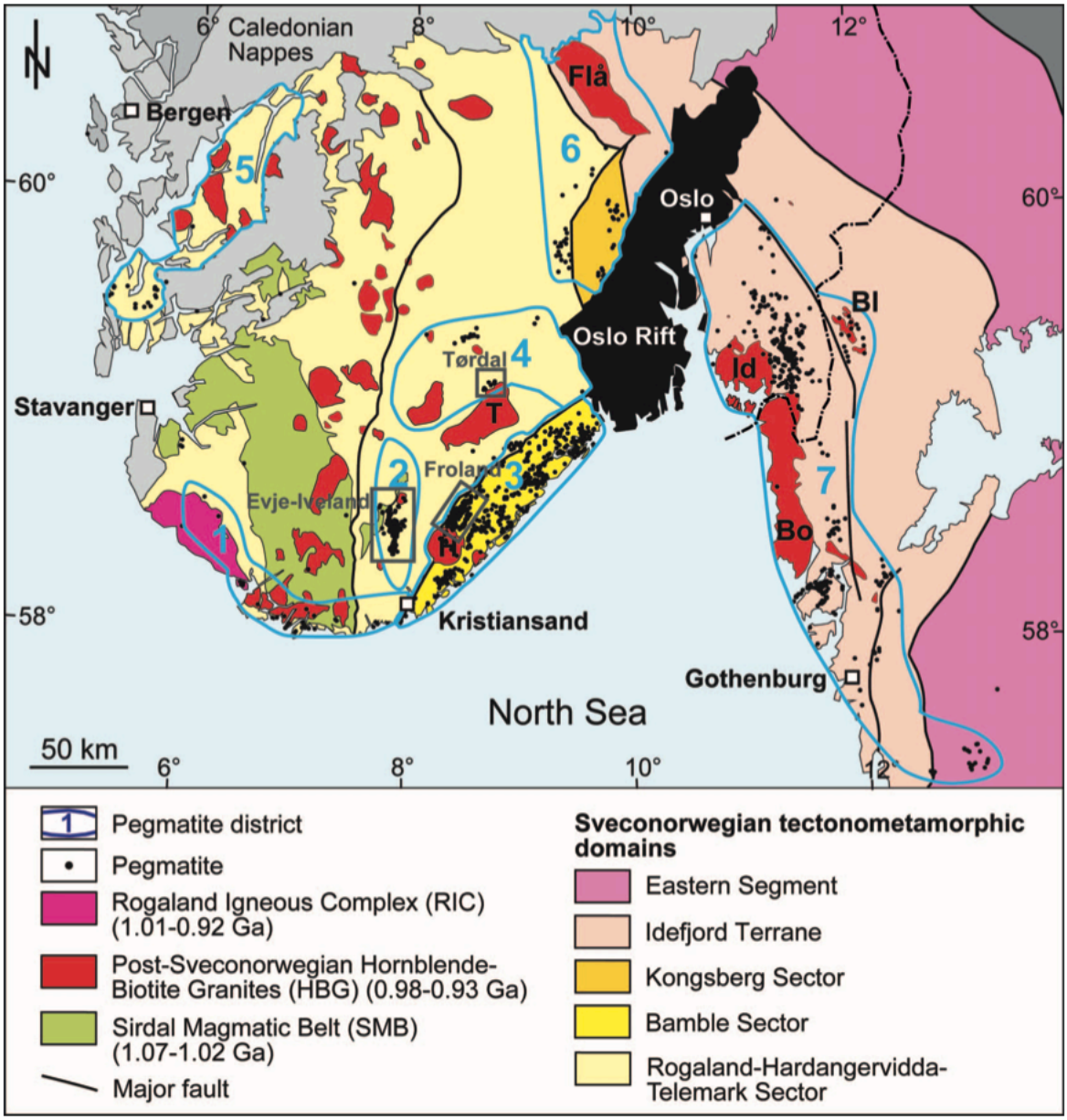

***Figure 8**: A simplified map covering Southern Norway illustrating The Sweconorwegian pegmatite provinces (Solid blue lines encircling the areas). 1) Mandal, 2) Setesdal, 3) Bamle, 4) Nissedal, 5) Hardanger, 6) Buskerud, 7) Østfold-Halland. Our interest lies with the letter T for the Tørdal-granite. From (Müller, Romer, & Pedersen, 2017; Rosing-Schow, 2020).*

3.4 Pegmatites located at Kleppsvatn

The pegmatites around Kleppsvatn are situated in the Nissedal district, located in the Rogaland-Hardangervidda-Telemark sector in a 10 km NE-SW striking area, marked with T (Tørdal) in **Figure 8**. The center of the Telemark-sector underwent extensive metamorphism during the Sveconorwegian orogeny, exactly where the present-day pegmatites are located. The belt is 3 km wide comprising of 300 pegmatite bodies in the Tørdal-Treungen granite (Rosing-Schow et al., 2018b; Steffenssen et al., 2020).

The pegmatites and Tørdal-Treungen granite intruded granitic gneisses and supracrustal rocks (1300-1200 Ma). They mainly comprise of amphibolite's with minor mafic to felsic intrusive and some intercalations of volcanic strata. The biotite granite is medium- to coarse-grained. More recent U-Pb zircon dating imply 957 ± 12 Ma (Slagstad et al., 2018) and 946 ± 4 Ma using Nb-Y oxide (Rosing-Schow 2020). This concludes that the Tørdal-Treungen granite is about 40 Ma older than the pegmatites in Tørdal, hence the pegmatites are not related to the Tørdalen-Treungen granite, as previously thought (Černý, 1991). Combined with the Nb-Y oxide dating were the Pb isotope signatures sampled (Rosing-Schow, 2020). The pegmatites had equal Pb signatures with its adjacent granites, implying alike source rock. This contributes to confirm the assumption that the Tørdal pegmatite field has been formed by anatectic melting of the surrounding host rock. The pegmatites represent a great variety and generally is no mineral zoning is observed, and the dominant texture is granitic with coarse crystals (>20 cm) of quartz and feldspar. Zoning can be found in the moderately evolved pegmatites. The zonation patterns typically exhibit a granitic border zone, the wall zone is coarse-grained followed by an intermediate zone of coarse-grained crystals and finally a quartz core.

The Pegmatites has an affinity to the NYF family, and the most common minerals are quartz, K-feldspar, albite, oligoclase, biotite and muscovite. With some locally occurrences of distributed amazonite and cleavelandite. They are locally rich in minerals as Mo, Y, Sc, Be, Sn and Li (Bergstøl & Juve, 1988). Some of the accessory minerals are cassiterite, fluorine, topaz, allanite, monzanite, beryl and lepidolite (Bergstøl & Juve, 1988; Raade & Kristiansen, 2000). The Tørdal pegmatites were misinterpreted as a mixed class until recently.

The mixed class conclusion was drawn due to the existence of cleavelandite and lepidolite, in addition to the NYF -typical minerals; monzonite (Ce), allanite (Ce) and gadolinite (Y). Combined with the LCT (Li-Cs-Ta) characteristics of Cs, Li, Be and Sn (Bergstøl & Juve, 1988; Rosing-Schow et al., 2018b; Wilberg, 1983).

Rune Wilberg (1983) suggested that the pegmatites were formed by an S-type magma, formed by partial melting of muscovite-bearing meta-sediments, so the felsic-alkaline peraluminous porphyries originated from the Tørdal granitic melt (Wilberg, 1983). The Tørdal granite is situated adjacent to the pegmatites. Hence, increasing distance from the pluton should increase the degree of fractionation. However, this classical pattern is not observed. The degree of fractionation indicates that the pegmatites must have travelled over large distances or fractionated from a voluminous magma source. The recent dating implying that the pegmatites were ca 40 Ma younger than the Tørdal granite, fed the interpretation that pegmatites were of anatectic origin. This interpretation is supported by field observations of partial melting structures including leucocratic veinlets (<1mm) forming networks in the amphibolite's observed at Kleppe, close to Kleppsvann. Pegmatites appear to grow out of the magmatic amphibolite over distances of 10 to 20 m's. This indicates a relatively short melting distance, since the veins forms 2-4 m thick pegmatite sheets (Steffenssen et al., 2020). This theory is supported by a study from Steffensen et. al in 2020 who identified high amounts of Sc in the pegmatites. Typically, would Sc behave as a compatible element in granitic systems, and the melt will not become enriched by fractional crystallization. This substantiates that the Sc-rich pegmatites cannot be derived from the Tørdal-Treungen granitic melt due to their high content of Sc.

Two groups characterize the Seconorwegian orogen based on new dating results. Both are believed to be of anatectic origin rather than from the residual melt of the granites. This helps explaining the large age gap between the pegmatites and granites, and even the chemical similarities and spatial coincidence. The first group (1090-1030 Ma) is synorogenic and suggested to be formed during compression and high-grade metamorphism. The melt is strain-induced with heat from mafic underplating. This is the same mafic underplating causing group two and the granitic melts. During post-orogenic extension were group 2 formed (920-890 Ma), as a continuation of the large-scale magmatism.

Since the heat-induced melting of group two stems from the same mafic underplating, are the chemical differences not related to the mode of melting, but rather to source variations (Rosing-Schow, 2020).

Muller (2015; 2017) suggested that the source rock of the pegmatites could be the amphibolite dominated supracrustal unit, present as host rock in the area. To produce a pegmatitic melt from an amphibolite dominated source rock must fractionation during melt movement or mixing with felsic compositions be present, as a tonalitic melt composition is expected based on melt experiments (Rapp, 1991).

4. Methodology

4.1 Field work

Fieldwork was completed in the area around Kleppsvatn, SE Norway, from 10. – 17. Sept. 2020 and is supplementary to a detailed study performed by Rune Wilberg in 1982. In the whole area did he identify five different generations of pegmatites based on mineralogy, shape, contact relationship, age etc.: 1.) Amazonite pegmatite, the most abundant type. 2.) Pegmatites where K-feldspar is not yet evolved as amazonite. Dominated by red K-feldspar and occur in dark gneisses. 3.) Cleavelandite pegmatite, rare but appear in cavities or along fractures in the amazonite pegmatite. Formed by replacement of primary magmatic minerals of late hydrothermal solutions. 4.) Rare aplite that occurs in small veins and can be found at the contact zone of amazonite pegmatite. 5.) Mineralized veins of quartz (Wilberg, 1983). Despite the numerous amounts of pegmatites did tree locally sections point out of a greater interest, and one of them were selected to a detailed study due to its popularity for previously tin tone washing.

The pegmatites are dominated by coarse-grained quartz, microcline, and plagioclase, with minor amounts of biotite, muscovite, sericite, garnet, and beryl. The grain size varies but is generally two to tens of cm's. The detailed study was performed over a 300 x 100m's area at the east side of Kleppsvatn, given previous observations of cassiterite during mineral washing at this site (Figure 9). The dominating rock is a bright quartz-feldspar gneiss with bands of amphibolite. Wilberg (1983) separated the pegmatites in this area into three different generations, and two different quartz zone generations. Geochronological are the following history represented 1.) Quartz veins with and without sulphide. 2.) Flat lying pegmatites with partially diffuse boundaries and anastomosing paths. 3.) Parallel, steep, narrow, and discordant pegmatites where dilatation is often observed. 4.) The last generation of pegmatites cutting older pegmatites and quartz vein, with beryl, cassiterite and molybdenite. 5.) The second generation of quartz and final generation of veins cutting all previous phases and carrying molybdenite, cassiterite and beryl (Wilberg, 1983). All these pegmatites belong to the 1.) Amazonite pegmatite in the first classification. Generation 4 and 5 was chosen for detailed studies because of the mineralization's and for comparison with the Land's End mineralizing system.

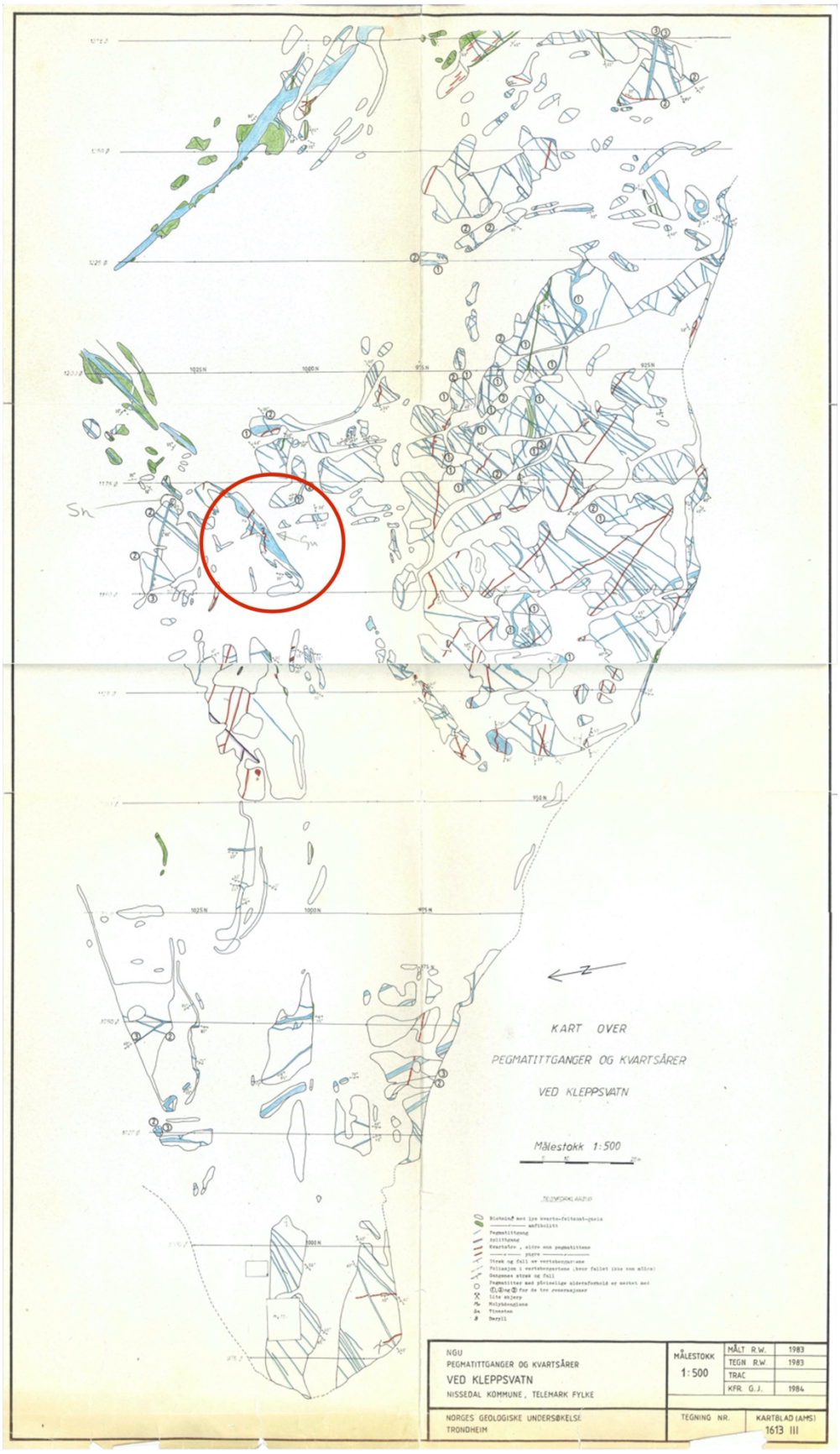

Figure 9: *Map of pegmatites and quartz veins around Siljestølen at Kleppsvatn. The green color is amphibolite, blue is pegmatite, purple aplite, red is quartz veins. Mo, Sn and B and the generations are also marked. The samples collected from field work was in the final quartz generation quartz vein, highlighted with a red circle. Modified from (Wilberg, 1983)*

4.2 Sample preparation

4.2.1 Thin sections

Six thin sections with dimensions 28x48mm and a standard thickness of 30μm were prepared by the laboratory technicians Kjetil Eriksen and Håkon Fjærli at the thin section laboratory at NTNU.

Two thin sections (TG20-001A and TG20-001B) originate from the same sample, a quartz vein with previous observations of elements such as B, Mo and Sn (**Figure 10**). Sample 1A is taken closer to the edge of the quartz vein, while sample 1B is taken closer to the core. The purpose of this is to record any zonation or differences throughout the veins. Two samples (TG20-002, TG20-003) had the purpose of representing the transition from the core to the edge of the quartz vein. In the borderline between the quartz vein and the surrounding aplite were sample TG20-004 taken. The sample had a quartz vein of 1 cm cutting through. Field observations only revealed Mo placed in the quartz vein border zone, so the final sample is from the transitions zone between the surrounding biotite-granite and the vein were also collected (TG20-005) (**Figure 10**).

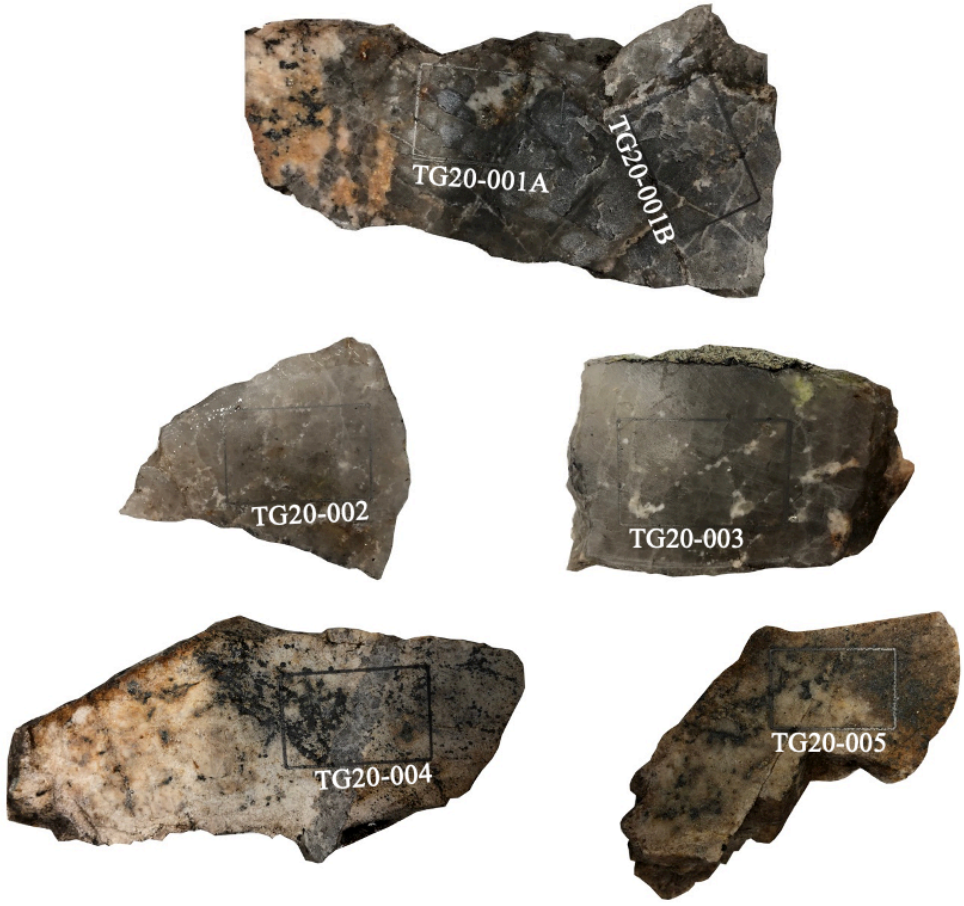

Figure 10: *Hand sections sampled in field that the thin sections are made of.*

4.2.2 Fluid Inclusion sections

Observations of the thin sections in a Nikon Eclipse Microscope revealed numerous well preserved fluid inclusions with various sizes (10-40 μm) in five sections (**Figure 11**). Based on those observations was a new round of thin sections created from the same samples as earlier at the thin section lab. Only this time with a thickness of 250 μm, to preserve the inclusions.

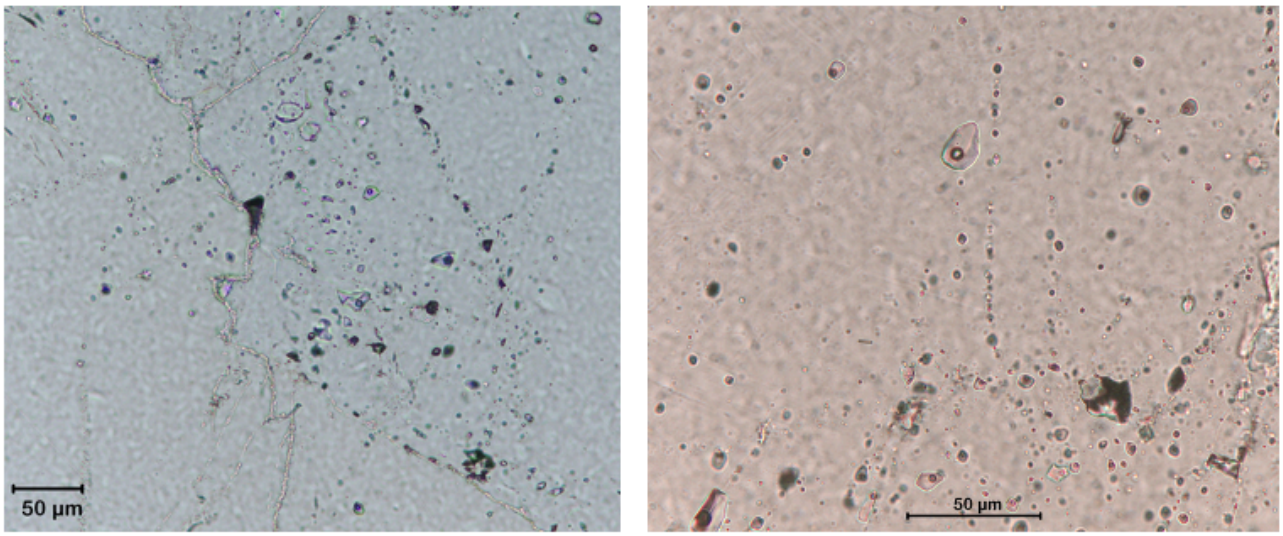

Figure 11: *Example of well-preserved fluid inclusions from section TG20-001A (left) and TG20-003 (right).*

4.3 Microthermometry

Microthermometry was performed on a Nikon Eclipse E600 microscope with a QICAM camera and Linkam MDSG 600 heating/freezing stage mounted to it. The temperature was controlled by a Linkam TMS 93 attached to a nitrogen pump. The microscope was calibrated using synthetic fluid inclusions of known compositions from Bubbles Inc, Blacksburg, VA, USA, at -56.6, -21.2, -6.6, 0.0, 9.8, 323.0, and 374°C.

The software Linksys 32 cooled the inclusions with a rate of 50 degrees pr. Minute to -197°C, and then kept for one minute to ensure sufficient undercooling and followed by gradual heating with a stepwise rate of 30 °C/min. Phase changes were observed at much slower heating rates of 1-5 °C/minute. First and final melting temperatures were recorded. Subsequently, each inclusion was heated to approximately 200-230 °C and the homogenization temperature was recorded. The same procedure by holding the temperature at T_h was implemented to ensure accurate readings.

After eight days of work and ca. One hundred measurements the NTNU microthermometry stage defaulted. However, the measurements were continued at The Arctic University of Norway, UiT. The equipment was a Linkam THMS 600 stage mounted on an Olympus BX 2 microscope. This microscope had 10x and 50x Olympus long-working distance objectives. In contrast to NTNU where 50x and 100x objectives were primarily used. For calibration were the synthetic fluid inclusion standards: SYN FLINC; pure H20 and mixed H2O-CO2 were used.

4.3.1 Salinity, pressure, and temperature estimations

The worksheet from Hokieflincs_H_2O-NACL is a numerical tool to calculate the pressure-volume-temperature-composition (PVTX) properties and trapping conditions of H_2O-NaCl fluid inclusions. The input data is dissolution temperature (T_{mf}), last melting phase (ice) and homogenization temperature (T_h). Output data for each inclusion is salinity, density, pressure, and temperature at homogenization, the dP/dT isochore slope and a unique trapping P/T condition for each inclusion.

Table 1: *Example from worksheet calculations for the H2O-NACL system. The blue cells are input parameters.*

T_{mf} (°C)	Phase	T_h L-V	Salinity (wt% NaCl)	T_{hom} (°C)	P_{hom} (Bar)	ρ (g/cm^3)	dP/dT (bar/°C)	Based on	T or P	T_{Trap} (°C)
-17,5	Ice	170	20,60	170	7	1,054	21,3	P est.	3270	323
-10	Ice	213	13,94	213	18	0,960	17,1	P est.	3270	403

To calculate an estimate of the trapping P/T along the isochore we used Ti in quartz geothemometry. Rutile solubility and TiO_2 activity in the silicate melts is confirmed by the appearance of Niobium-rutile in the system (section 5.3), so the requirements of Borisov A. and Aranovich L. (2020)'s equations is satisfied i.e. that the $\propto Ti = 1$. The hydrothermal fluids were derived from and co-existed with the rutile-bearing pegmatites (Section 5.3).
The equation calculates a temperature based on pressure estimate and input parameters (SiO_2, Al_2O_3, FeO, MgO, CaO, Na_2O, K_2O), sampled from EPMA in the hydrothermal quartz (section 5.5.1). This output temperature was used as temperature correction for the hydrothermal fluid inclusions in the Hokieflincs_H_2O-NACL worksheet. For the magmatic fluid inclusions was EPMA measurements from quartz in the aplite used to calculate a temperature estimate for the magmatic fluid inclusions.

The properties of the H_2O-NaCl thermodynamic system considering P-V-T-X properties are well characterized by numerous theoretical and experimental studies (R. Bodnar, Burnham, & Sterner, 1985; R. J. Bodnar, 2003). The given information is used to calculate the slope of the isochore, and the P-T conditions are estimated by combination with other methods. Isochores are lines with a constant density in a pressure-temperature diagram. Isochores are used to estimate the FI formation's PT conditions.

4.4 Scanning electron mincroscope (SEM)

SEM provides information on mineralogy, petrography, and mineral chemistry. This methodology came prior to Electron Probe Micro Analysis (EPMA) to identify major chemical components and suspected phases. The equipment used was a Hitachi SU-6600 scanning electron microscope with an acceleration voltage set to 20kV. It investigates a sample by scanning a beam of electrons across the sample in a specimen chamber under a vacuum. Detectors collect the electrons scattered back from the sample's surface or emitted secondary electrons (Lloyd, 1987). Each scan is visualized as an image on a monitor and allows magnifications significantly. Heavier elements yield more electrons because of their atomic number, which is directly proportional to the atomic number of the constituent elements in the minerals. All images from SEM are grey, and different grey tones interpret the result on the screen. A spectrum and table with normalized wt% of each element is supplementary information, all found in Appendix B.

4.5 Cathodoluminescence (CL)

Cathodoluminescence was obtained with a Hitachi SU-6600 scanning electron microscope. The acceleration voltage was set to 20kV with an attached Robinson panchromatic CL detector. The work was done at the Norwegian University of Science and Technology. Dr. Kristian Drivenes, helped to set up and run the instrument. During analysis the section is excited with a beam of electrons that causes backscattering of electrons. Local heating and X-rays are generated because of energy transfer to the lattice, facilitating the backscattering of electrons (Nasdala et al., 2004; Richter & Zinkernagel, 1981; Ten Have & Heijnen, 1985). Scan of thin sections TG20-004 was performed two times to detect variations within the hydrothermal vein and the pegmatite. The scattered images were stitched and visualized as one photo found in Appendix C.

A scan of TG20-005 was set up to identify noticeable changes in the pegmatite further away from the hydrothermal event. Nonobvious alteration seems affiliated in TG20-004, so a comparison of the two sections could disclose this.

4.6 Electron microprobe analysis (EMPA)

The electron microprobe analysis was determined at the Norwegian University of Science and Technology on thin section TG20-004 and TG20-005. Electron microprobe analysis uses a polished thin section to determine the main element composition of the mineral grains. The first scanning of the feldspar performed on thin section TG20-004, while quartz analysis was performed on both TG20-004 and TG20-005 afterwards. The analysis was performed by a JEOL JXA 8500 hyperprobe, with an acceleration voltage set to 15 kW, and the beam current was set to 20nA. The X-rays are generated by a high-energy focused beam of electrons and reveal the character of the elements in the sample (Reed, 2005). Standard X-ray intensity from Astimex Scientific Limited is compared with the X-rays from the investigated sample to determine the exact chemical composition. An overview of reference materials and detection limits is listed, found in appendix D.

The second round of EPMA was to detect trace elements, such as Ta, Dy, Y, U, Fe, Er, Gd, Th, Yb, Ho, Nb and Ti. A 100 Nm step size with a beam current of 10nA and acceleration voltage of 10kV was set up assisted by Dr. Kristian Drivenes. A lower voltage is set to avoid atomic sputtering and reduce the beam-specimen grant analysis of highly narrow and trim points.

4.6.1 Titanium in quartz (TitaniQ) thermobarometer

The affinity between the Ti content in quartz and the equilibration temperature is described systematically as titanium-in-quartz geothermometer, dubbed “TitaniQ” (Wark & Watson, 2004). In quartz traces of Ti substitute for silicon, so the TitaniQ can be calculated in the presence of rutile and hydrous silicate melt or fluids. Ti from sample TG20-005 and TG20-004 were collected using EPMA. The uncertainties of Ti measurements in EPMA are maybe the most significant factor.

The equilibrium $TiO_2^{rutile} = TiO_2^{quartz}$ controls the solubility of Ti in quartz. The TiO_2 activity (α_{TiO2}) is set to 1 as the system is saturated in Ti since rutile is present. TitaniQ may be used as a thermobarometer for P-T dependencies combined with isochores from the fluid inclusions.

Formula (3) was used for pressure calculations and formula (4) for temperature.

$$P(kbar) = \frac{-a + bT + RTln\alpha_{TiO_2} - RTlnX_{TiO_2}^{Qtz}}{c} \quad (3)$$

$$T°C = \frac{a + cP}{b - R \times lnX_{TiO_2}^{Qtz} + R \times ln\alpha_{TiO_2}} \quad (4)$$

R is the gas constant 8,3145 J/K, α_{TiO_2} is the activity of TiO_2 in the system and $X_{TiO_2}^{quartz}$ is the mole fraction of TiO_2 in quartz. The parameters a=60952 $\pm$ 3122, b=1,520 $\pm$0,04, c= 1741 $\pm$ 63. An independent constraint on temperature were listed for calculations of pressure, and subsequently an input for calculating the temperature. Practical limitations of this method is ~20 kbar upper pressure limit, as changes in Ti-in-quartz solubility behaviour appear at ~20 kbar. The lower pressure is limited by the sensitivity of available analytical techniques. This thesis is simplified by the presence of Rutile to that α_{TiO_2} is fixed at unity and the intersection of results from fluid inclusions analysis. Compositions were calculated for each Ti_{ppm} value, but an average composition of all result was concluded to represent the results and draw the isochore. This method is as the fluid inclusion worksheet best fit together with other assumptions. The main result is represented as the point of intersection between the isochore of fluid inclusions and TitaniQ analysis (Section 5.7).

5. Results

This chapter addresses the field observations with the following petrographic descriptions. Further on, some chemical identifications from SEM, CL, EPMA and microthermometry. The last chapter combines the previous results to make a pressure-temperature estimate. Sources of error are included in all chapters consecutively.

5.1 Field descriptions

The dominating host rock at the NE corner of Klepsvatnet is a pale quartz-feldspar gneiss with amphibolite bonding. Most of the pegmatites had weak or poorly developed zonation. Where zonation was developed it typically occurred as a narrow boundary zone towards the host rock with a finer-grained quartz and feldspar and incrementally increasing grain size towards the quartz dominated core zone (**Figure 12: A).** Accumulations of irregular aplite and quartz zones exist in the wider veins. The quartz is primary smoky grey and coarse-grained, and feldspar variates from light green amazonite to plagioclase (**Figure 12: C).** Beryl was observed as well-developed crystals at 4-5 cm crystallized out in the contact zone of the veins.

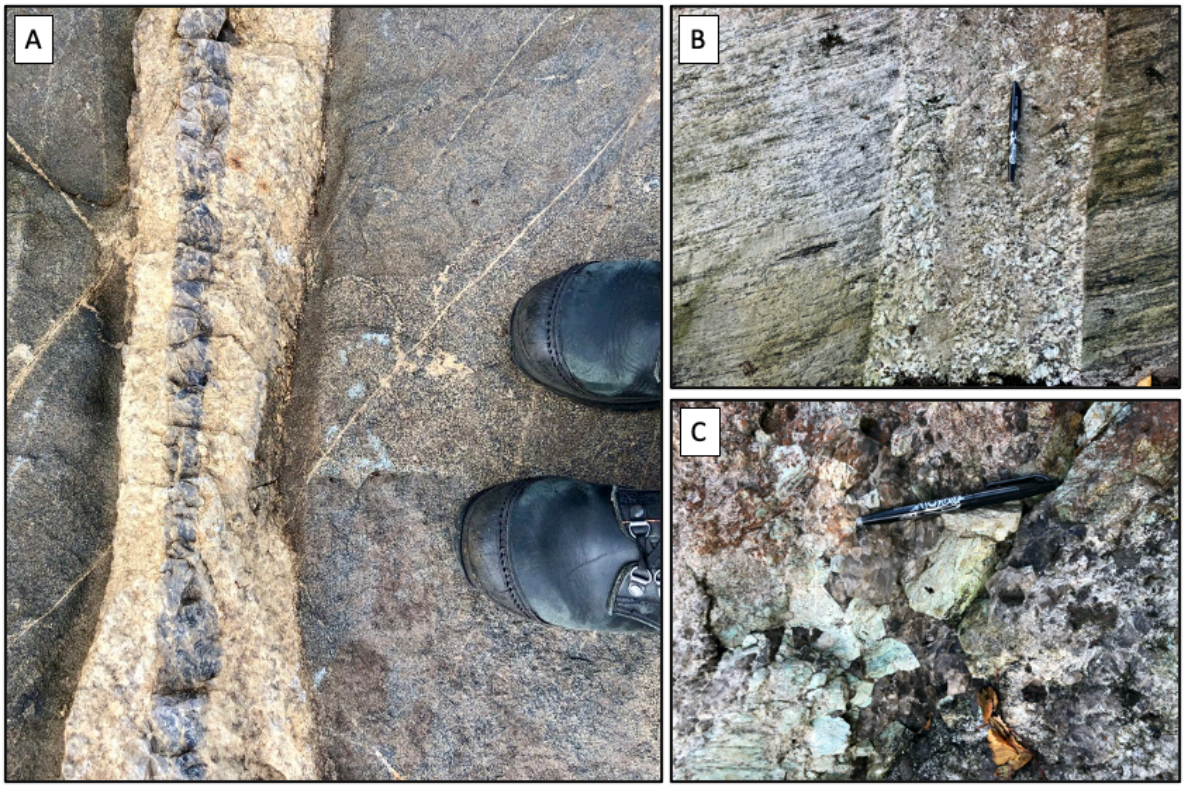

Figure 12: *Field observations. A) Example of a sonation pattern in a pegmatite. B) Amazonitepegmatite cutting the pale quartz-feldspar gneiss. Black lines are amphibolite bonding. C) Close up photo of the amazonitepegmatite. Coarse grained amazonite and smoky quartz.*

Ore minerals were observed in the field due to their characteristic dark colours and preserved grain sizes. However, they are not easily separated from each other in the field, and only positive observations are made of molybdenite. Strong assumptions regarding the others to be cassiterite or magnetite based on previously documented observations (Wilberg, 1983). Most of the pegmatites cut the host rock discordantly with sharp and straight contacts.

5.2 Petrographic descriptions

5.2.1 Quartz vein

In the samples from the quartz vein is >80% holocrystalline quartz. The dominant quartz is phaneritic and coarse grained, allotriomorphic, with dark smoky colour. Fluid inclusions are prominent in almost all quartz grains. It has undulating extinction and a mix of straight and lobe grain boundaries. Chessboard deformation are present in some of the grains, then typically with more uneven grain boundaries (Figure 13). Evidence of dynamic recrystallization is seen as both grain boundary migration (GBM), subgrain rotation (SGR) and bulging (BLG).

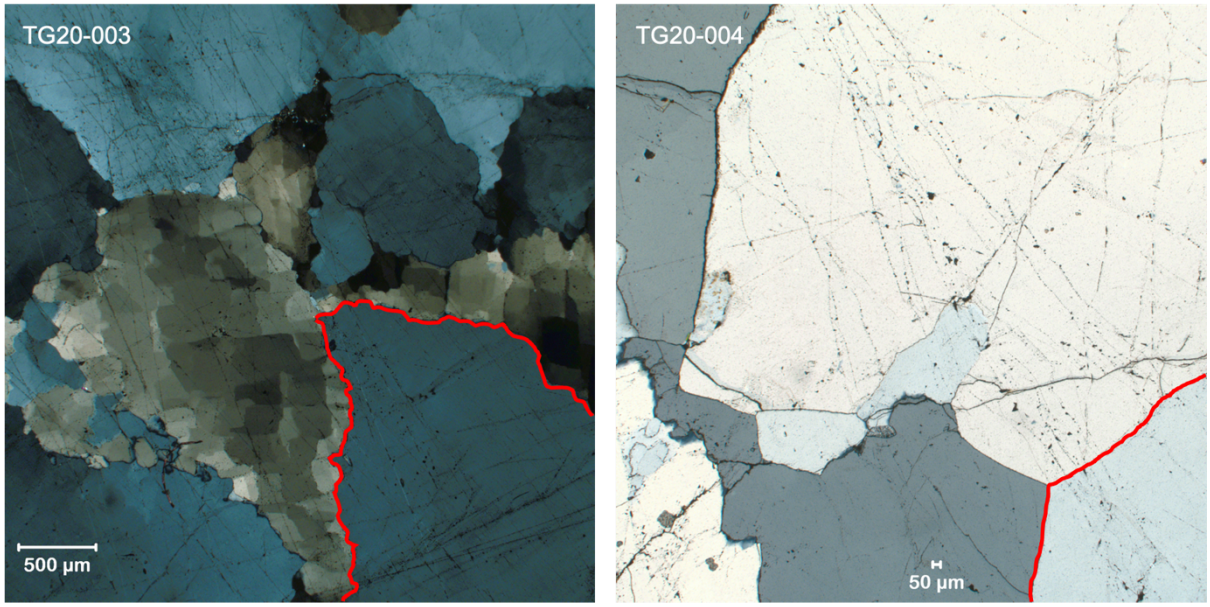

Figure 13: *Example of variations in grain boundaries in hydrothermal quartz from thin section TG20-003 and TG20-004. See appendix A for whole scan of the thin section.*

Some feldspar grains are seen in xenoblastic accumulations dominated by microcline and K-feldspar (**Figure 14**). Both biotite and muscovite are present in all sections, but rarely more than 3%.

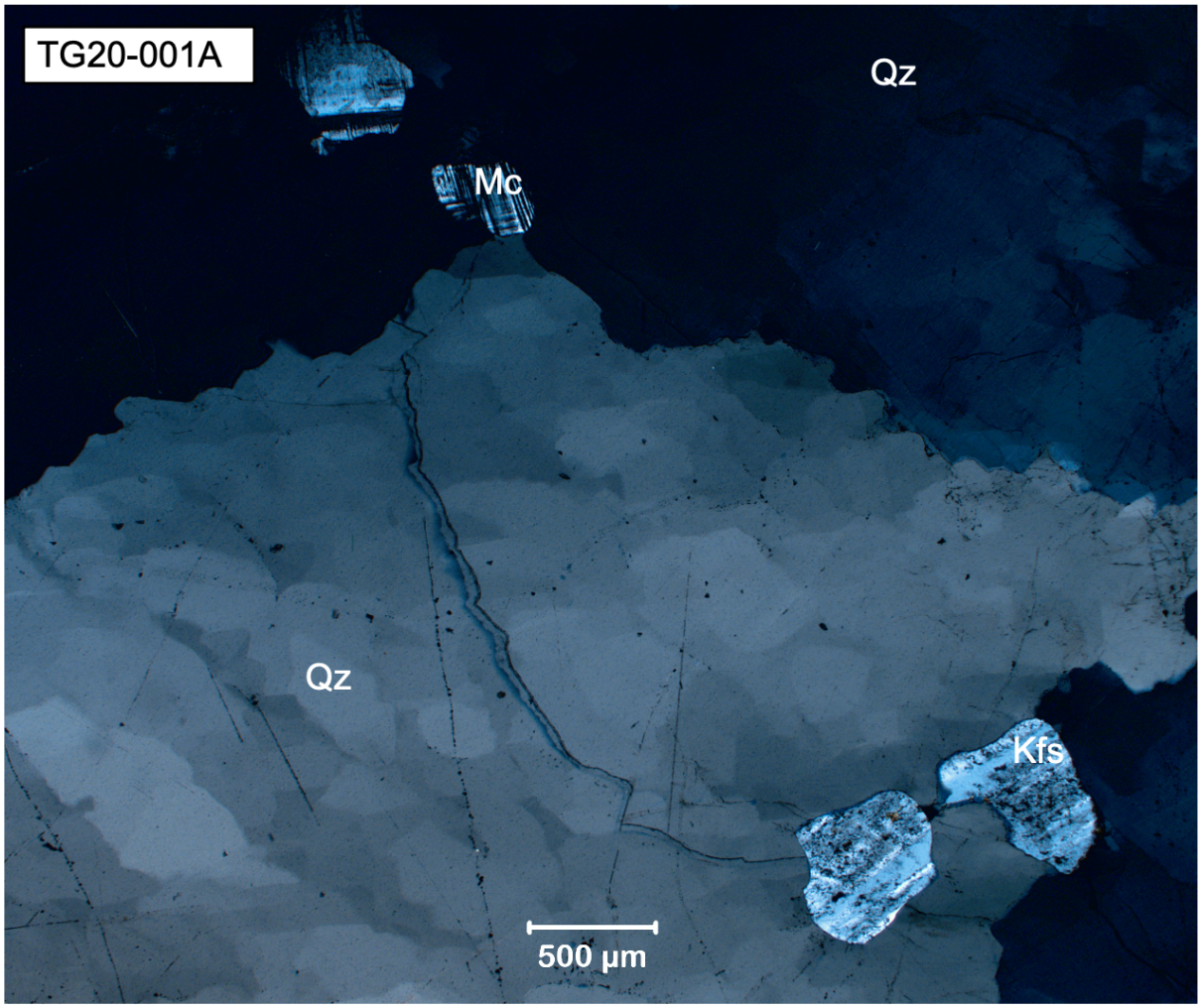

Figure 14: *Quartz and feldspar from thin section TG20-001A. Chessboard texture in the quartz. See appendix A for whole scan of the thin section.*

5.2.2. Aplite

The aplite is allotriomorphic-granular, overall equigranularity with smaller grain sizes and bigger variations, but still >50% is quartz and feldspar. Many opaque minerals. The dominating quartz is dark smoky, anhedral with undulating extinction. No distinct difference in quartz textures is observed between the hydrothermal quartz and the magmatic quartz. Another great difference is the degree of transformation in the feldspar, that is both microcline and plagioclase. Locally in the microcline can appearances of plagioclase inclusions in optical continuity be observed. Feldspar alteration is present as both sericitization and saussuritization, but it was found difficult to separate the processes only in optical microscope (**Figure 15**).

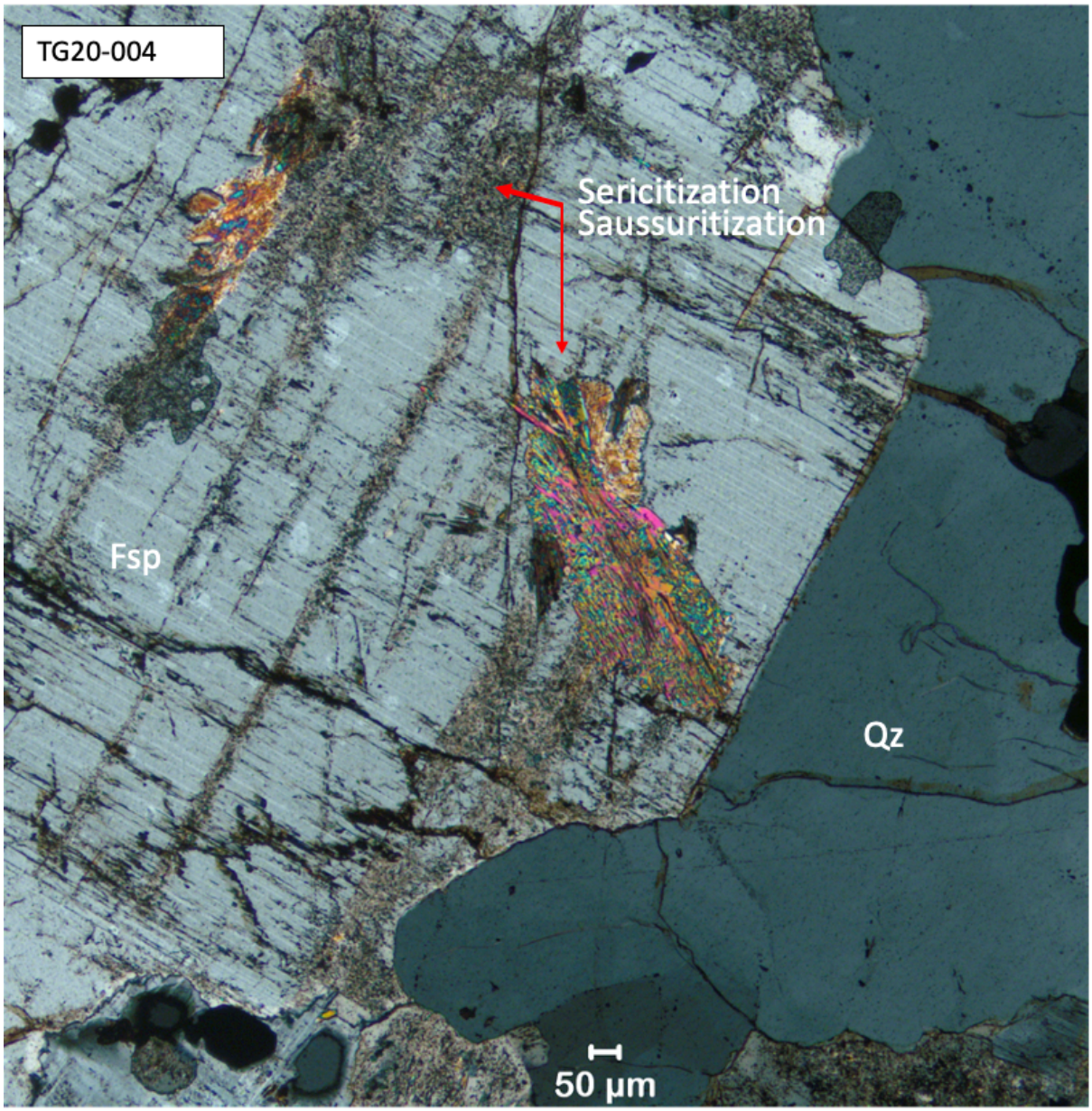

Figure 15: *Example from thin section TG20-004 in cross polarized light. Neighboring quartz veins of a feldspar with both saussuritization and sericitization. See appendix A for whole scan of the thin section.*

Greater amounts of both biotite and muscovite are observed. A euhedral diamond shaped titanite is observed, strongly altered with poikiloblastic textures. The altered minerals are opaque or pleochroic halos in both plan and cross polarized light, so no identification was made but they can be of radioactive varieties. Pyroxenes are present, with green colours in plan polarized light. Chlorite is observed and separated from muscovite and biotite because of green colour in plan polarized light and pleochroism. Typically, in clusters around the opaque minerals close to the rim between the hydrothermal quartz vein.

5.3 SEM

SEM results were primary used for mineral identification and textural studies. Cassiterite (SnO_2) is very fine-grained varying from 10 - 20 µm with bright SEM colors since Sn is heavier than surrounding feldspar and quartz (Figure 16). The cassiterite in this sample is mainly located in the contact between the hydrothermal quartz when intersecting pegmatite. Cassiterite is generally precipitated in veins with quartz.

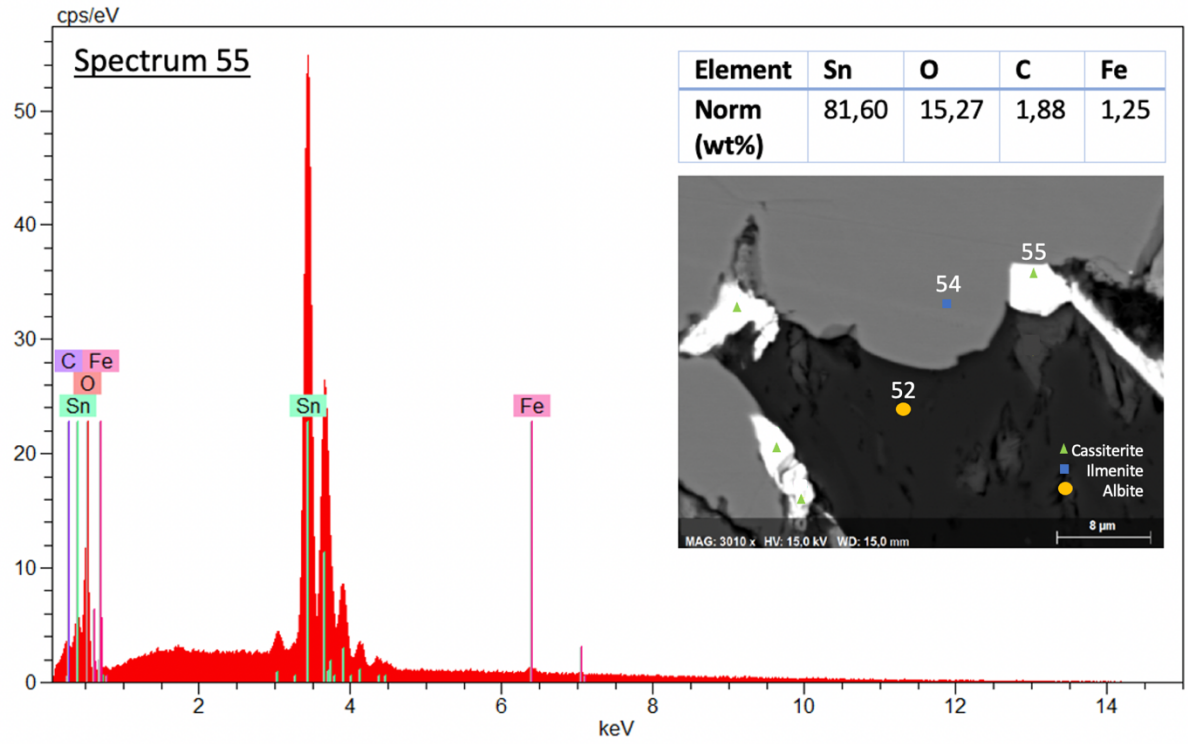

Figure 16: *SEM photo with spectrum and normalized weight percent from spectrum 55. Cassiterite has the brightest signatures due to higher densities. See appendix B for several examples.*

The next identified mineral is magnetite (Fe_3O_4) that confirms the field assumptions. Fe solubilities also manage to link us towards the next observed mineral, Ilmenite ($FeTiO_3$) (Figure 17).

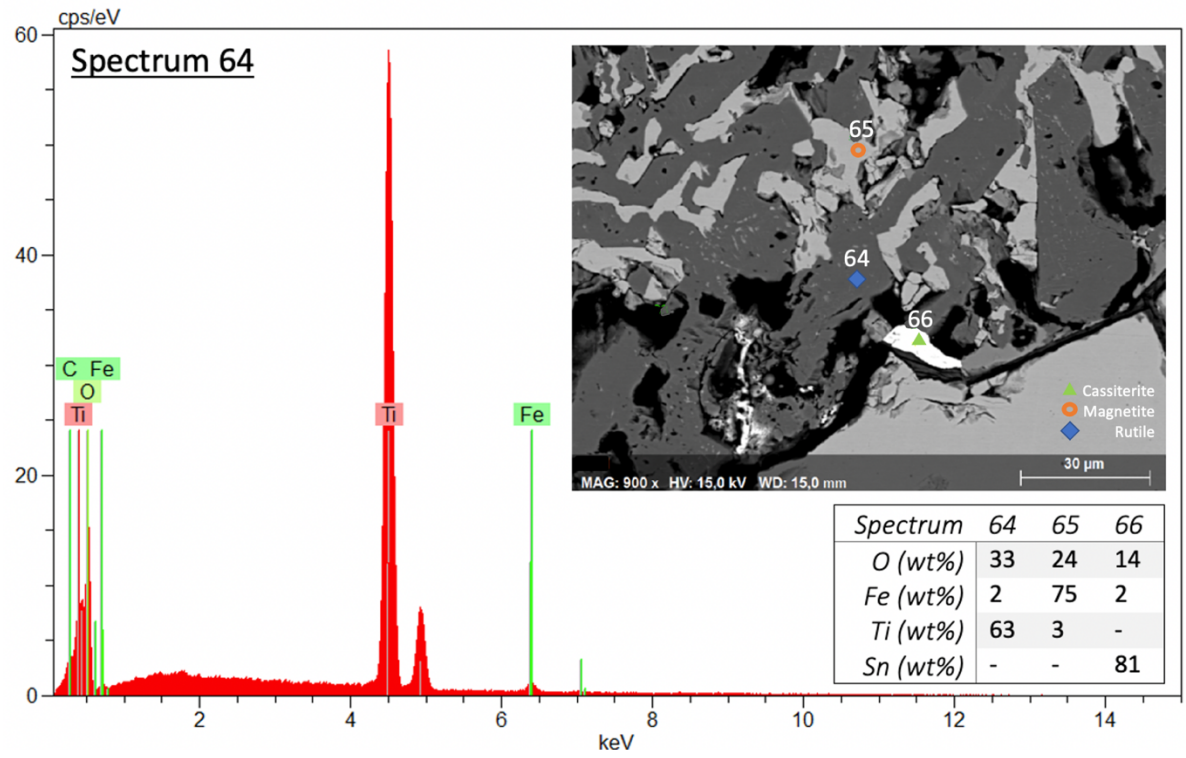

Spectrum	64	65	66
O (wt%)	33	24	14
Fe (wt%)	2	75	2
Ti (wt%)	63	3	-
Sn (wt%)	-	-	81

Figure 17: *SEM photo of spectrum 64 (rutile), 65 (magnetite) and 66 (cassiterite) with normalized weight percent. Taken from the borderline between cross cutting hydrothermal vein and magmatic aplite. See appendix B for several examples.*

5.4 CL

The main purpose of CL recordings is to distinguish different growth episodes, resorption, possible hydrothermal events, or post magmatic recrystallization. CL can also visualize different inclusions in the quartz grains. The first CL scan was of the quartz vein in thin section TG20-04 to evaluate the hydrothermal quartz (Figure 18). The CL-signatures are homogeneous and relatively dark, indicating only one growth episode caused in a high temperature environment with low content of Ti (Breiter, Ďurišová, & Dosbaba, 2020). Quartz textures are important sources of petrological information since it partially maintains its primary features during later alteration processes.

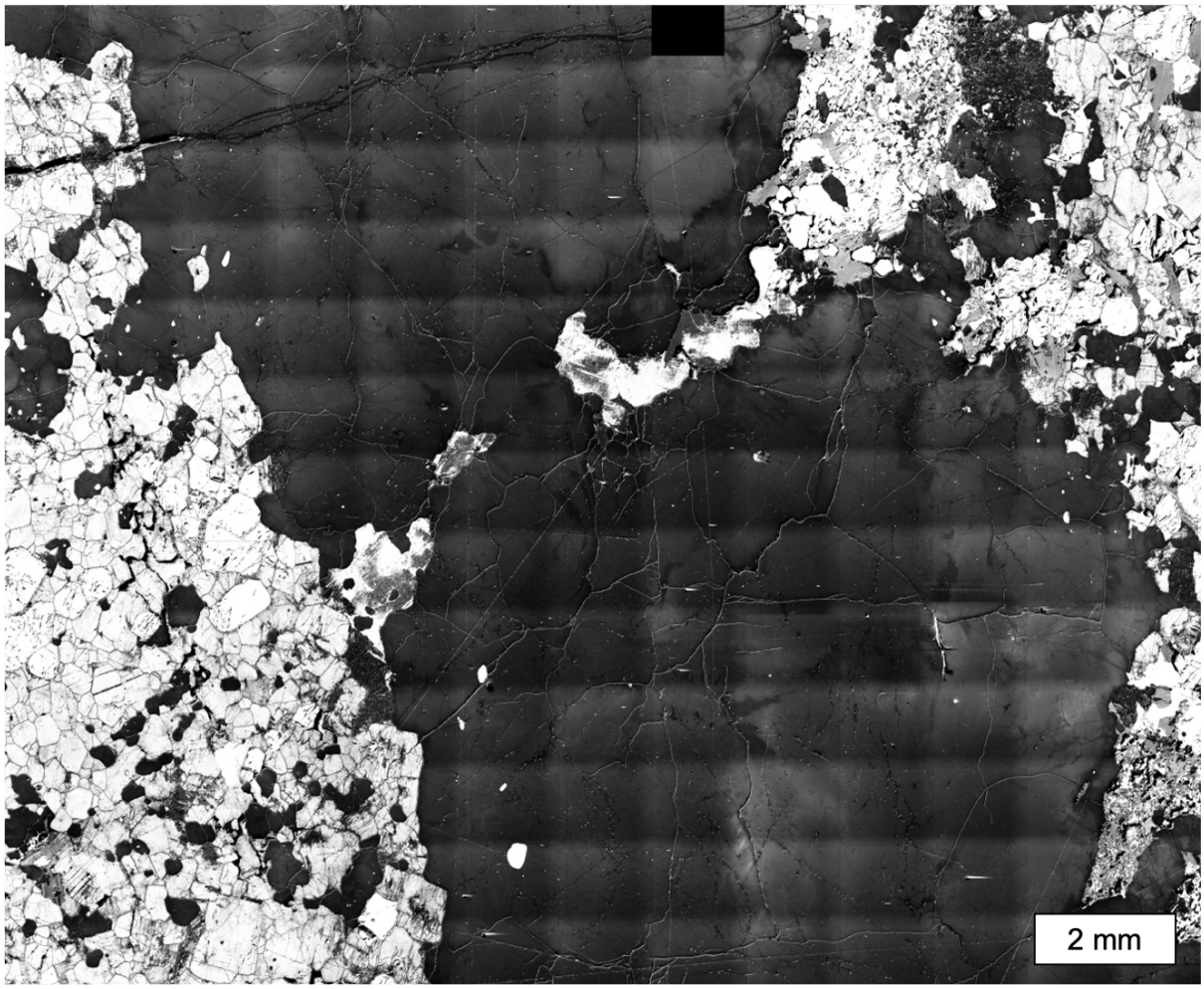

Figure 18: *CL photo of the quartz vein cutting through the aplite in section TG20-004. The chessboard formation is caused by the stitching program and scans. Main result is the small contrasts in grey-color, also found in Appendix C.*

The CL signature from the magmatic quartz in thin section TG20-004 and TG20-005 is bright at the grain boundaries and darker in the core (Figure 19). By Breiter et. al (2020) does this mean an inward decrease in Ti. CL results is therefore combined with the Al/Ti results in (section 5.5.2).

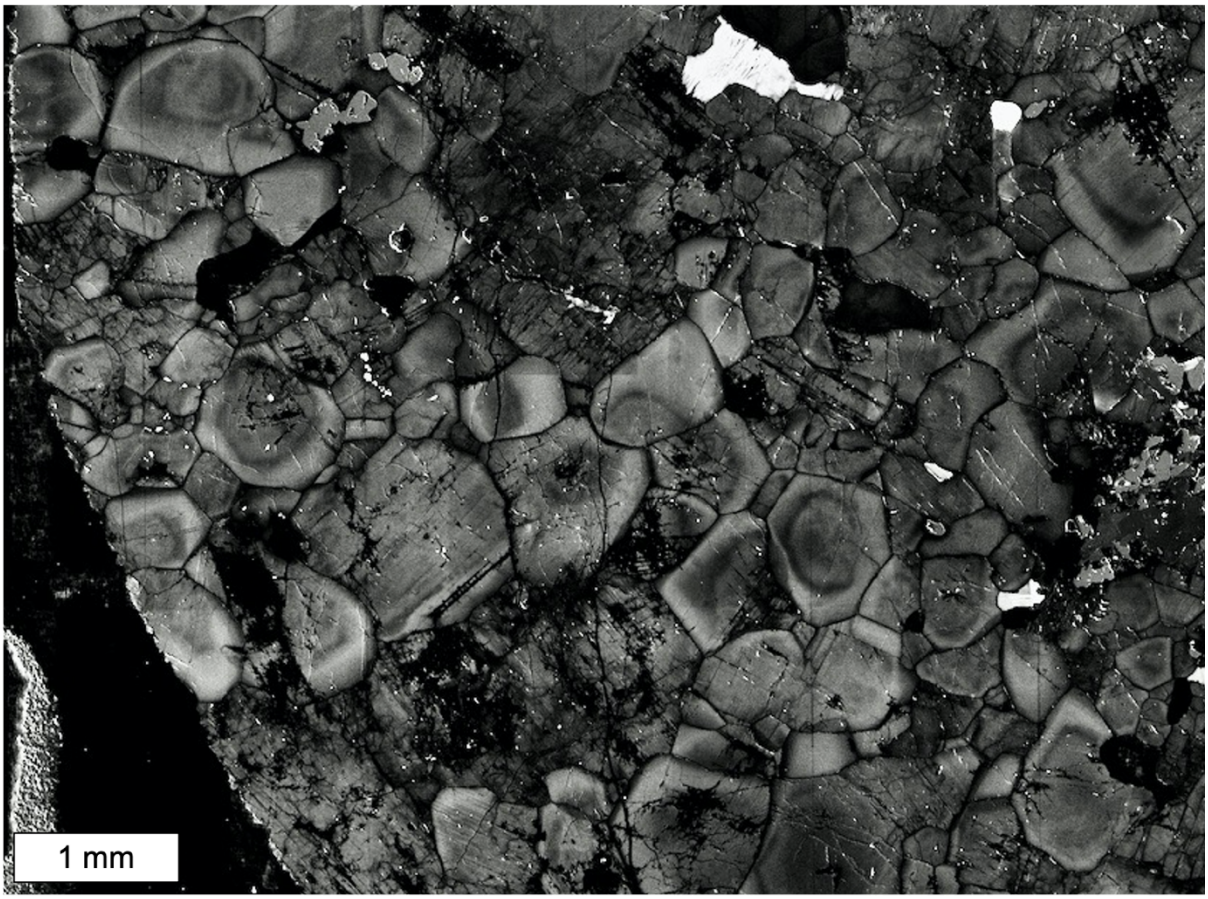

Figure 19: *CL image from thin section TG20-004. A sonation pattern with a lighter contrast close to the rim and darker inwards to the core. See appendix C for whole section.*

Reviews of thin sections in CPL and PPL are combined with the CL-photo to determine where EPMA points should be taken (**Figure 20**)

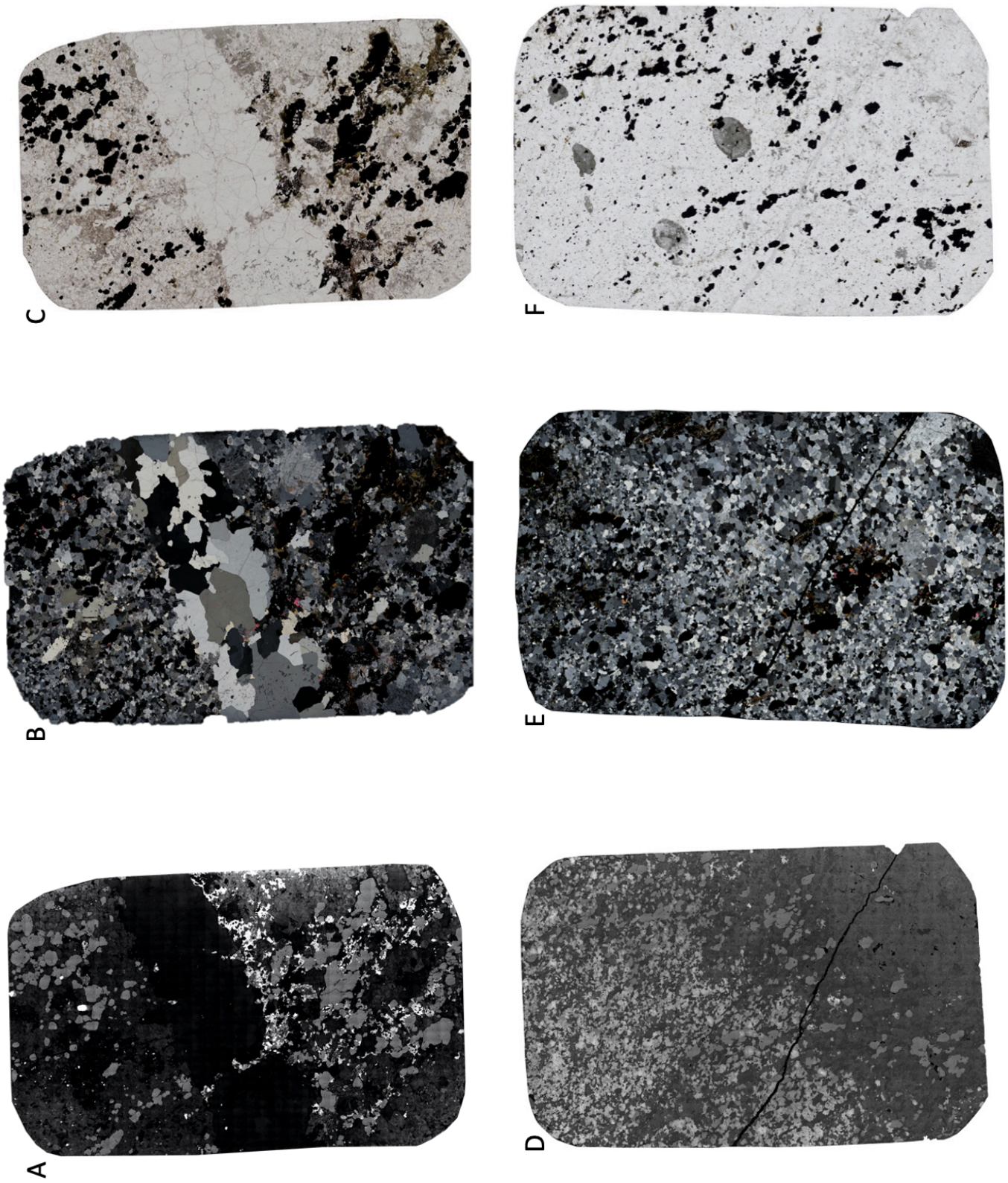

Figure 20: *Photos of thin section TG20-004 from both CL (A), CPL (B) and PPL(C).*

5.5 EPMA

Electron microprobe analysis were used to obtain exact chemical composition of the minerals observed from SEM.

5.5.1 Feldspar analysis

The average bulk composition in the measurements of plagioclase in thin section TG20-04 was $An_{13,5}Ab_{85,6}Or_0$. The dominant feldspar is an Oligoclase with the chemical formula $Na_{0,8}Ca_{0,13}Al_{1,1}Si_{2,8}O_8$. The average bulk composition of the K-feldspar $An_{0,2}Ab_5Or_{94,9}$ and the dominating K-feldspar is orthoclase. (**Figure 21**).

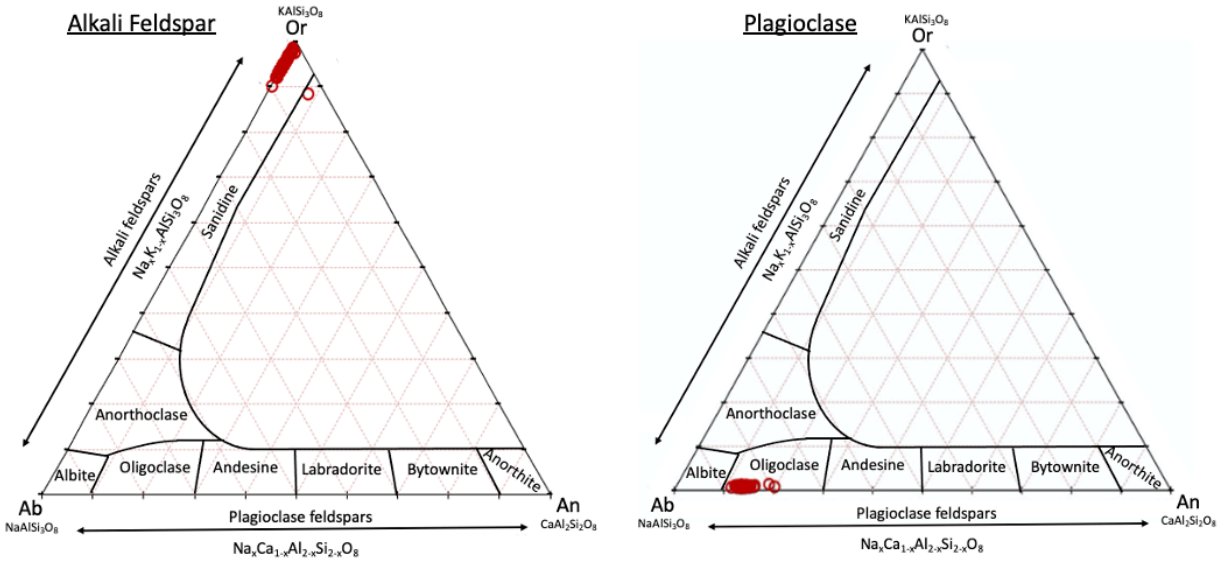

Figure 21: *Composition from felspar in thin section TG20-04. Measurements was sampled from both plagioclase and K-feldspar.*

K/Rb and Rb/Sr in k-feldspar were plotted against each other due to their sensitivity to ingenious differentiation (Figure 22). Since all the plots are from the same thin section, it only represents the location of thin section TG20-004, and evaluations of variations are difficult to determine. If the total value were below 99 were the points disregarded due to uncertainties, only if the stoichiometry also did not make sense. The K/Rb relationship has an average of 191, and Rb/Sr has average of 8,95. The axes illustrate variation of pegmatitic system and allows comparison to other pegmatites systems (Figure 22).

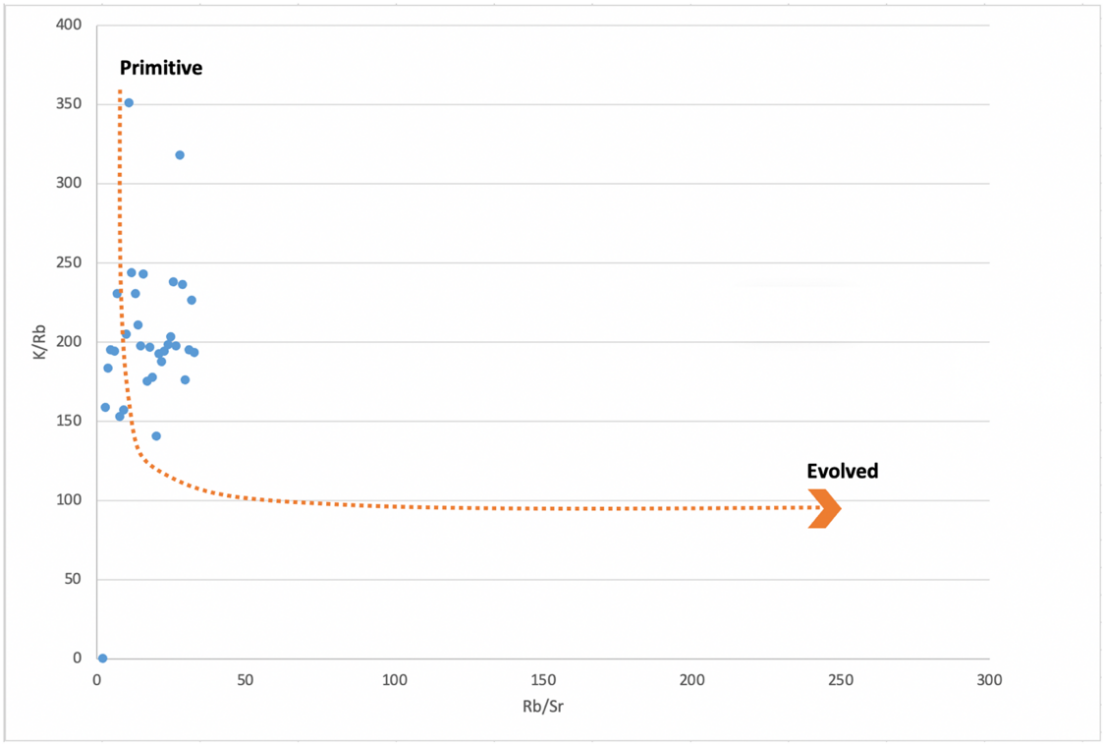

Figure 22: *K/Rb plot against Rb/Sr from K-feldspar from sample TG20-004.*

5.5.2 Quartz analysis

Quartz was analysed for Al and Ti content. The Al/Ti content in quarts has previously provided petrogenetic indicators such as geothermobarometer and the granite type. Ti is temperature and alkaline dependent and compatible, while Al is dependent of the melt composition and crystallisation physics (Larsen, 2004). Analysis was done in transverse over the quartz grains in the hydrothermal quartz to detect variations in Al. It can vary from 2 ppm to 2000 ppm even in primary grains being in contact.

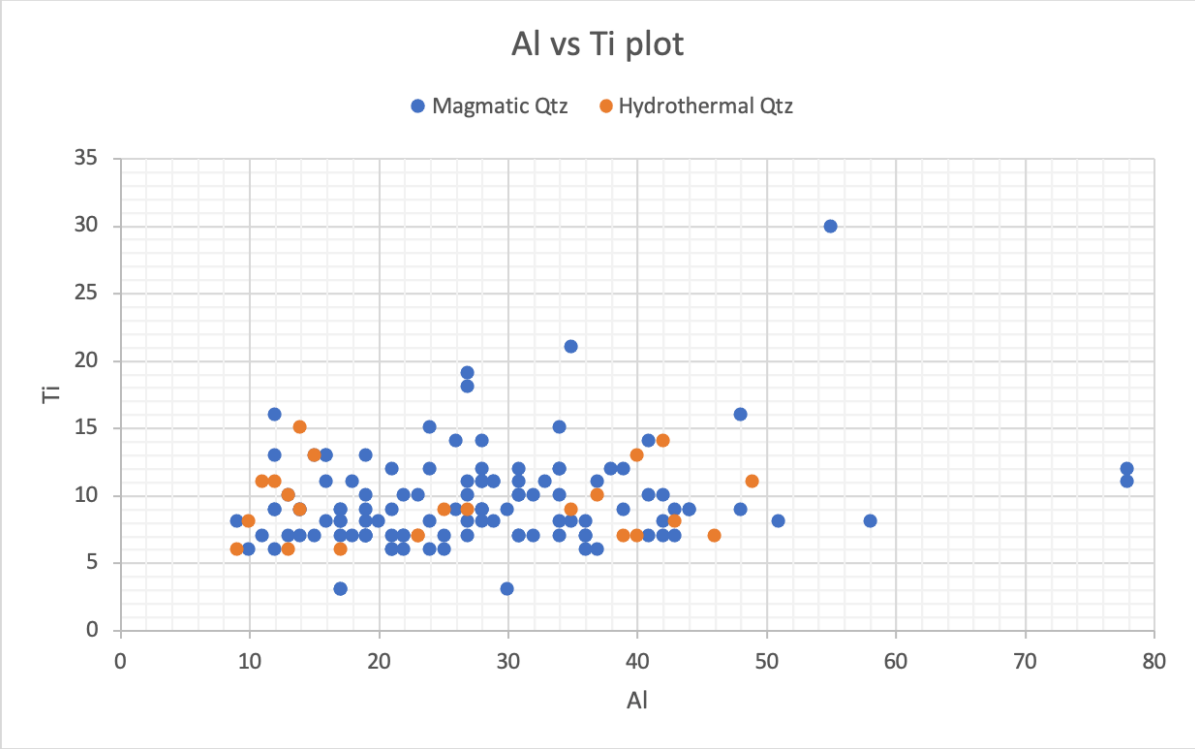

Figure 23: *Plot of Ti against Al. Hydrothermal quartz with orange and magmatic with blue.*

260 points were analyzed but values below 3 ppm were classified as below detection limit and rejected from the dataset. Other contaminated analyses and outliers were excluded from the dataset. Al_{max} = 78 ppm and Ti_{max}= 30 ppm. This plot shows no immediate trends or correlations. It seems like the magmatic quartz generally has more Ti than the hydrothermal quartz, however, there is considerable overlap amongst hydrothermal and magmatic quartz.

To determine if there were any correlation between Al and Ti in the samples, some statistical analyses were performed. Only these two variables are included because the interest lies in weather or not, they show any correlation. A Pearson's test could not be done because the dataset did not fulfill the required obligations. A spearman's correlation test could be performed as one or both variables were not normally distributed, or the relationship was non-linear and complicated. The relationship is linear and uncomplicated, but Ti is not normally distributed. The null hypothesis (H0) is: There is no correlation between Al and Ti. H1: There is a correlation between Al and Ti. Values of the correlation coefficient (ρ) close to 1, indicate a strong, positive correlation between the ranked data. There is a weak, but positive correlation between Al and Ti (correlation coefficient ρ = 0,0766, S = 498840, p-value = 0,3542).

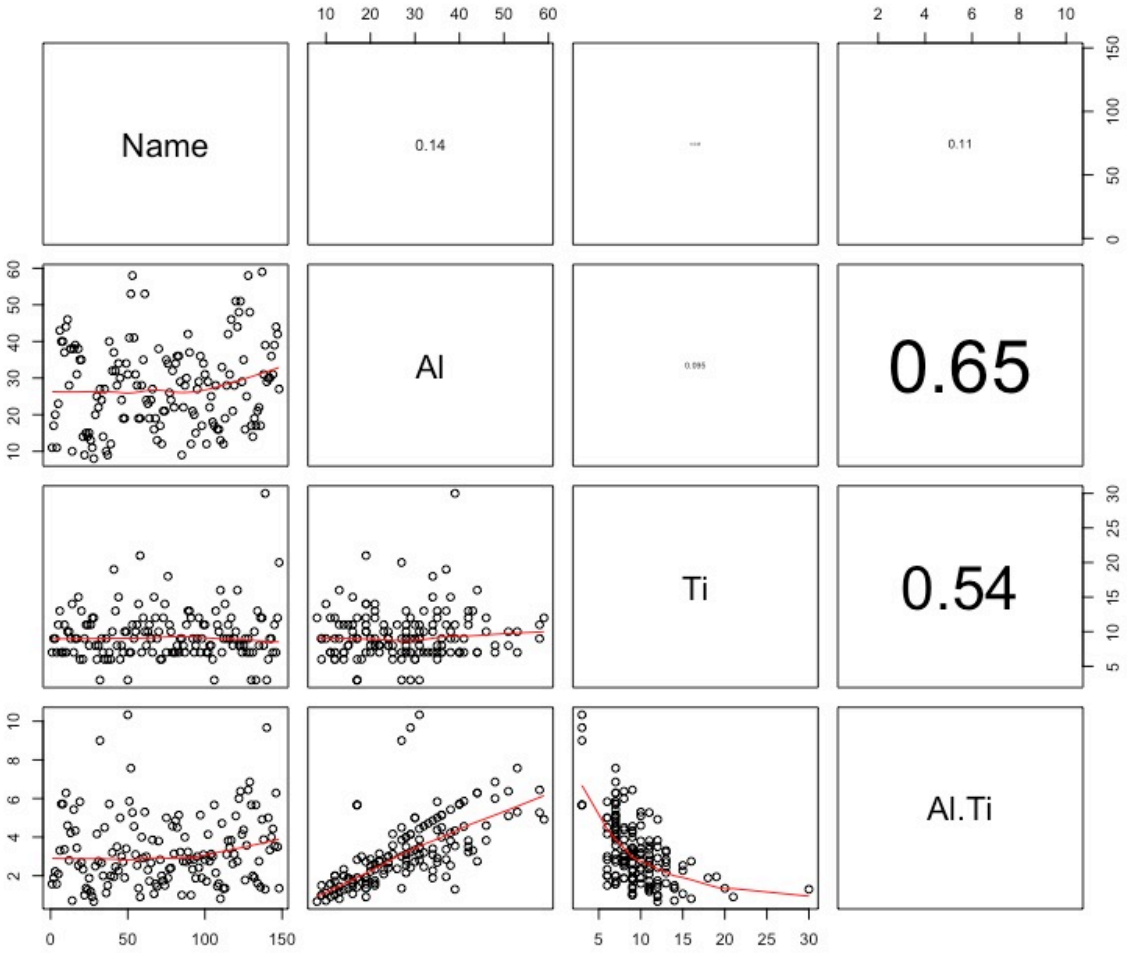

Figure 24: *Plot of Al/Ti relationship. The upper panels show correlation coefficients, and the lower panels draw line between the datasets. A flat line indicates a typical non-related.*

The upper panels indicate correlation coefficients to visualize what variables that are correlated. Both Al and Ti are correlated to Al/Ti, but not to each other. The lower panels are a red line added to represent the “smoothing function” in attempting to draw a linear or curvy line through the datapoints. This demonstrates the presence or absence of a potential relationship. The lines are dominantly flat that is typical for non-related variables.

Each grain got several analyzing points attempting to detect Ti- or Al- variations within and correlation between CL-intensity and Ti/Al content (**Figure 25**).

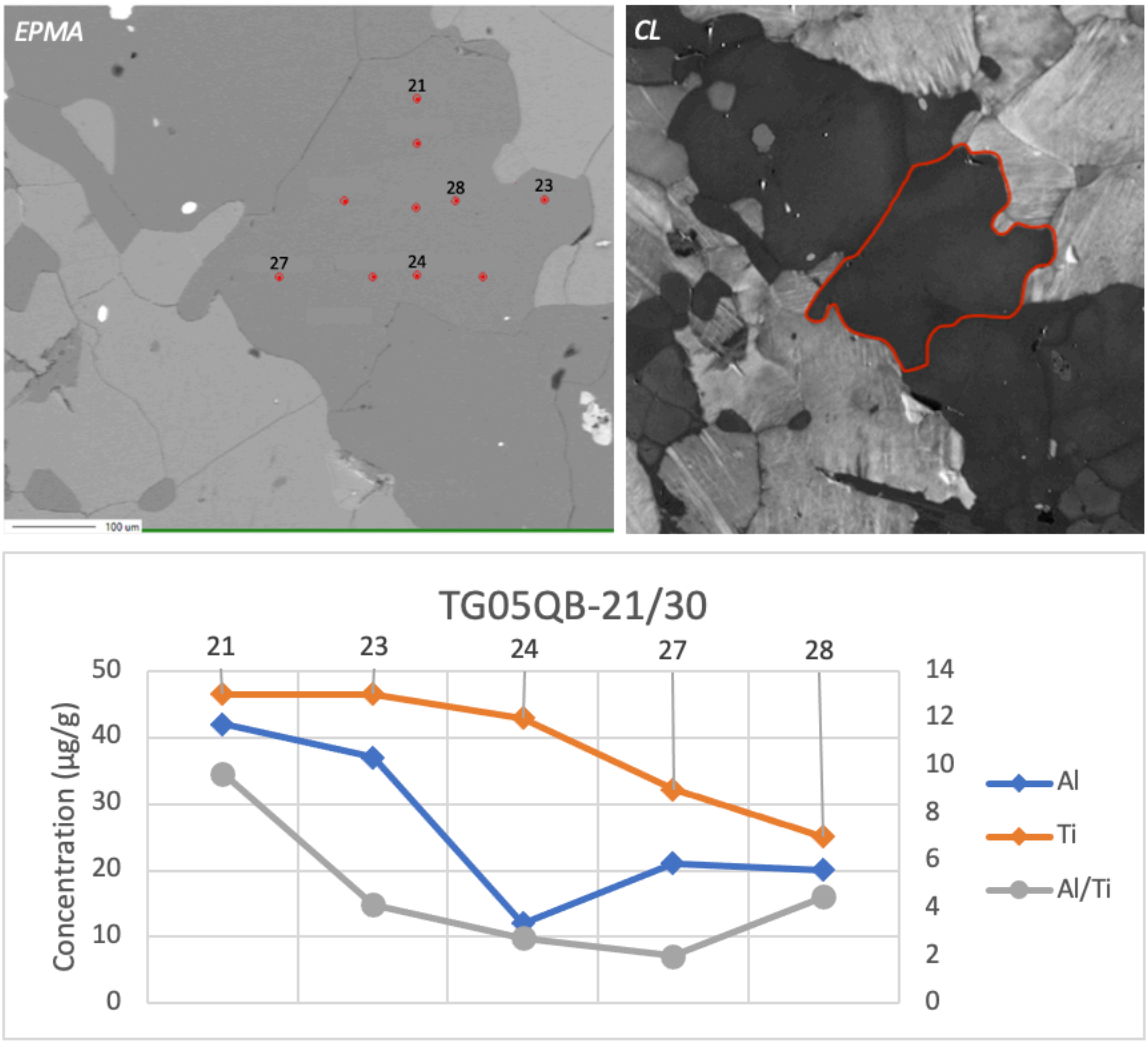

Figure 25: *Overview of the points sampled from EPMA and CL photo. A plot of TG20-005, analyze point 21-30.*

The CL-signatures show small or no degree of variation. Point 21, 23 and 24 lie closes to the grain boundary with 28 closest to the core. The trend implies a decrease in Ti towards the core, but only based on one point. No significant pattern was found in any other samples (Se Appendix D).

5.5.3 Rare earth elements

The distribution of REE's in pegmatites are one of the main factors controlling the different pegmatite families LCT and NYF. The minerals of interest were first detected in SEM with observations of possible Nb-rutile and accompanying Y, Ta, C, U and Th signatures (**Figure 26**). The selected mineral is a good example representing most of the Nb-rutile in the section as all of them has that same petrographic feature i.e. small grain size, and bright back scatter features. It has an unknown texture, perhaps it is rather an aggregate of Nb-rutile than just being one mineral, is it multiple minerals. The circles can be rutile that have grown together. The anhedral inclusion on the right side is zircon, a common accessory mineral in NYF-pegmatites. Zircon excludes Pb and accept U to its atomic structure.

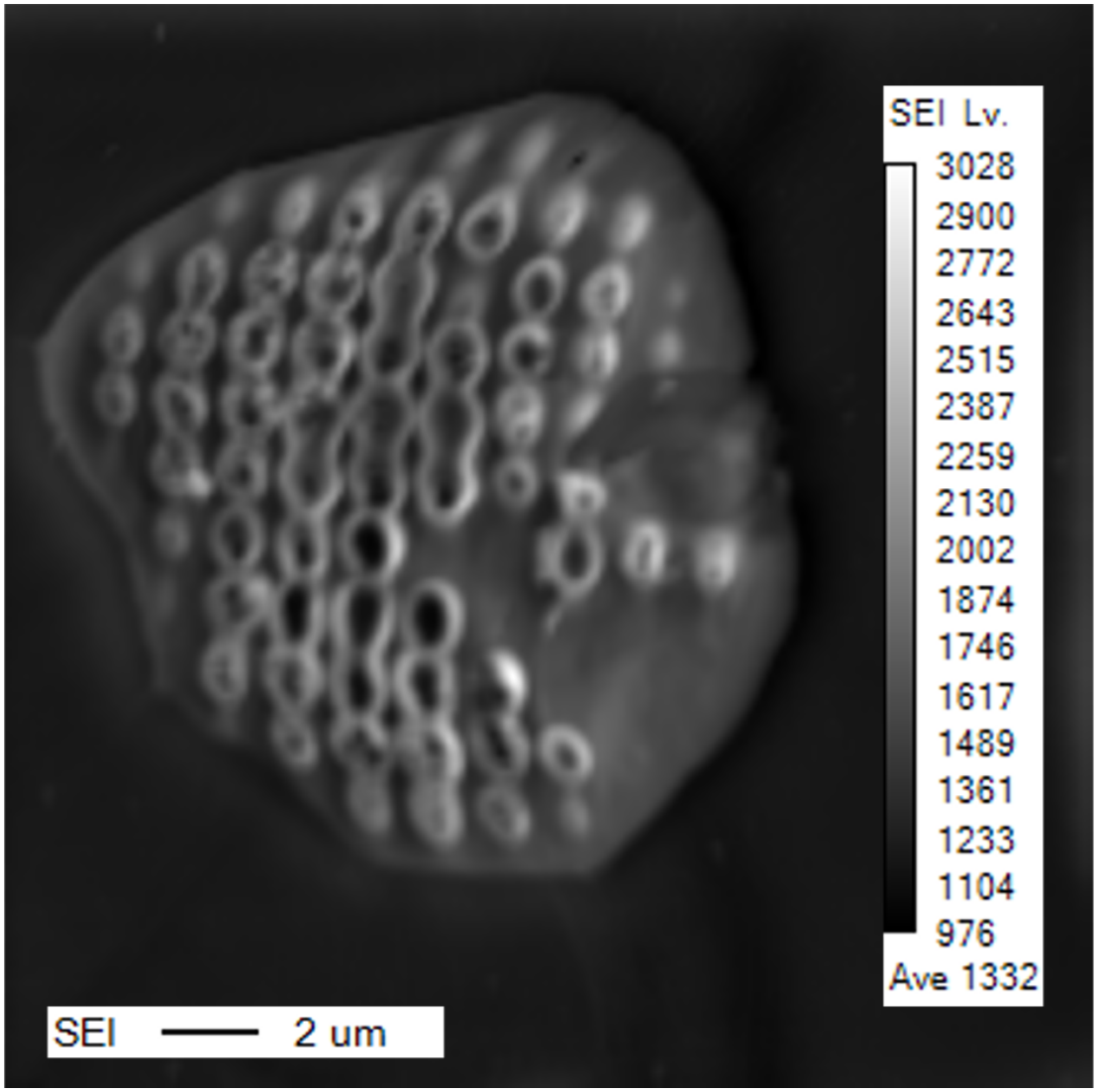

Figure 26: *The grain of interest, a Nb-Rutile with a characteristic texture.*

REE often accompanies Y as many elements have the same atomic charge 3+, and predominantly the same ionic radius. This equity allows the minerals to substitute easily for

Y. This pertains especially to the fact that NYF pegmatites carry more REE-minerals whereas only negligible amounts are observed in LCT pegmatites. The grain was mapped in detail with focus on Fe, Ta, Dy, Y, U, Yb, Er, Gd, Tg, Ho, Nb, Si, Ti and Zr (**Figure 27**, **Figure 28**).

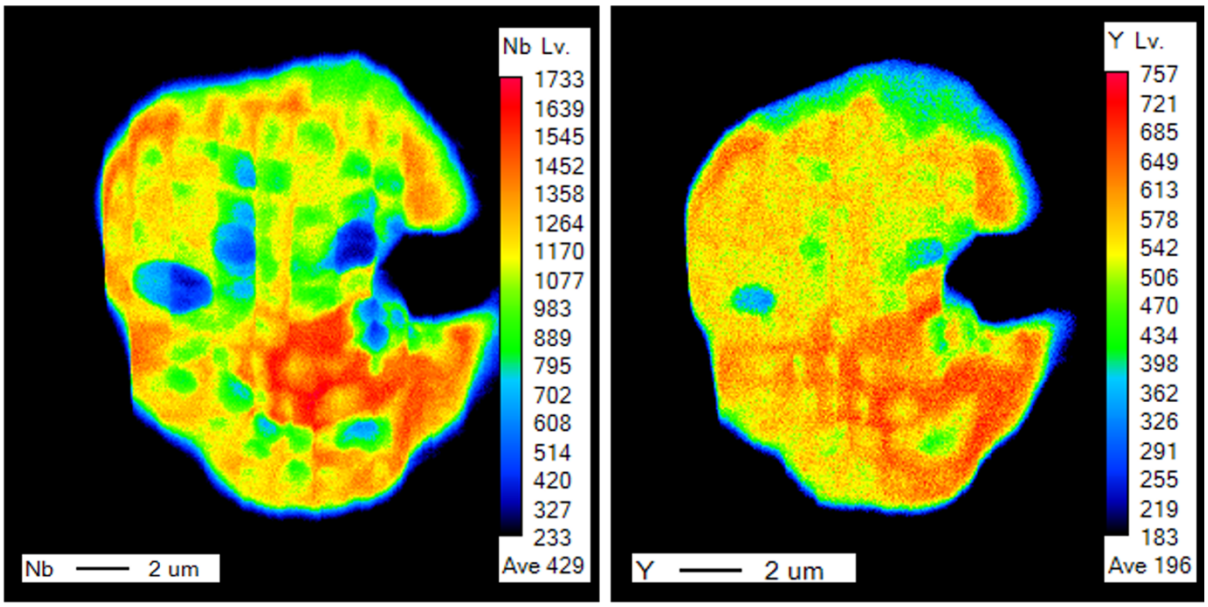

Figure 27: *High concetrations of Nb and Y in Nb-Rutile mapped from EPMA.*

High signatures of both Nb and Y, strong affinities to the NYF-family. U correlate positively with Th, the separation is proven. The same area of high Th has also high values of Nb and Y, so it is a hydrogen phase.

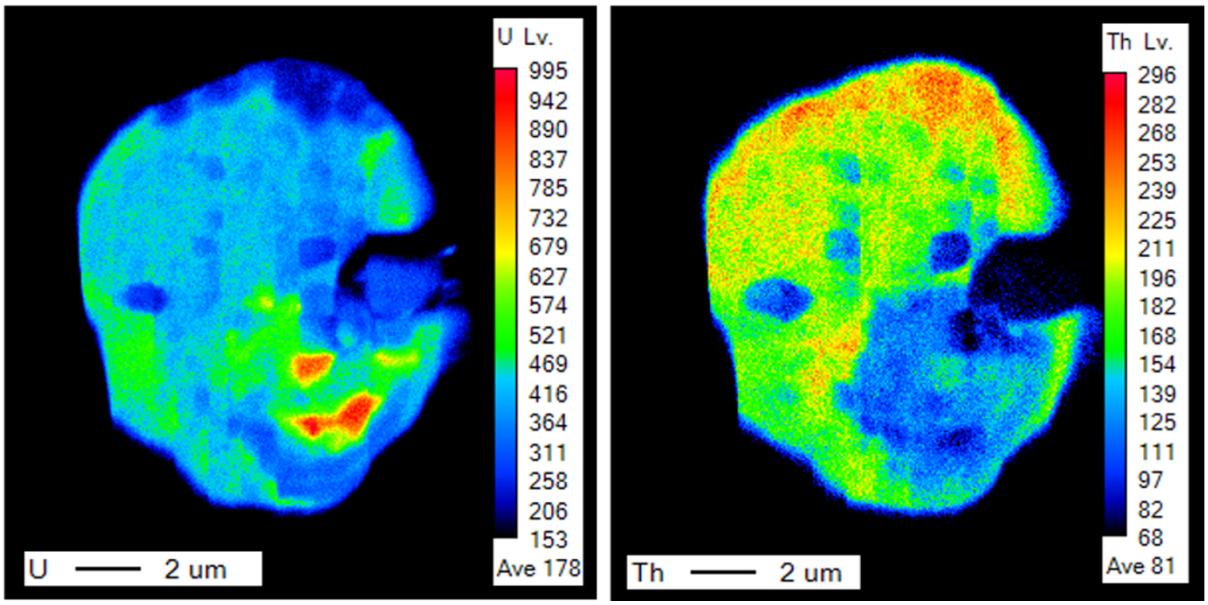

Figure 28: *EPMA photo showing correlation between U and Th.*

5.6 Microthermometry

The fluid inclusions were measured in quartz from the aplite and the quartz vein. They were generally between 5 and 30 µm in diameter and well preserved. Most of the inclusions contained liquid water and vapour i.e. they are simple L-V types (Figure 29). Rare inclusions also contained a halite crystal (LVS-type) while the third phase of water, vapor, halite crystal and second tabular solid (LVSS) was not observed. Most measurements were performed on primary clusters, and in rare cases pseudo secondary inclusions. Compositions as well as freezing-heating behavior between primary and pseudosecondary inclusions was indistinguishable.

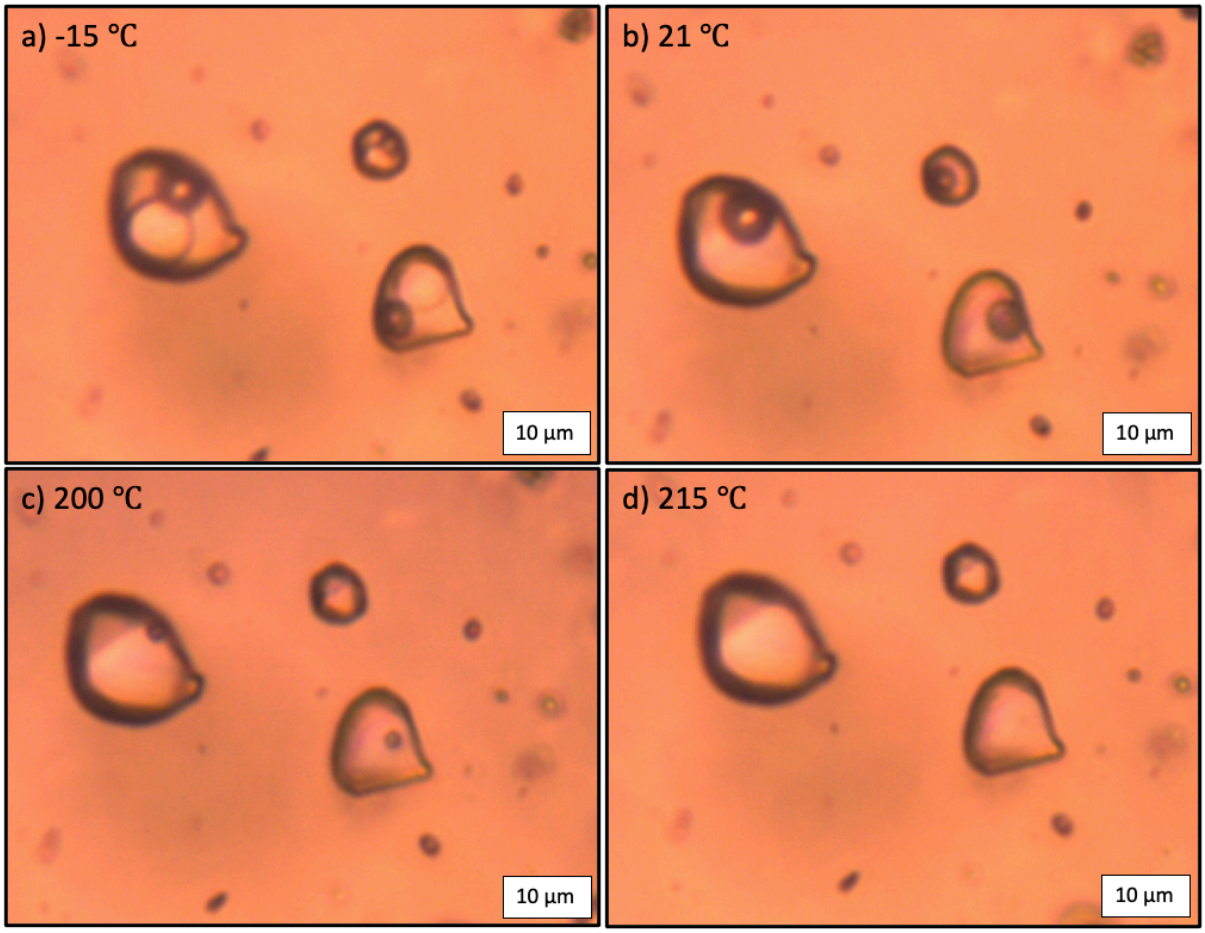

Figure 29: *Fluid inclusions in thin section TG20-002 (38850) a) At -15 °C after sufficient undercooling at -197 °C and gradually heating. Three phases are observed, solid ice crystal, gas and a liquid. During the observations, final melting temperature (T_{mf}) noted. b) Inclusions at room temperature, vapor, and liquid phase. c) Heated to 200 °C, the gas bubble sublimates in the liquid. d) Only liquid phase remains, and the temperature of homogenization (Th) is noted.*

The dataset was recorded in both excel and the statistical program R to validate the measurements. When all outliers and uncertain observations were excluded, the mean value of the final melting of ice (T_{mf}) was recorded to -10,71 °C, with a standard deviation of 4,57 °C. Total homogenization (T_h) occurred at the mean value 204,123 °C with a standard

deviation of 26,96 °C. A Saphiro test gave a p-value of first melting (T_{mi}) of 7.935e-06 and for T_h a value of 4.62e-10. The dataset was normally distributed and concluded to be worked on with (Figure 30).

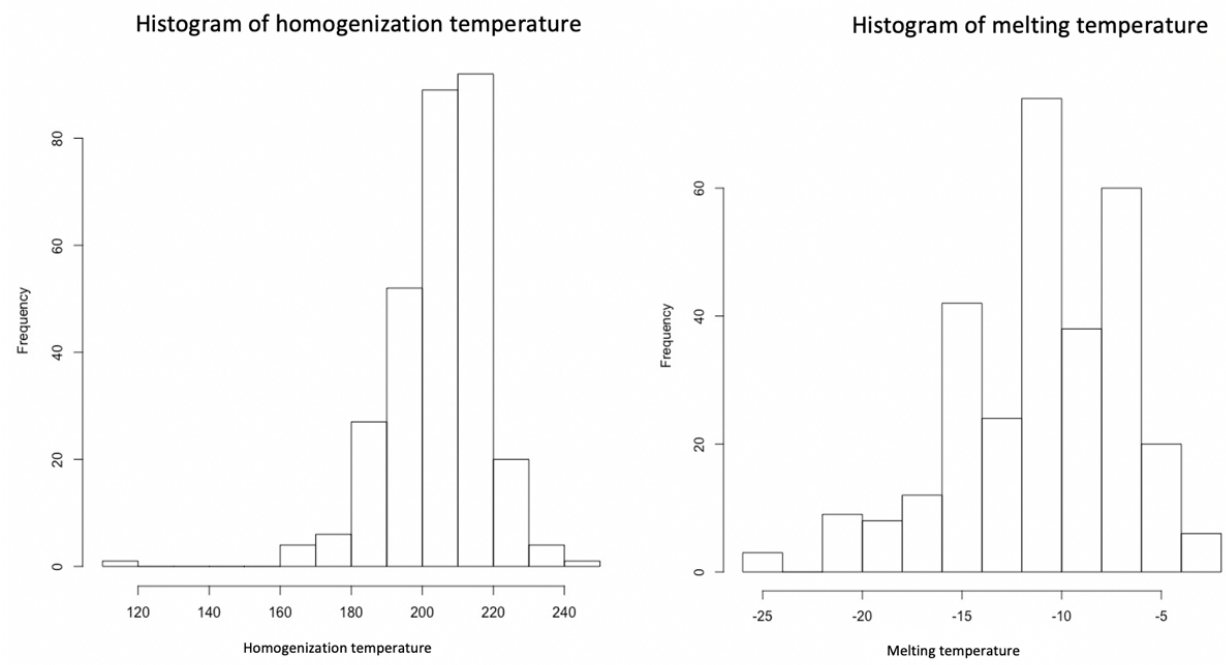

Figure 30: *Histogram of homogenization temperature and melting temperature for alle measurements performed on thin section TG20-001 to TG20-005.*

To better constrain the system is histograms of initial melting (T_{mi}) and temperature of final melt, (T_{mf}) produced (**Figure 31**). Phase diagrams for the NaCl-H_2O system, CO_2 system, H_2O-NaCl-$CaCl_2$ were used and given a T_{mi} median for hydrothermal samples of -35 °C and a T_{mi} median for magmatic samples of -30 °C, it is concluded that the system is NaCl-H_2O. However, the fact that some samples deviate with considerably lower T_{mi}'s imply that other salts such as FeCl and $CaCl_2$ may also be present together with NaCl.

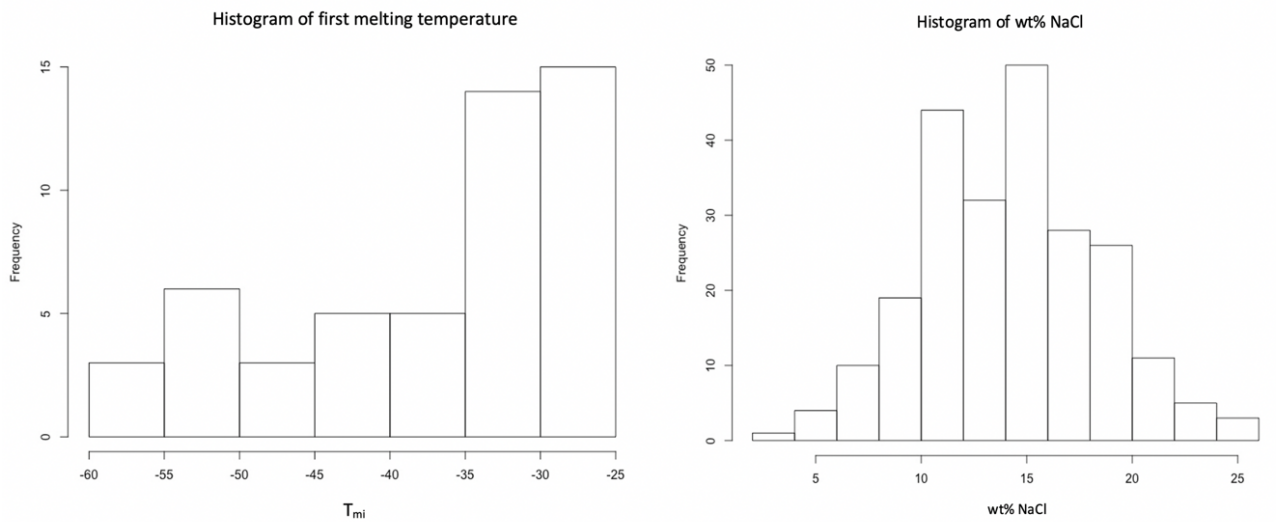

Figure 31: *Histogram of first melting temperature and wt% Nacl from thin section TG20-001 to TG20-005.*

The normally distributed histogram of salinity has an average composition of 14,27 equivalent NaCl with a standard deviation of 4,17. T_m was plotted against T_h to detect if there was any trend between melting and homogenization temperature (**Figure 32**).

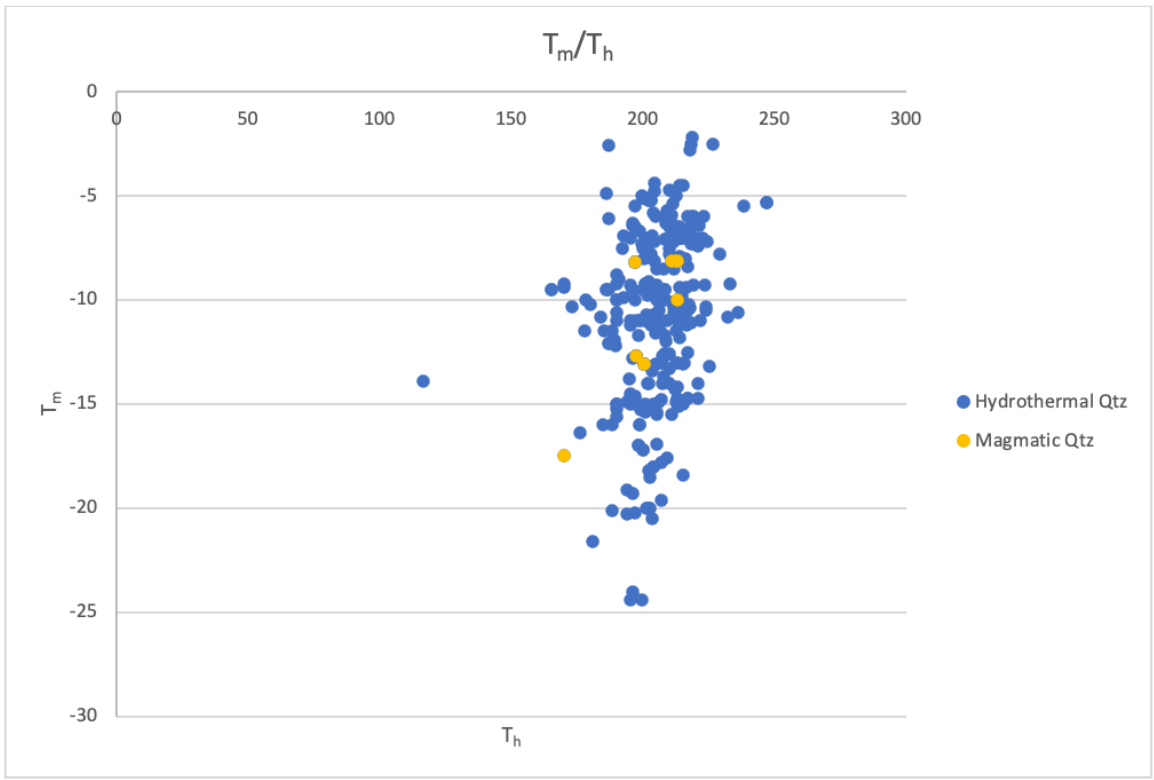

Figure 32: *Plot diagram of hydrothermal and magmatic quartz regarding to melting temperature and homogenization temperature of the fluid inclusions.*

The plots indicate a slight trend between homogenization temperature and melting temperature. Temperatures with a low melting temperature also has a lower homogenization temperature.

The hydrothermal quartz show more scatter than magmatic quartz and they are falling on the same trend line although the number of measurements on magmatic quartz is too low to make any firm conclusions (**Figure 33**).

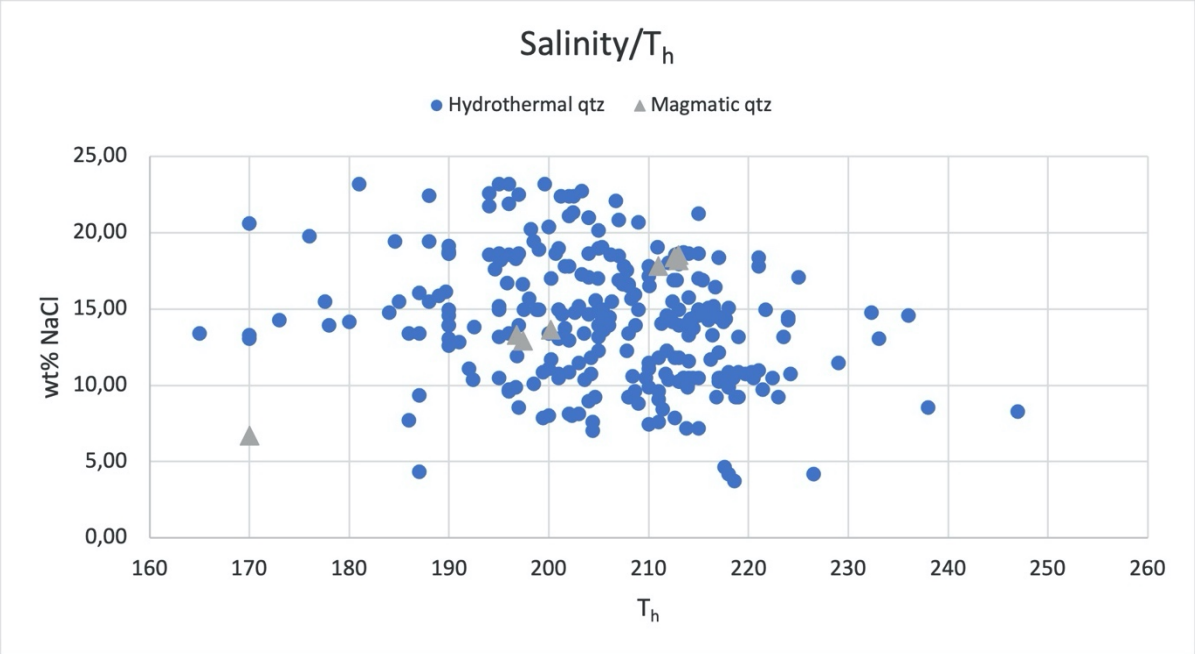

Figure 33: *Plot of T_h against wt% NaCl. Hydrothermal quartz and magmatic quartz show opposite trendlines.*

The trend of hydrothermal quartz has a negative slope number y=-0,2026x+54,793. The trend of magmatic quartz cannot be estimated due to the scarcity of samples. In conclusion, the trends are poor and a clear correlation between T_h and not found.

Variations between each section was not observed as all the analysed samples fall on the same trendline due to the same trend when salinity and density is compared, with an average salinity of 14,5wt% NaCl equivalents (**Figure 34**).

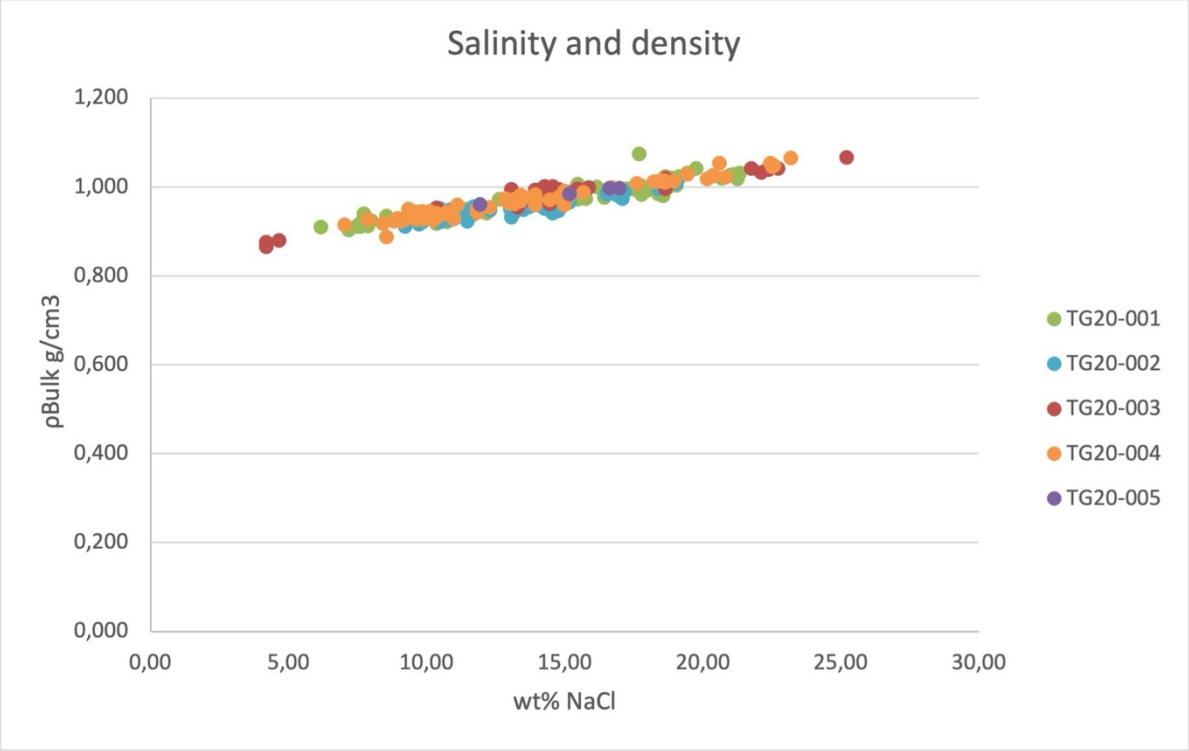

Figure 34: *Plot of all thin sections in a wt% NaC and density diagram illustrating small degree of variation.*

Calculations from the excel sheet (see section 4.3.1) provided information about both density and salinity. This information was used to produce a line with a constant density in a pressure-temperature diagram, also known as an isochore (section 5.7.2). Isochores are used to estimate the P and T of FI formation. This provided that either trapping temperature or the pressure are known, or tentatively assumed based on the mineral assemblage or other geothermobarometric constraints.

5.7 Pressure and temperature estimates

5.7.1 Fluid inclusions

The plagioclase and K-feldspar analyses from EPMA were used to calculate an average of each composition (wt%) before applying it to the Borisov A. and Aranovich L. (2020) spreadsheet (**Table 1**). Compositions of SiO_2, TiO_2, Al_2O_3, FeO_2, MgO, CaO, Na_2O, K_2O were used as input parameters to give a temperature estimate. Feldspars are also known to contain a bit of OH and some iron could be present as Fe_2O_3, so a total value of 99 were accepted inaccuracy.

The output temperature is used to assume a temperature estimate for the fluid inclusions in Hokieflincs (2012) spreadsheet. T_m and T_h from the fluid inclusions measurements are amongst the input parameters, last melting phase (ice), and salinity, T@Homogenisation, P@homogenisation, density and dP/dT are output variables. It is required to assume an independent pressure or temperature estimate based on other assumptions. The temperature estimate is based on the Ti in quartz geothermometer. The T_{output} is 384 °C. The Ti-content from the pegmatites were also used to calculate a likely temperature estimate for the system. When this is transferred to the equilibrium phase diagram of Ti we can see that such low contents the temperatures are likely <500 °C.

Detection of differentiates between hydrothermal and magmatic quartz is found when plotting pressure and salinity against each other (**Figure 35**). The salinity is equal, but the pressure is lower.

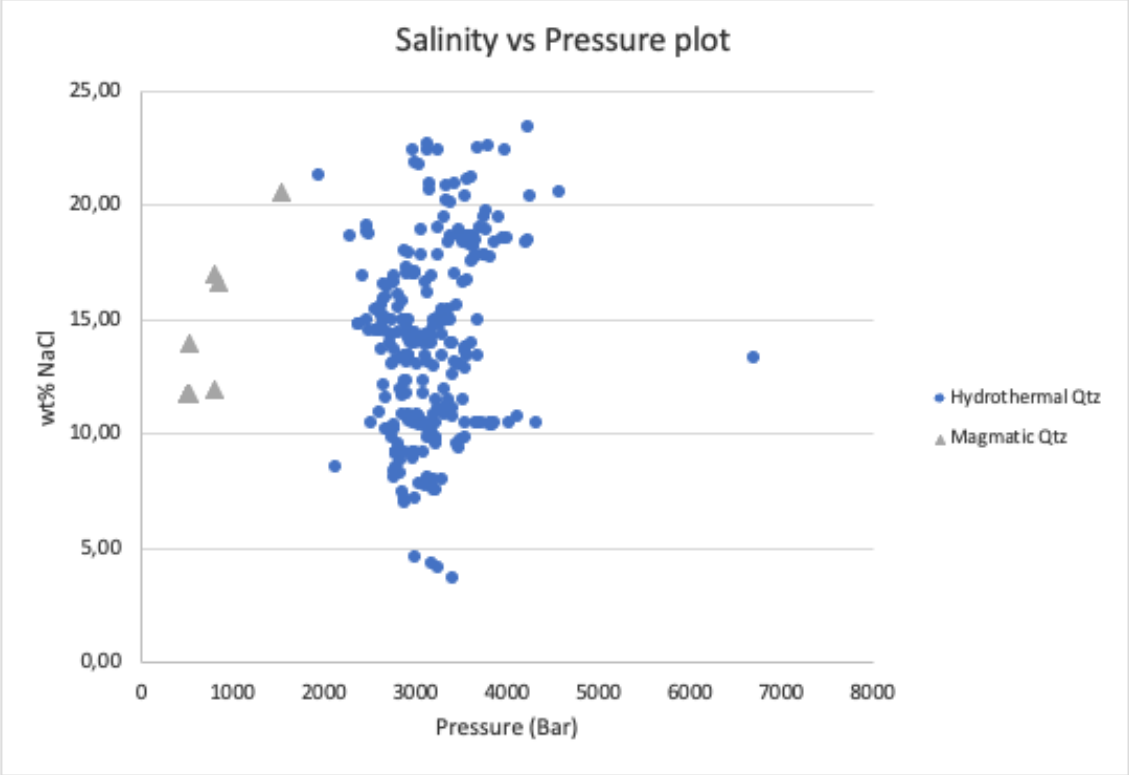

Figure 35: *Pressure and salinity plotted against each other. The blue dots are hydrothermal Quartz analyzed from section TG20-001 to TG20-004. FI measurements from the pegmatite were difficult to collect, and only eight samples were politely and included.*

5.7.2 EPMA

As the isochores from fluids inclusions are combined with the isochores from TitaniQ, T of 450-550 °C and P of 3,4-5,2 Kb. The orange square is included to indicate the variety it can have been formed under. Even if the fluid inclusions are believed to be formed under precisely equal pressure and temperature conditions within an FIA is it not possible not know if this is the case. The synthetic fluids inclusions are reasonable reference points, and the variation within salinity is therefore included.

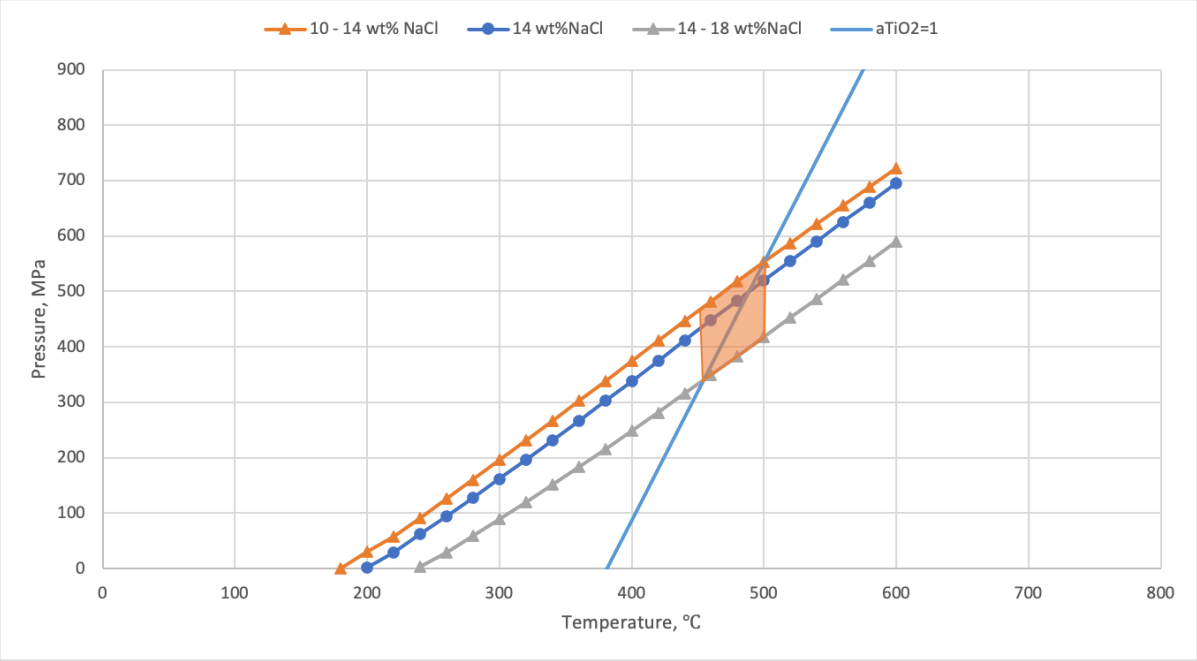

Figure 36: *Isochores from fluid inclusion plotted with average composition ± standard deviation, against TitaniQ isochore from Wark and Watson, 2010.*

6. Discussion

6.1 The mineral assemblage

The petrographic description is divided in two sections. The first concerns textures belonging to the hydrothermal phase (section 5.2.1) whereas the other sections is on the magmatic (section 5.2.20). Hydrothermal quartz indicate low-temperature plasticity, due to dynamic recrystallization such as both grain boundary migration (GBM), subgrain rotation (SGR) and bulging (BLG)(**Figure 13**). Indicators of low-temperature transformation includes formation of perthite. In the transition zone between the magmatic quartz and the hydrothermal quartz vein in TG20-004 is intragranular alteration in the plagioclase is observed. Opaque minerals are wrapped in chlorite, recognised by the green colour in plan polarized light, undulating extinction and pleochroic halo. Both sericitization (to fine grained muscovite) and saussuritization (to muscovite and some epidote) was observed, but difficult to distinguish in optical microscopy. Both are phyllic alteration products, being an evidence of the hydrothermal transition (**Figure 15**). The alteration products could be formed by hydrolysis of feldspar. They typically form over a wide range of temperatures and is a common mineral assemblage of hydrothermal ore deposits. The acidic reaction (Kfs ↔ ms + qz) only require the presence of H^+ ions (formula 5).

$$^3/_2\, KAlSi_3O_8 + H^+ \leftrightarrow {}^1/_2\, KAl_3Si_3O_{10}(OH)_2 + 3SiO_2 + K^+ \qquad (5)$$

The hydrothermal solutions percolated through fractures during H^+ consumption by wall-rock reactions. This contributed to an increase in fluid pH that changed the prevailing fluid properties.

Change in fluid properties or temperature drop are two common mechanisms to cause precipitation of ore-forming minerals (Robb, 2005). SEM analysis confirmed the field observations that cassiterite (SnO_2), magnetite (Fe_3O_4), rutile (TiO_2), and ilmenite ($FeTiO_3$) formed from the hydrothermal event is present (Section 5.3) at Klepsvatnet. Cassiterite can be present in oxidizing conditions as the quadrivalent Sn^{4+}, and in reducing conditions as both Sn^{4+} and divalent Sn^{2+} (section 2.1.3). In this acidic system tin may have been transported as hydroxychloride $Sn(OH)_2Cl_2$ at low temperatures over far distances. A temperature decrease is expected as the fluid migrated away from the heat-source and through fractures into a cooler host rock. This process could facilitate precipitation of cassiterite.

But also, evidence of phyllic alteration from the thin sections indicate a system moving towards oxidation and increasing pH while the fluid/rock ratio decreased. Cassiterite was normally observed where hydrothermal quartz intersected the pegmatites. Accordingly it appears that reactions with the pegmatite changed the fluid properties towards destabilization of cassiterite. The frequency of sericitization and saussuritization decreased with increasing distance away from the quartz vein in section TG20-004. Thin section TG20-005 was sampled further away from the hydrothermal quartz and sericite it observed to a much lesser extent. As the system evolved towards more oxidizing conditions and higher pH the Sn^{2+} complexes were destabilized and cassiterite precipitated probably dominated by the reaction

$$SnCl_x^{2-x} + 2H_2O = SnO_2 + 2H^+ + xCl^- + H_2^0 \quad (6)$$

The next identified minerals Ilmenite ($FeTiO_3$) and Magnetite (Fe_3O_4) are variations within Fe-oxides. The majority of iron in aqueous solutions are transported as the divalent Fe^{2+}, as the ferric Fe^{3+} is less soluble and only forms under relative oxidizing conditions. Dissolved iron does not preference hard or soft bases in the aqueous solution implicating a great variety of metal-lingand complexes, such as Cl^-, OH^- and HCO^-. When hydrolysis is present in the system the hydrated Fe^{2+} ion is implicated in fluid transport. These minerals can be present as accesory products in the phyllic alteration assemblage, and are associated with high temperatures (500-600°C). The assemblage can also be transferred into the paragenic sequence in many hydrothermal ore deposit (Robb, 2005) from (Guilbert and Park, 1986). Molybdenum and Cassiterite fit into the mesothermal part of related alteration assemblages.

Ti in quartz geothermometry is a growing discipline since it is more stable during secondary processes than feldspar and micas (Section 2.4.5 and 4.5). CL-patterns from hydrothermal quartz generally varies from CL-free signatures to occilatory zonation (Breiter et al., 2020). Sample TG20-004 shows even homogeneous CL-colours in quartz from the hydrothermal vein which indicates only one growth episode from the aqueous fluids (section 5.4). Decreasing temperatures during the magmatic hydrothermal transition are documented by systematically decreasin in Ti in quartz, so values of Ti_{max}= 30 ppm and Ti_{min}<3 ppm can indicate a low-temperature late stages.

EPMA-data shows that Al and Ti are present in both the hydrothermal and magmatic quartz, but CL-pattern from magmatic quartz are distinctly different.

The prominent zonation pattern In the pegmatitic quartz from SEM-CL recordings show dark cores and bright rims. This indicates higher Ti at the rim and decreasing amounts towards the core. This is opposite the typical sonation pattern for magmatic quartz (Breiter et al., 2020). The Ti/Al relationship from EPMA of both hydrothermal and magmatic quarts are quite equal with an average of only 1,53 ppm separating them. The CL signatures can be affected by other factors than the Ti content, but a visual and tangible difference is observed. The diversity of CL-intensities can be due to the sensitivity of the detector since it is panchromatic. The result is only showing the amount of light on a photo, a relative result dependent on brightness and contrast settings. Different defects have different voltages (e.g Ti=2,7 V), and the results is based on several wavelengths, not only one. It was expected a difference in pressure/temperature conditions for the magmatic and hydrothermal quartz, here firstly identified by CL.

6.2 Pressure and temperature estimate

Rosing-Schow et. al (2020) leaves the unanswered question of the temperature and pressure conditions during the formation of the Sweconorwegian pegmatites. Furthermore, she explains how fluid inclusion studies can reveal the composition and the spatial relation to the granites in depth. Measurements from this thesis may contribute to a deeper understanding of the magmatic hydrothermal transition in Tørdal.

Plot of the FI-dataset seems to indicate a slight trend of increasing T_h with increasing T_{mi}, and the Pearson's correlation test had a p-value of 0,07 being statistically significant. However, there are not enough data points to make this conclusion with certainty. Fluid inclusions in the magmatic quartz had experienced post entrapment changes, and only eight reliable measurements were sampled. Nevertheless, based on the prominent presence of well-preserved fluid inclusions in the pegmatite, crystal growth in the presence of a fluid phase may be confirmed. These, and fluid inclusions from the hydrothermal quartz are base for the microthermometric measurements.

The FI's belong to the NaCl-H_2O system, dominated by a salinity varying from ~3,71 wt% to ~24 wt%. T_{mi} for this system is -21,1 °C, and the eutectic point lies at 23,3% salt. This binary system is well studied and thermodynamically very well constrained. The lowest pressure and temperature conditions are defined at the dew point curve for a specific density, the phase boundary between liquid and vapor. The salinity is therefore plotted against the homogenisation temperature, weakly indicating an increasing T_h and decreasing salinity in hydrothermal quartz, while increasing salinity with increasing T_h in magmatic quartz. (Figure 32). This may indicate inclusions being captured at equal temperatures in a system with reducing salinity for the hydrothermal veins. The fluids may be equilibrated chemically and isotopically prior to their ore-deposit site, in which they are transported through a cooler environment. This magma evolves from high salinity to low salinity due to the common dilution effects of these systems. The concentration of salts is declining as the first aqueous fluids escapes. Accordingly, aqueous fluids subsequently unmixing from the melts will have progressively lower salt concentrations. The first Cl aqeuous fluids to form increase the solubility of many incompatible elements that complex with Cl, e.g Sn, Fe, Na etc. As the system evolves, the salinity decreases. Less water is saturated in the melt, and the system has less of the intermediate Cl to complex in the aqueous solutions, also dependent on the pressure and temperature.

The temperature range between 450 – 500 °C with a pressure between 3,5-5,5 MPa. This is relatively high for these fluids but is a good match for a system dominated by cassiterite and molybdenite, as they may form at high T conditions, particularly when the pressure is high (section 5.7).

6.3 The magmatic hydrothermal transition in Tørdal

6.2.1 Igneous differentiation

The pegmatites are formed during extension after the Sweconorwegian collapse and is dated to ca. 900 Ma. The large-scale tectonism caused great temperature and pressure conditions at amphibolite-facies conditions. Since the surrounding bedrock is amphibolite, the probability of this being the source rock of both the Tørdal-granites and the pegmatites increases.

The variations regarding salinity and homogenisation temperature should be considered with caution, due to the fact that all samples originate from the same quartz vein.

Previous articles from the Tørdal area contains an abundance of information on the mica chemistry, K/Rb ratios from K-feldspar and dating of the igneous evolution (Granseth et al., 2020; Rosing-Schow, Müller, & Friis, 2018a; Steffenssen et al., 2020). The pressure and temperature estimate is a supplement to already existing result. The technique regarding K/Rb and Rb/SR relationship provides information about the igneous differentiation because K and Sr are compatible in these granitic systems whereas Rb is incompatible. Accordingly, the greatest enrichment of Rb is expected in the most evolved parts of the pegmatite (Simmons & Webber, 2008). The Tørdal pegmatites appear quite primitive, indicating a less fractionated pegmatitic melt because they are plotting with high K/Rb and low Rb/Sr ratios. The most primitive pegmatites have highest K/Rb values while the most evolved has higher Rb/Sr. Also compared to other granitic pegmatite fields such as Tanco, Red Cross Lake and Greer lake (**Figure 3**) does exacly these sections represent a primitive pegmatite part, but it must be noted that great variations are previosly proven in the Evje-Iveland pegmatite field (Larsen, 2004).

The final generation of hydrothermal veins are recognized in the field as discordant veins cutting the earlier pegmatite generations. This vein turns out to be the intensely Sn-Mo mineralized generation, as confirmed in the field by the mapping of (Wilberg, 1983). Pegmatite genesis indicates that the final phases of melt often are the most primitive, since the residual melt are scavenged of incompatible elements (Robb, 2005). The pegmatites lie adjacent to the Tørdal granites so they could represent the absolute final phase of melt from this intrusion. However, recent gechronology revealed over 40 Ma years difference and by that indicating that the pegmatites may not be derived from the same magmatic event(Rosing-Schow, 2020). However, an equal parent of pegmatites and the Tørdal granite is likely due to similar Pb isotope signatures but with different ages of origin.

It is proposed that a melt by direct anatexis of proper lithologies can gain equal composition as a pegmatite melt formed by protracted fractional crystallization (Simmons & Webber, 2008). The ore-forming minerals reveal that fluxing components and incompatible elements probably was present in the system fed by the meta-sedimentary host rock. It also indicates that they must have been sourced into the low-degree partial melts, as if they were derived from a magma chamber by igneous differentiations. This sourcing is dependent on the chemical composition of the source rock, and critical factors for the formation of rare element pegmatites is the presence of B, F, P, and Li combined with H_2O and other network modifying components (Thomas et al., 2012).). The source rock can be more related to the composition of the pegmatites rather than the tectonic setting. Of course, the pressure and temperature conditions will also be controlling factors of the degree of partial melting. Given the right conditions, the nucleation rate and the melt polymerization is lowered, while the diffusion rate increases. This sourcing argues for why the final phase of quartz vein formation might be the most mineralizing events, as differentiation is not the mechanism to determine the order of enriched fluids, but partial melting. The previous generations of primitive pegmatites are not necessarily related to the first liquids escaping from a differentiated magma chamber, but of melt derived from partial melting.

The properties of the melts and the escaping hydrothermal fluids are often generalized by the commonly accepted pegmatite families, LCT or NYF (section 0). Discussions regarding the classification of the Tørdal-pegmatites as NYF or mixed class are ongoing. Several NYF-elements such as Nb and Sc are precent but LCT elements such as Li, Sn and Be are also common (Bergstøl & Juve, 1988). Mapping of the Nb-rutile revealed strong signatures of $Nb_{average}$ = 429 and $Y_{average}$ = 196, indicating an affinity to NYF pegmatites. The observed rare earth elements (Ho, Yb, Er, Dy, Gd, Ti and Zr) is also associated in NYF-type pegmatites. Observations of beryl points towards LCT pegmatites. Mixed pegmatites can plot with NYF pegmatites in the metaluminous area, even if their minerals resemble both groups.
A classification of the Tørdal pegmatites being of a mixed class sounds reasonable (Ihlen & Müller, 2009; Rosing-Schow, 2020).

6.4 Origin of the Tørdal pegmatite field

The Sweconorwegian orogeny underwent multiple events, both geographically and tectonically between 1140 to 920 Ma, before the extensional collapse phase. The post-orogenic extension was followed by mafic underplating causing heat-induced melting, which both the Tørdal granite and the Tørdal pegmatites seems to be derived from (Rosing-Schow, 2020). As a conquence, the hydrothermal fluids are also ultimately related to the underplating event. Both the Tørdal-granites and the pegmatite field, is probably formed by partial melting of the amphibolites (Rosing-Schow, 2020). However, partial melting of the Tørdal-granite or the surrounding amphibolite can also be the source for the 40 Ma younger pegmatites (Rosing-Schow, 2020).

Calculations of the pressure and temperature conditions represented in this thesis, seems to fall within the precipitation conditions of the observed ore-forming minerals. The P and T conditions also seems to lie inside the amphibolite-facies at P-T diagrams, supporting the origin. Field observations from Tørdal show that the pegmatites appear to grow out of the magmatic amphibolite over a very short melting distance, also confirmed by the enrichment of Sc (Steffenssen et al., 2020). All pegmatite generations are probably derived from a limited area since they cluster in an isolated area, perhaps indicating short -distance melt migration. They cut each other discordantly and are easily separated. The fluid inclusions for the final hydrothermal events are well preserved, indicating both water over-saturation and minimal overprinting by later events. The relatively high pressure imply that the ore-forming melts must have been very rich in dissolved water prior to formation of the magmatic hydrothermal fluids. It is difficult to point out the precise mechanism exsolving water from the melt, i.e the magmatic hydrothermal transition. But during melt migration through cooler fractures increased the distance to the melt-induced heat source, combined with continous wall-rock reactions changing the chemical properties of the melt. The transition to hydrothermal fluids are evidentially found in alteration products identified in the thin sections. The acidic system with high activity of H^+ had also high abundances of positive charge and low pH. As the system was percolating through fractures H^+ ions could be consumed by wall-rock reactions and the fluid/rock ratio decreased.

This contributed to an increase in fluid pH that changed the prevailing fluid properties. These changes facilitated destabilization of the ore-forming complexes and facilitated precipitation of magnetite, ilmenite, cassiterite and rutile (section 5.3).

6.5 Comparison to pegmatites of Land's End

This chapter aims to represent the diversity of granitic pegmatites caring ore-forming minerals. The genesis of Cornwall and Tørdal will be compared with respect to pressure, temperature, and the composition of the magma-derived ore-forming hydrothermal fluids. The results from microthermometry on fluid inclusions, trace elements in quartz and feldspar and added SEM-CL performed by Drivenes et. al (2016) is discussed.

6.5.1 Petrogenesis

Both Cornwall and Tørdal are emplaced during orogenic collapse. The youngest Land's End pluton originate from the Variscan Orogeny, emplaced about ~275 Ma, and the Tørdal pegmatite field is derived from the collapse of the Sweconorwegian orogeny, ~900 Ma. The Land's End granite is a part of the Cornubian batholith, comprising five granitic complexes. Continuation of this thesis will be focusing only on the Land's End complex where the magmatic hydrothermal transition and the formation of Sn-deposits are particularly well studied (Drivenes, 2015; Müller et al., 2006). The Lands End originates from peraluminous, S-type melt whereas Tørdal is more uncertain with both S and I type signatures (Rosing-Schow, 2020). Both origins are somewhat controversial, but The Land's End granites may be differentiated from a single reservoir.

The formation history of the Tørdal pegmatites has recently been revised. Both by implying an anatectic origin by heat-induced melting and by implying that they are NYF-pegmatites originating from I- or A-type melts that are subalkaline with enrichments of REE. LCT-pegmatites are normally derived from peraluminous melts formed by partial melting of quartzo feldspatic sediments with low contents of REE. The pegmatites from both The Land's End and Tørdal areas have some enrichments in REE. As previously discussed, the degree of differentiation is often the primary mechanism determining the evolution of each generation connected to a pegmatite field. Combined with the degree of differentiation, the composition of the magma-derived ore-forming hydrothermal fluids is important. The protolith of the Tørdal pegmatites is either partial melting of the Tørdal granite or the host rock amphibolite. The protolith of the Land's End granite is voluminously feldspar-rich greywacke, giving a composition of sedimentary material with dominating continental footprints. The granites of the Land's End are peraluminous with a high K-content and indications of high-grade differentiation due to high values of Rb, Cs, Pb, Ta, Sn and Nb.

The great popularity of the area is closely related to its rich Sn-Cu-As deposits, genetically representing a relationship between hydrothermal mineralisations and granite intrusions. This chapter will illustrate the essential factors that contributes to these mineralizing ore-forming fluids in different tectonic environments.

Both scenarios have evidence of multiple intrusive events. The main stages in Cornwall are separated by (1) Megacrystic fine grained biotite granite, FGG, (2) megacrystic coarse-grained biotite granite, CGG and (3) fine- to medium grained porphyritic and equigranular Li-sideophyllite granites, all fed by dykes. In Tørdal, the main stages a pre-pegmatites quartz vein, three generations of pegmatites and a post-pegmatitic quartz vein. Their evolution is more unknown, but some comparison can be made.

6.5.2 Magmatic hydrothermal transition

Comparison of the situations will be concentrated around the magmatic hydrothermal transition in Cornwall, rather than the whole petrogenesis. Multiple generations indicate an evolving system, with known processes such as dilution and differentiation (Drivenes et al., 2015). Trace-element fingerprints in tourmaline during the evolution of granitic melt to a pneumatolytic stage, is one of the most preferred and reliable methods regarding The Land's End granites. The Massive Quartz Tourmaline (MQT) are studied in detail as they were formed at the transition from the magmatic to the hydrothermal stage (section 3.2) and three main quartz generations are defined. The primary quartz with bright CL, overprinted by secondary quartz and the final hydrothermal quartz with relations to cavities. The most interesting part concerns the hydrothermal processes. CL patterns from the final hydrothermal quartz are identified as low luminescent, overprinting and truncating earlier quartz generations along grain boundaries, along fractures and in mineral inclusions. Typically euhedral grains with oscillatory zoning. The hydrothermal quartz also had significally higher content of Sn and Sr, and were isotopically heavier. CL-signatures from the hydrothermal quartz vein from Tørdal are also low lumicent and homogeneous. Samples were only sampled from one vein, but that whole fracture are filled with only hydrothermal quartz. This can indicate one growth episode in an high temperature environment and low enrichments of Ti, also with enrichments of Sn.

Where zonation is missing from the Land's End, it is proposed that the magmatic growth-stages was followed by hydrothermal overprinting. Also, quartz might lose its CL signatures by metasomatic processes in post-magmatic environments. CL-images of magmatic quarts is also conducted to understand the evolutionary history.

Occurrences of light core zonation and no zonation are observed in the magmatic fine-grained matrix quartz and the MQT-orbicules from The Land's End, so great variations are prominent. The CL signatures from the magmatic Tørdal quartz indicate a high-temperature environment with decreasing Ti from margin to core. A significant isothermal drop in pressure could have allowed higher Ti in newly formed quartz grains to give a brighter CL signature and explain the Tørdal SEM-CL pattern. The contacts are wavy, indicating episodes of resorption. Drivenes found abundant evidence of a correlation between Ti contents and the CL-intensity, and this is also generally accepted in the literature (Breiter et al., 2020; Drivenes et al., 2016; Müller et al., 2006). This indicates that the trends of a magmatic orbicule quartz at Lands End and Tørdal is opposite (Figure 37). From magmatic quartz in Tørdal there is no correlation between CL-intensity and Ti found during single grain analysis, however, several of the analysis were below the limit of detection i.e. this conclusion is uncertain.

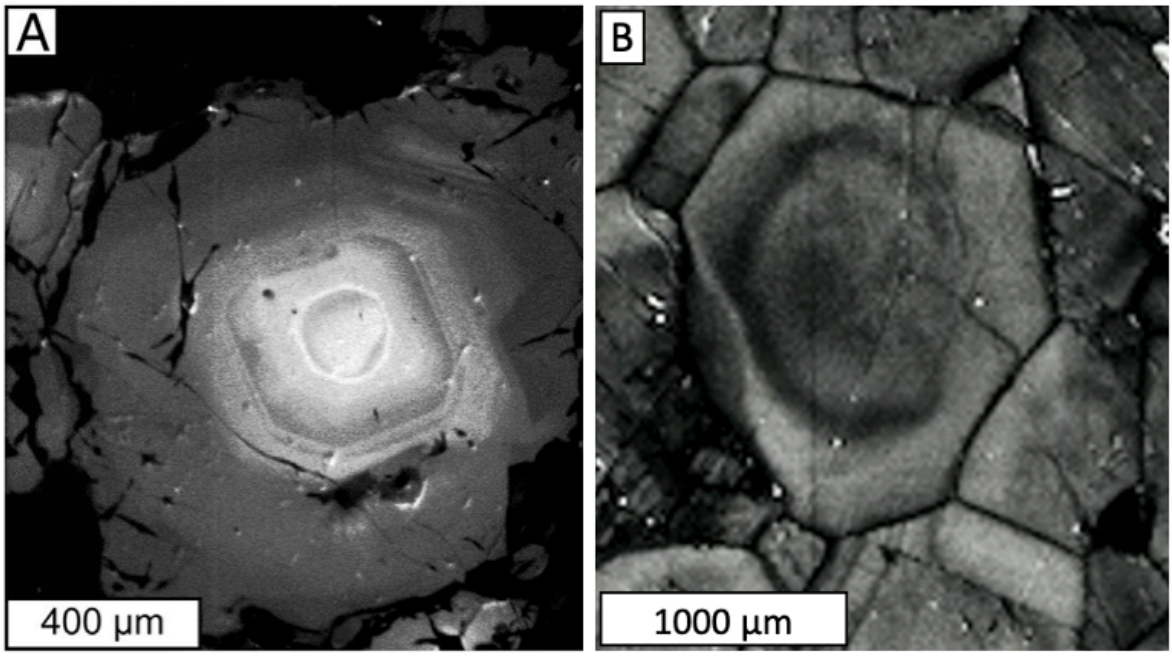

Figure 37: *A) From The Land's End granite, light core with decreasing intensities towards the rim. B) Opposite trends from Tørdal, with a dark core and light randzone.*

Bimodal distribution of the Ti content from The Land's End are assumed to show both the primary quartz evolution and later overprinting by the hydrothermal quartz generation. Despite this, caution should be applied when considering the ratio between Al/Ti. The incompatible Al ratios depends strongly on the peraluminousity of the melt, water and flux components of the melt while Ti are compatible (Drivenes et al., 2016; Larsen, 2004). Drivenes et. al (2016) managed to detect an increasing differentation from the granite to the MQT, but in the final stage it was overprinted by the hydrothermal fluids prominent as CL intensities with lower grey scales. He tried to explain this overprint by resorbtion by the hydrothermal fluids. Any precice Ti measurements of the hydrothermal quartz is not taken. Müller et. al (2006) also got values below detection limit (33 ppm) during his analysis of the overgrowing hydrothermal quartz from the MQT samples. Despite this was high Al values detected in both cases, indicating enrichment of Al in a transitional phase where both hydrothermal and magmatic components co-existed. This assumptions is based on both the Fe-content, CL-pattern and mobility of K- and Na-. To make similarities to the hydrothermal vein in Tørdal, also here we had several of the analysis below the detection limits for both Ti and Al. The increased content of Al from magmatic quartz to hydrothermal quartz is not detected, and it can with great uncertainty indicate a more strict transition from magmatic to hydrothermal. No field evidence show that several phases co-existed in the field area, and some of the pegmatite vein actually demonstretes a gradual transition from pegmatites to hydrothermal quartz veins (Steffenssen et al., 2020; Wilberg, 1983). In a sense, this is the most tangible evidence for the magmatic-hydrothermal transition in Tørdal.

The evolutionary path of the hydrothermal fluids may be better understood by studying fluid inclusions. The main difference is the amount of data used to produce results and draw conclusions. Drivenes had measurements from different localities as his goal was to determine the gradual evolution of the system. Different phase relations separated the inclusions into three groups. Type I (liquid water and vapor), type II (liquid water, vapour and halite crystal), and the final type III (liquid water, vapor, halite crystal and a second tabular solid) (Drivenes et al., 2016). Only the final stages of the hydrothermal continuum are analysed from this study, with well-preserved fluid inclusions without any later overprints. The phase relations found in Tørdal was liquid water and vapor, equal to type I from the Land's End granite.

Since Cl partitions in favor of the aqueous phase rather than the silicate melt, type III inclusions are believed to be the first hydrthermal fluids in the Lands End system,follwed by type two and type one, representing the internal magmatic event (Drivenes et al., 2016). Type I is also the most prominent type. This is a challenging point as the hydrothermal overprinting fluids from The Lands End system does not have any fluid inclusions, and thereby no analysis from it. This is opposite of the situastion in Tørdal, where almost all measured inclusions are from the hydrothermal quartz vein. Only eight reliable measurements are sampled from the magmatic quartz.

The hydrothermal fluids at Lands End belongs to the H_2O-NaCl-CaCl system whereas Tørdal belongs to the H_2O-NaCl system. Another difference is the great range of temperatures for the Land's End LV-inclusions (type I) lie within, with Tm_{ice} -8,5 °C to -31,0 °C, and T_h from 134 °C to 429 °C. As both environments contain salty solutions, phase separation in highly saline fluids may happen at higher P and T than salt poor solutions. Remarkably, the salinity in the inclusions increases as the system moves towards higher P and T because the concentration of water is doubled from 1 to 3 kBar, so a pressure increase saturates the melt in more water. In the Land's End granite a drop in pressure is thought to have formed greater volumes of aqueous fluids and facilitate dilution regarding the salinity. But phase separation of a single fluid is not believed to have formed the fluid inclusions, but a gradual equilibrating flow between the silicate melt and fluids during different stages of crystallization. All of the samples from Tørdal were sampled from the same locality, and interpretations of the evolutionary path for the fluid inclusions is not obtained. Also, the amount of data from magmatic quartz from Tørdal is not sufficient to discuss changes in pressure or temperature. The calculated P-T condition is only fit for the hydrothermal quartz, but still indicating a system of high pressure and temperature conditions.

An interesting detail to point out is the great amounts of Molybdenite in Tørdal, but not in The Land's End. Only field observations and existing litterature is base for this part of the discussion, as none of the analysis reveal exact what triggered the different events. During Second World War was Mo mined in Tørdal, and Cu-W in Cornwall. Generally are Cu-Mo typically assosiated with I-type or "calc-alkaline" magmas and separated into two groups.

In the first subdivition is Cu- most prominent with only accesorry amounts of Mo referred to as Cu-(Mo), while the second divition is opposite, with great amounts of Mo and Cu to a smaller extent known as Mo-(Cu) (Robb, 2005). The difference is controlled by the water content and pressure. The magma forming Cu-(Mo) deposits are emplaced at more shallow levels where the low pressure ensure low water saturation. Vapor-saturation occurs early, and despite the fact that Cu is compatible has only small amounts crystallized at this point. Cu will favour to enter the Cl^- rich vapour phase, and the granitic melt is scavenged. Mo is incompabtible with a small partitioning coefficient and are also unaffected by Cl^-, so significant consentrations in the fluid phase will not be attained. This might be the case for The Land's End, as its evolution is believed to be differentation from a magma chamber, and high amounts of Cu is deposited by the hydrothermal veins.

By contrast has the Mo-(Cu) scenario a higher water content, and the magma is emplaced at deeper levels. Due to both higher pressure and water content is degree of crystallization greater before archievement of water-saturation. This early crystallization extract the melt of Cu while the concentration of Mo continues to increase in the residual melt. At saturation is Mo concentrated into its favorable partion coefficient, a H_2O-fluid phase. The residual melt is depleted of the compatible Cu, and significant concentrations will not be partioned.

The discussion of the Tørdal pegmatite being of anatectic origin must be concerned here. Well preserved fluid inclusions and relatively high calculated pressure imply that the ore-forming melts must have been very rich in dissolved water prior to the formation of the magmatic hydrothermal fluid. This votes well for the hydrothermal veins carrying Mo, and the situation may be transferred to equal mechanisms, only dominated by the degree of partial melt rather than differentation in a magma chamber. That is assumptions about Tørdal, and the evolution of the Land's End granite is proposed to be early crystallization of quartz cores with dark CL at ca. 640-840 MPa. Followed by transportation to 550 MPa where the main magma is deposited and the majority of the phenocrystic quartz develops, befor they are being transported through tectoic structures to emplacement level at 300 MPa (Drivenes et al., 2016). The system has a great range of both pressure and temperature conditions, but no pressure estimate is calculated on the final hydrothermal veins. An interesting annontation is that in Cornwall are Cu in a degree accompanied by W instead of

Mo, even though W is normally not accosiated with Cu-Mo deposits. W is not found in The Land's End, but in Roche Rock, anouther part of the Cornubian Batholith and therefore presented. In a peraluminous hydrous melt with reducing conditions behaves W as incompatible and Mo will behave more compatible. When the H_2O-fluid phase exsolve in the highly differentiated melt with enrichments of W is the melt scavenged of W, giving higher amounts of W and minor Mo.

7. Conclusion

By analysing samples from the ore-forming hydrothermal veins in the Tørdal-Treungen pegmatite field, was temperatures ranging from 450°C-550°C and a pressure between 340-520 MPa estimated. These calculations are based on microthermometry of fluid inclusions and EPMA analysis of Ti- in quartz. The high P/T conditions agree especially to the precipitation of the identified ore minerals, Cassiterite and Molybdenite. The mineral assemblage and textures identified by optical microscope and SEM-analysis gave important information regarding the hydrothermal processes. Phyllic alteration products and great amounts of magnetite and ilmenite tell a story about fluids moving from acidity towards oxidation during decreasing fluid/rock ratios. Differenties in SEM-CL signatures from the magmatic and hydrothermal quartz indicate an evolving system, even if no correlation between Ti-content and CL-signatures was documented. Documented Nb-Y-Fe in an detailed EPMA-mapping of a Nb-Rutile indicate a system with NYF-affinity, feeding the assumptions of the Tørdal-pegmatites being a mixed-class rather than LCT, despite occurences of LCT characteristics. Small degree of variation in the salinities, field observations and the final events being the most mineralised confirms previos assumtions about the system being formed directly by anatecic rather than differentation from a magma chamber. This announce that tectonically settings with a highly induced heat-source, can form NYF-pegmatites carrying ore-foming minerals, if the right persisquents are present.

8. References

Bergstøl, S., & Juve, G. (1988). Scandian ixiolite, pyrochlore and bazzite in granite pegmatite in terdal, Telemark, Norway. A contribution to the mineralogy and geochemistry of scandium and tin. *Mineralogy and Petrology, 38*(4), 229-243. doi:10.1007/BF01167090

Bingen, B., Nordgulen, Ø., & Viola, G. (2008). A four-phase for the Sveconorwegian orogeny, SW Scandinavia. *Norwegian journal of geology, Vol. 88*, pp 43-72.

Bodnar, R., Burnham, C., & Sterner, S. (1985). Synthetic fluid inclusions in natural quartz. III. Determination of phase equilibrium properties in the system H2O-NaCl to 1000 C and 1500 bars. *Geochimica et Cosmochimica Acta, 49*(9), 1861-1873.

Bodnar, R. J. (2003). Introduction to aqueous-electrolyte fluid inclusions. *Fluid inclusions: analysis and interpretation, 32*, 81-100.

Borisov, A., & Aranovich, L. (2020). Rutile solubility and TiO2 activity in silicate melts: An experimental study. *Chemical Geology, 556*, 119817.

Bott, M. H. P., Day, A. A., & Masson-Smith, D. (1958). The Geological Interpretation of Gravity and Magnetic Surveys in Devon and Cornwall. *Philosophical Transactions of the Royal Society of London. Series A, Mathematical and Physical Sciences, 251*(992), 161-191. doi:10.1098/rsta.1958.0013

Breiter, K., Ďurišová, J., & Dosbaba, M. (2020). Chemical signature of quartz from S-and A-type rare-metal granites–A summary. *Ore Geology Reviews, 125*, 103674.

Burnham, C. W. (1979). Magmas and hydrothermal fluids. *Geochemistry of Hydrothermal Ore Deposits.*, 71-136.

Chappell, B. W., & Hine, R. (2006). The Cornubian Batholith: an Example of Magmatic Fractionation on a Crustal Scale. *Resource geology, 56*(3), 203-244. doi:10.1111/j.1751-3928.2006.tb00281.x

Chen, Y., Clark, A. H., Farrar, E., WASTENEYS, H. A. H. P., HODGSON, M. J., & BROMLEY, A. V. (1993). Diachronous and independent histories of plutonism and mineralization in the Cornubian Batholith, southwest England. *Journal of the Geological Society, Volume 15*(Issue 6), 1183-1191. doi:https://doi.org/10.1144/gsjgs.150.6.1183

Chesley, J. T., Halliday, A. N., Snee, L. W., Mezger, K., Shepherd, T. J., & Scrivener, R. C. (1993). Thermochronology of the Cornubian batholith in southwest England: Implications for pluton emplacement and protracted hydrothermal mineralization. *Geochimica et cosmochimica acta, 57*(8), 1817-1835. doi:10.1016/0016-7037(93)90115-D

Černý, P., & Ercit, T. S. (2005). The classification of granitic pegmatites revisited. *The Canadian Mineralogist, 43*(6), 2005-2026.

Drivenes, K. (2015). Late-magmatic immiscibility during batholith formation: assessment of B isotopes and trace elements in tourmaline from the Land's End granite, SW England.

Drivenes, K., Larsen, R. B., Müller, A., & Sørensen, B. E. (2016). Crystallization and uplift path of late Variscan granites evidenced by quartz chemistry and fluid inclusions: Example from the Land's End granite, SW England. *Lithos, 252-253*, 57-75. doi:10.1016/j.lithos.2016.02.011

Drivenes, K., Larsen, R. B., Müller, A., Sørensen, B. E., Wiedenbeck, M., & Raanes, M. P. (2015). Late-magmatic immiscibility during batholith formation: assessment of B isotopes and trace elements in tourmaline from the Land's End granite, SW England.

Contributions to mineralogy and petrology, 169(6), 1-27. doi:10.1007/s00410-015-1151-6

Drummond, S., & Ohmoto, H. (1985). Chemical evolution and mineral deposition in boiling hydrothermal systems. *Economic Geology, 80*(1), 126-147.

Goldstein, J., Newbury, D., Joy, D., Lyman, C., Echlin, P., Lifshin, E., . . . Michael, J. (2003). Scanning Electron Microscopy and Microanalysis, New York: Kulwer Academic. In: Plenum Publishers.

Goldstein, R. H., & Reynolds, T. J. (1994). Fluid inclusion microthermometry.

Goode, A. J. J., Taylor, R. T., Dangerfield, J., Hawkes, J. R., Scrivener, R. C., & Wilson, A. C. (1988). Geology of the country around Penzance: memoir for 1:50 000 geological sheets 351 and 358 (England and Wales). *Memoir of the British Geological Survey, Sheets 351 and 358*.

Granseth, A., Slagstad, T., Coint, N., Roberts, N. M., Røhr, T. S., & Sørensen, B. E. (2020). Tectonomagmatic evolution of the Sveconorwegian orogen recorded in the chemical and isotopic compositions of 1070–920 Ma granitoids. *Precambrian Research, 340*, 105527.

Ihlen, P. M., & Müller, A. (2009). Rare-metal pegmatites in the Sveconorwegian orogen (0.9–1.1 Ga) of southern Norway. *Estudos Geológicos, 19*(2), 140.

Jahns, R. H., & Burnham, C. W. (1969). Experimental studies of pegmatite genesis; l, A model for the derivation and crystallization of granitic pegmatites. *Economic Geology, 64*(8), 843-864.

Larsen, R. B. (2004). The distribution of rare-earth elements in K-feldspar as an indicator of petrogenetic processes in granitic pegmatites: examples from two pegmatite fields in southern Norway. *The Canadian Mineralogist, 40*(1), 137-152.

LeBoutiller, N. G. (2002). *The Tectonics of Variscan Magmatism and Mineralisation in South West England.* (Doctor). University of Exter, Academia.

Lloyd, G. E. (1987). Atomic number and crystallographic contrast images with the SEM: a review of backscattered electron techniques. *Mineralogical Magazine, 51*(359), 3-19.

London, D. (2018). Ore-forming processes within granitic pegmatites. *Ore Geology Reviews, 101*, 349-383.

Müller, A., Romer, R. L., & Pedersen, R.-B. (2017). The Sveconorwegian pegmatite province–thousands of pegmatites without parental granites. *The Canadian Mineralogist, 55*(2), 283-315.

Müller, A., Seltmann, R., Halls, C., Siebel, W., Dulski, P., Jeffries, T., . . . Kronz, A. (2006). The magmatic evolution of the Land's End pluton, Cornwall, and associated pre-enrichment of metals. *Ore geology reviews, 28*(3), 329-367. doi:10.1016/j.oregeorev.2005.05.002

Nasdala, L., Götze, J., Hanchar, J. M., Gaft, M., Krbetschek, M. R., Beran, A., & Libowitzky, E. (2004). Luminescence techniques in Earth sciences. *Spectroscopic methods in mineralogy, 6*, 43-91.

Patterson, D. J., Ohmoto, H., & Solomon, M. (1981). Geologic setting and genesis of cassiterite-sulfide mineralization at Renison Bell, western Tasmania. *Economic Geology, 76*(2), 393-438. doi:10.2113/gsecongeo.76.2.393

Pearson, R. G. (1963). Hard and Soft Acids and Bases. *J. Am. Chem. Soc, 85*(22), 3533-3539. doi:10.1021/ja00905a001

Pirajno, F. (2008). *Hydrothermal processes and mineral systems*: Springer Science & Business Media.

Pownall, J. M., Waters, D. J., Searle, M. P., Shail, R. K., & Robb, L. J. (2012). Shallow laccoliti emplacement of the Land's End and Tregonning granites, Corwall, UK: Evidence from aureole field relations and PT modeling of cordierite-anthophyllite hornfels. *Geosphere, 8*(6), 38.

Raade, G., & Kristiansen, R. (2000). Mineralogy and geochemistry if the Heftetjern granite pegmatite, Tørdal: a progress report. *Norsk Bergverksmuseum, Skrift. 17*, 19-25.

Reed, S. J. B. (2005). *Electron microprobe analysis and scanning electron microscopy in geology*: Cambridge university press.

Richter, D. K., & Zinkernagel, U. (1981). Zur Anwendung der Kathodolumineszenz in der Karbonatpetrographie. *Geologische Rundschau, 70*(3), 1276-1302.

Robb, L. (2005). *Introduction to ore-forming processes*. Malden, Mass: Blackwell.

Roedder, E. (2005). Iain Samson Alan Anderson Dan Marshall Fluid Inclusions, Analysis and Interpretation Mineralogical Association of Canada Short Course Series Volume 32 2003 Mineralogical Association of Canada 0-921294-32-8 374 pp. In (Vol. 69, pp. 5133-5134): Elsevier Ltd.

Rosing-Schow, N. (2020). The Sveconorwegian pegmatite province: Identifying the parameters controlling the abundance and genesis of the pegmatites.

Rosing-Schow, N., Müller, A., & Friis, H. (2018a). A comparison of the mica geochemistry of the pegmatite fields in southern Norway. *The Canadian Mineralogist, 56*(4), 463-488.

Rosing-Schow, N., Müller, A., & Friis, H. (2018b). A comparison of the mica geochemistry of the pegmatite fields in Southern Norway. *The Canadian Mineralogist, Vol. 56*, pp. 463-488. doi:10.3749/canmin.1700086

Samson, I., Anderson, A., & Marshall, D. (2003). *Iain Samson Alan Anderson Dan Marshall Fluid Inclusions, Analysis and Interpretation Mineralogical Association of Canada Short Course Series Volume 32 2003 Mineralogical Association of Canada 0-921294-32-8 374 pp*. Department of Geology,

Acadia University,

Wolfville, Nova Scotia

Canada, B4P 2R6: Elsevier Ltd.

Simmons, W. B. S., & Webber, K. L. (2008). Pegmatite genesis: state of the art. *European Journal of Mineralogy, 20*(4), 421-438.

Slagstad, T., Roberts, N., & Kulakov, E. (2017). Linking orogenesis across a supercontinent; the Grenvillian and Sveconorwegian margins on Rodinia. *Gondwana Research, 44*, 109-115. doi:10.1016/j.gr.2016.12.007

Slagstad, T., Roberts, N. M. W., Coint, N., Høy, I., Sauer, S., Kirkland, C. L., . . . Bybee, G. (2018). Magma-driven, high-grade metamorphism in the Sveconorwegian Province, southwest Norway, during the terminal stages of Fennoscanadian Shield evolution. *Geosphere, vol. 14*, 861-882. doi:10.1130/GES01565.1

Sorby, H. C. (1858). On the Microscopical, Structure of Crystals, indicating the Origin of Minerals and Rocks. *Quarterly Journal of the Geological Society, 14*(1-2), 453-500. doi:10.1144/gsl.jgs.1858.014.01-02.44

Steffenssen, G., Müller, A., Munnik, F., Friis, H., Erambert, M., Kristoffersen, M., & Rosing-Schow, N. (2020). Unusual scandium enrichments of the Tørdal pegmatites, south Norway. Part I: Garnet as Sc exploration pathfinder. *Ore Geology Reviews, 126*, 103729. doi:https://doi.org/10.1016/j.oregeorev.2020.103729

Ten Have, T., & Heijnen, W. (1985). experimental approach. *Geologie en Mijnbouw, 64*, 297-310.

Thomas, R., Davidson, P., & Beurlen, H. (2012). The competing models for the origin and internal evolution of granitic pegmatites in the light of melt and fluid inclusion research. *Mineralogy and Petrology, 106*(1), 55-73.

Wark, D., & Watson, E. (2004). *The TITANiQ: a titanium-in-quartz thermometer.* Paper presented at the Geochimica et Cosmochimica Acta.

Wilberg, R. (1983). *En geologisk og geokjemisk undersøkelse innenfor kartblad Nissedal i Telemark med detaljert geologisk kartlegging i Kleppsvatnområdet.* Norges tekniske høgskole,

Zhang, L., Audétat, A., & Dolejš, D. (2012). Solubility of molybdenite (MoS2) in aqueous fluids at 600–800° C, 200 MPa: A synthetic fluid inclusion study. *Geochimica et Cosmochimica Acta, 77*, 175-185.

Černý, P. (1991). Rare-element Granitic Pegmatites. Part I: Anatomy and Internal Evolution of Pegmatitic deposits. . *Geoscience Canada, 18, Number 2*, 49-67.

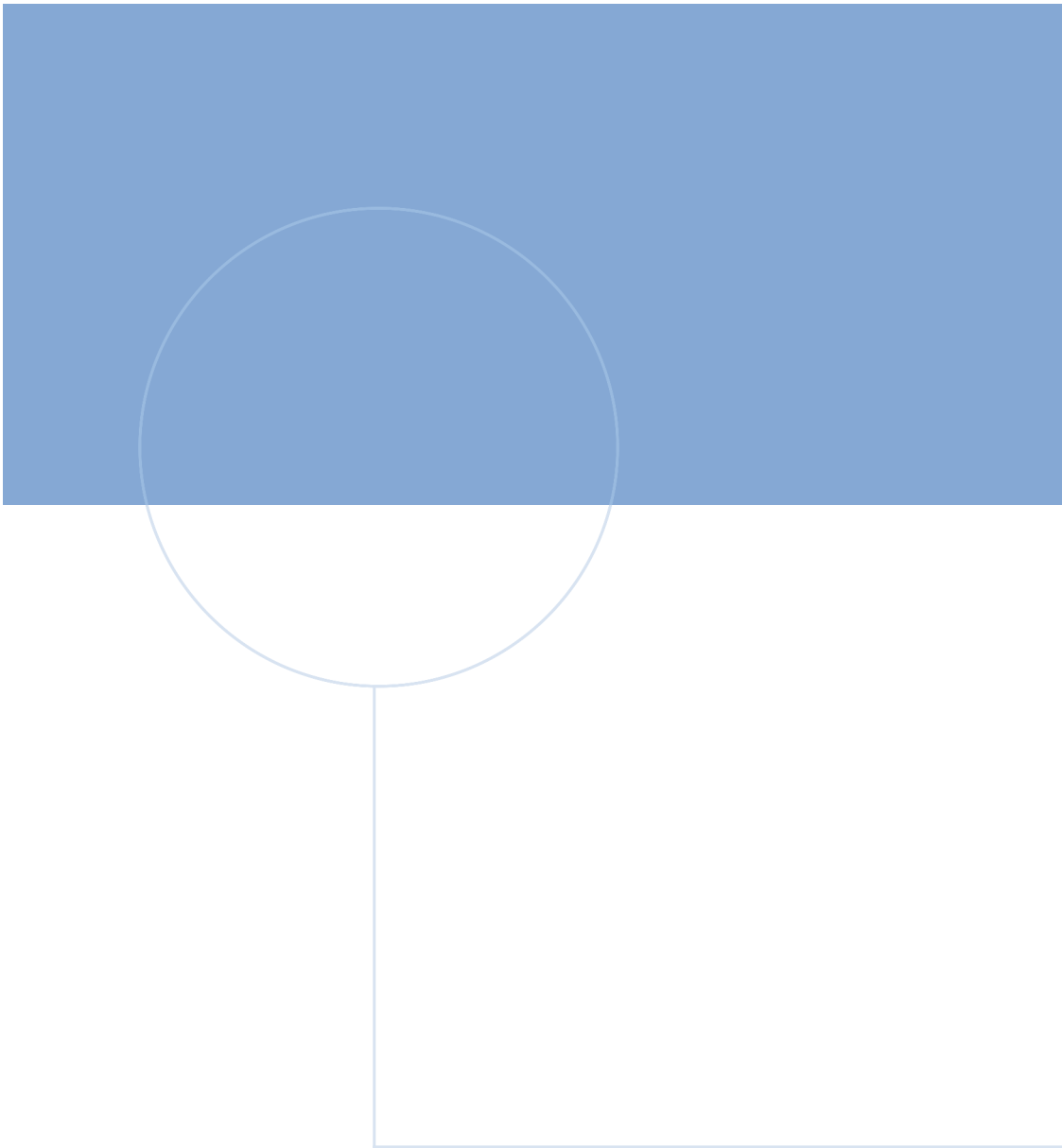

NTNU

Norwegian University of
Science and Technology